An Anatomical and Biomechanical Study of the Human Iliotibial Band's Role in Elastic Energy Storage

A dissertation presented
by

Carolyn Margaret Eng

to
The Committee on Human Evolutionary Biology & Organismic and Evolutionary Biology

in partial fulfillment of the requirements
for the degree of
Doctor of Philosophy
in the subject of
Human Evolutionary Biology & Organismic and Evolutionary Biology

Harvard University
Cambridge, Massachusetts

April 2014

Dissertation Advisors: Professors Andrew A. Biewener and Daniel E. Lieberman Carolyn Margaret Eng

An Anatomical and Biomechanical Study of the Human Iliotibial Band's Role in Elastic Energy Storage

Abstract

The iliotibial band (ITB) is a complex structure that is unique to humans among apes and is derived from the fascia lata (FL) of the thigh. Although the ITB evolved in the hominin lineage, it is unclear whether it evolved to improve locomotor economy, increase stability, or serve a different function. This dissertation tests the hypothesis that the ITB stores and recovers elastic energy during walking and running.

Because the goat FL shares many convergent features with the ITB, I conducted experiments on the goat FL to gain insight into its potential for energy storage. The capacity for a fascial structure to store energy depends on its stiffness. Biaxial tests revealed that FL stiffness is not strongly influenced by the FL's biaxial strain environment despite its complex structure. To examine *in vivo* FL function, I measured FL strains during goat locomotion. I found that the goat FL is stretched by muscle forces during stance phase and potentially stores a fraction of the limb's kinetic energy as elastic energy.

To assess the human ITB's role in elastic energy storage, I created computer models that characterize the 3D geometry and isometric force-generating capacity of muscles that insert into the human ITB and chimp FL. The models are based on quantitative measurements of the muscle architecture, 3D anatomy, and hip and knee

moment arms of the tensor fascia lata and gluteus maximus muscles in human and chimpanzee cadaveric specimens. Using the human model, I found that the ITB has the potential to store and recover elastic energy during walking and running, with eight times greater energy storage in running compared to walking.

By comparing factors that contribute to elastic energy storage in the human and chimpanzee models, I showed that differences in muscle attachments and hip motion during bipedal walking explain the human ITB's greater capacity for energy storage compared to the chimp FL. Together, these data suggest that the human ITB is specialized for elastic energy storage during locomotion, especially during running. Stronger selection for reduced locomotor costs during endurance running may have favored traits that increased ITB energy storage in humans.

Table of Contents

List of Figures

List of Tables

This work is dedicated to two wonderful people I met while at Harvard.

Farish A. Jenkins, Jr. was an inspiring mentor, teacher, anatomist, and friend. He was one of the best things about Harvard and the lessons I learned from him will be with me for the rest of my life.

Andrew McQueen Carroll and I shared many passions including muscle physiology, nature, and music. His guidance and friendship in my first years of graduate school were invaluable.

Acknowledgements

Although the process of completing a thesis is long and arduous at times, the last seven years at Harvard have been some of the best years of my life. I have met many amazing people that have given me advice, mentorship, and friendship and they have collectively made my experience at Harvard extremely valuable and unique.

My thesis committee has been immensely supportive. I am very lucky to have had two advisors through this process, Dan Lieberman and Andy Biewener. Dan has been supportive from the outset and our many conversations helped shape this project. Dan's door is always open and his contagious enthusiasm made doing science more fun. Andy, too, has been an amazingly supportive advisor. I learned so much from our many conversations about locomotion and energy storage, and I have especially appreciated our more philosophical chats about life in general. I honed my surgical techniques under Andy's guidance as he sat in on all goat surgeries and experiments. Both Andy and Dan are very invested in me, both personally and academically, and I appreciate their selfless dedication to my success. Allison Arnold-Rife has been nothing short of a third advisor on this project. My thesis benefited greatly from her support and guidance. From helping to design my moment arm frame to assisting with all human and chimp experiments, it would have taken me seven more years to complete this thesis without Allison's help. Allison is also an excellent writer and editor and she helped make this a better thesis. I would also like to thank Tom Roberts for our many fruitful conversations about my thesis research and future research plans. I look forward to working with him in the years to come.

I am thankful to the many people who made me excited about musculoskeletal research in the first place including Andrea Taylor and Sam Ward. Andrea is a great scientist and an even better person, and she taught me many skills that are essential to being a good scientist. She has been an important role model and mentor for me and I would not be where I am now were it not for her guidance and support. Sam has also been a tireless supporter and great friend. He taught me so much about anatomy, muscle physiology, and most importantly, mentorship. Sam is just about the smartest person I know, and yet he has this great ability to admit what he does know and more importantly, what he doesn't know, which makes him an amazing teacher. When my enthusiasm was flagging in the first years of graduate school, Sam brought the fire back. He told me to get a plane ticket to San Diego and he would provide the cadaver. Our iliotibial band dissections and materials testing helped shape my thesis experiments and I am very thankful for that time with him.

I am grateful to the many students that have worked with me on this project including Yasmin Rawlins, Casey Boyle, and Andrew Reed. I am especially appreciative of the hard work of Delande Justinvil. I appreciate others at Harvard who have helped me along the way including Lee Gehrke, Sid Paula, Mark Omura, and Judy Chupasko.

Thank you to everyone in the Human Evolutionary Biology department including Meg Lynch, Zarin Machanda, Amanda Lobell, Tanya Smith, Dan Green, Katy Sharrock, Lenia Constantinou, Meg Jarvi, David Pilbeam, Michele Morgan, and Larry Flynn. Your support and guidance made my time at Harvard truly special. I am especially grateful for the many fruitful conversations with members of the Lieberman lab past and present including Neil Roach, Campbell Rolian, Maureen Devlin, Eric Castillo, Kristi Lewton, and

Katie Zink. My conversations with Herman Pontzer greatly benefited my research. I am thankful to Herman and Jim Cheverud for procuring the chimpanzee specimen that provided pilot data for my thesis and inspired future chimp experiments.

Thank you to the crew at Concord Field Station, my home away from home. I appreciate the guidance and friendship of the CFS students and staff including Peg Hedstrom, Lisa Litchfield, Somer O'Brien, Ken Wilcox, Pedro Ramirez, Chris Richards, Ed Yoo, Carlos Moreno, Angie Berg, Talia Moore, Glenna Clifton, Jen Carr, Dave Williams, Andrew Mountcastle, Fuzz Crompton, Stacey Coombes, Jay Iwasaki, Maria Miara, James Crall, Mary Salcedo, Susie Gagliardi, Jake Peters, and Callin Switzer. Ivo Ros, many thanks for your support at the end. Those freshly cooked meals were the fuel that helped me bring this beast home.

My parents were awesomely supportive throughout this process, even offering to fly out to Boston to help with a cadaver experiment. I am thankful for their love and guidance through it all. Thank you to the many friends I have made in graduate school, you know who you are. We have had so much fun canoeing, camping, biking, backpacking, drinking, and dancing. You have kept me sane through it all. Thank you also to my oldest and dearest friends, Jenny Carnival, Kathleen Semerad, and Colleen Terschluse. Finally, much love and appreciation to Zack for his help and support during my dissertation. He had a hand in every aspect of this project (literally had a hand in several human and chimp limbs) and I could not have done it without him. I also have my dissertation to thank for Zack, had I not been interested in imaging the fascia in his lab three years ago, we may never have had the opportunity to get to know each other. I have been so lucky to have Zack by my side through it all.

Introduction

Bipedalism may be the first major behavioral and anatomical innovation of the human lineage. Many hypotheses exist regarding the selective pressures that favored the evolution of bipedalism including reducing heat stress in open habitats (Wheeler, 1984), favoring hand-assisted stabilization during arboreal movement on small, flexible branches (Thorpe et al., 2007), and increasing load carrying abilities (Hewes, 1964). Another hypothesis is that natural selection favored a shift to bipedal walking from a costly mode of quadrupedalism, such as knuckle-walking, to reduce the energetic cost of travel as climatic shifts increased the distance between food patches (Taylor and Rowntree, 1973; Rodman and McHenry, 1980; McMahon et al., 1987; Sockol et al., 2007). Although the origins of bipedal locomotion probably reflected selection for walking, at some point in human evolution selective pressures favoring the evolution of endurance running also must have occurred, probably in the genus *Homo* (Bramble and Lieberman, 2004). Derived features in *Homo* that improve running performance include a stabilized sacroiliac joint, which allows effective weight transfer from the trunk to the pelvis (Rose, 1984); an expanded attachment surface on the ilium for gluteus maximus, which helps stabilize the trunk (Lieberman et al., 2006); and short toes which decrease the extension torques the foot muscles must counteract during stance (Rolian et al., 2009).

The iliotibial band (ITB) is a complex structure in the lower limb, unique to humans, and is derived from the fascia lata (FL) of the thigh. The human ITB is an insertion site for the gluteus maximus (GMax) and tensor fascia lata (TFL) muscles and is anatomically distinct from the FL of apes, which is small and has fewer connections

with hip muscles. Thus, the derived anatomy of the fascia lata in humans must have evolved at some time in hominin evolution, perhaps to improve locomotor economy or to increase bipedal stability. The ITB's role in human locomotion is not well understood, in part because it is difficult to model and experimentally test the structure's function. The primary goal my dissertation was to test a new model of ITB function during bipedal locomotion in humans. My major hypothesis is that the ITB stores and recovers elastic energy during walking and running. A role for the human ITB in energy storage is likely to improve the economy of human gait. Uncovering such a role for the human ITB may provide insight into the evolution of bipedal locomotion in hominins.

Like a tendon, the ITB acts as a spring that connects muscles to bones. Locomotor economy is determined, in large part, by the metabolic energy used by muscles to produce the forces needed to support and propel the body. Muscles can shorten to produce work, lengthen to absorb energy, or contract isometrically. Because the rate of metabolic energy consumed by a muscle is proportional to the amount of force it produces and its rate of shortening (Alexander, 1997), muscles that produce force isometrically are most economical. Compliant tendons or fascial structures that are in series with isometrically contracting muscles may further decrease the metabolic cost of movement by storing elastic strain energy that would otherwise be dissipated by muscles. Recovering energy, that would otherwise be dissipated, through tendon recoil decreases the amount of work required by active muscle (Roberts et al., 1997).

The ITB is traditionally considered a hip stabilizer, particularly in the frontal plane (Inman, 1947; Fredericson et al., 2000). However, muscles with short fibers in series with a long tendon often play a role in economical force generation through energy

storage and recovery (Biewener and Roberts, 2000; Biewener, 2008). This arrangement is found in the ITB and inserting muscles, suggesting that the ITB may store and recover elastic energy. However, accurate estimates of ITB energy storage cannot be generated without more accurate estimates of musculoskeletal geometry and muscle architecture.

The goal of my dissertation research was to test the model that the ITB's anatomy and material properties, together with kinematics and muscle activity, evolved in humans to improve locomotor economy through energy storage and recovery. To test this model, my research integrated experimental data from humans and nonhuman primates as well as from goats, which have a FL that is convergently well developed. Additionally, materials testing was performed to estimate the behavior of FL in response to muscle forces during locomotion.

The potential for fascial structures such as the human ITB and the goat FL to store energy, transmit forces, and/or stabilize joints is dependent on their material properties including stiffness and hysteresis. Because fascia is a sheet-like structure often attaching to muscles and bones at multiple sites, it is exposed to different states of biaxial strain, and its properties cannot be captured with a simple uniaxial testing protocol. Therefore, in chapter 1 of my thesis I used biaxial materials testing to measure the influence of biaxial strains on the material properties of the goat FL. The goat FL is composed of two layers of highly aligned collagen fibers that are oriented approximately perpendicular to each other, and biaxial tests were performed on both longitudinally-oriented and transversely-oriented samples in each goat. Histology and scanning

electron microscopy were also used to examine the structural differences underlying differences in material behavior.

Results suggest that although the collagen layers in the goat FL are not independent, loading in one layer does not greatly influence the other layer's material properties. Varying strain in the perpendicular direction did not affect the FL's stiffness or hysteresis. Additionally, material properties vary between longitudinal and transversely oriented samples. The FL's modulus, hysteresis, and strain energy density are greater in the longitudinal than in the transverse direction. Imaging results suggest that increased stiffness in the longitudinal layer is likely due to its greater thickness and greater average fibril diameter compared to the transverse layer. The differing material properties observed between the longitudinal and transverse orientations suggest that differential loading in these directions during growth and development may lead to these structural changes, enhancing the ability of the longitudinal FL to transmit force, store energy, and/or stabilize the goat limb. Additionally, these results suggest that the FL transmits force predominantly in the longitudinal direction, despite the complex 3D geometry of the tissue and surrounding muscles. Furthermore, these data suggest that the origin-to-insertion paths of the TFL-ITB and GMAX-ITB complexes can be reasonably modeled as a series of independent, proximal-to-distal muscle-tendon compartments.

Because *in vivo* measures of human muscle and tendon function are limited to non-invasive protocols and the FL of cursorial quadrupeds may be convergent with the human ITB, in chapter 2 of my thesis I used a goat model to test whether the goat FL stores elastic energy during the stance phase of locomotion and recovers the elastic

energy in swing phase. By measuring muscle and fascia length change patterns and muscle activity during both inclined and level locomotion, I assessed whether the FL contributes to the increased demand for mechanical work on an incline. Results suggest that the goat FL stretches during stance phase through both passive joint angles excursions and active muscle shortening. Distal FL stretch increased on the incline versus level walking, suggesting that the distal FL may store and release more energy as a result of the increased force (and work) produced by the inserting muscle.

While data describing the material properties and *in vivo* behavior are important for demonstrating the potential for elastic energy storage in fascial structures similar to the ITB, the ultimate goal of my dissertation was to test the hypothesis that the ITB stores and recovers energy during human walking and running. Therefore in chapter 3 of my thesis, I used a musculoskeletal model of the human ITB to estimate the strains and forces transmitted by this structure during walking and running. An existing human lower limb model was modified using measurements of muscle architecture and moment arms from five human cadavers. The model was used, in combination with measured joint kinematics and published EMG recordings, to examine the capacity of the ITB to store elastic energy during walking, endurance running, and sprinting. I found that forces generated by the TFL and GMax muscles are likely to stretch the ITB during walking and running, resulting in ITB energy storage in both gaits. The anterior and posterior ITB have distinct length change patterns and periods of predicted elastic energy storage because of different MAs. The anterior ITB potentially stores energy in stance phase, which may be recovered in swing phase. Estimates of energy storage in the posterior ITB are greater than in the anterior ITB because of larger maximum

muscle forces. The potential for ITB energy storage is eight times greater in walking than running, suggesting that selection for reduced locomotor costs during running may have increased ITB energy storage in *Homo*.

Chapter 4 of my thesis tests whether the human ITB's ability to store energy or counteract hip adduction moments during walking is unique to humans among apes. To do this, I compared the functions of the chimp FL and human ITB using musculoskeletal models. An existing chimp model was refined using measurements of muscle architecture and moment arms from four chimpanzee cadavers. The model was used with estimates of the chimp's hip and knee angles during bipedal walking to compute loading and displacement of the FL and to predict its capacity for elastic energy storage and recovery relative to the human ITB. Our modeling results support the hypothesis that the human ITB is anatomically derived compared to the chimp FL in ways that suggest the human ITB is specialized for elastic energy storage. Differences in both locomotor mechanics and anatomy contribute to the human ITB's greater capacity to store elastic energy compared to the chimp FL. Chimpanzees walk with a smaller range of hip flexion/extension than humans, so chimpanzee FL muscle-tendon units (MTUs) undergo smaller length changes during bipedal walking compared to human muscle-ITB MTUs. Additionally, the muscles inserting in the human ITB have a greater mass-specific force-generating capacity than the muscles inserting in the chimp FL. Specialization of the human ITB for energy storage suggests that it may have evolved to enhance locomotor economy.

References

Alexander, R. (1997). Optimum muscle design for oscillatory movement. *Journal of Theoretical Biology* **184**, 253-259.

Biewener, A. (2008). Tendons and ligaments: Structure, mechanical behavior and biological function. In *Collagen: Structure and Mechanics*, (ed. P. Fratzl). New York: Springer.

Biewener, A. and Roberts, T. (2000). Muscle and tendon contributions to force, work, and elastic energy savings: a comparative perspective. *Exercise and Sport Sciences Reviews* **28**, 99-107.

Bramble, D. and Lieberman, D. (2004). Endurance running and the evolution of *Homo*. *Nature* **432**, 345-352.

Fredericson, M., Cookingham, C., Chaudhari, A., Dowdell, B., Oestreicher, N. and Sahrmann, S. (2000). Hip abductor weakness in distance runners with iliotibial band syndrome. *Clinical Journal of Sport Medicine* **10**, 169-175.

Hewes, G. (1964). Hominid bipedalism: Independent evidence for the food-carrying theory. *Science* **146**, 416-418.

Inman, V. T. (1947). Functional aspects of the abductor muscles of the hip. *The Journal of Bone and Joint Surgery* **29**, 607-619.

Lieberman, D. E., Raichlen, D. A., Pontzer, H., Bramble, D. M. and Cutright-Smith, E. (2006). The human gluteus maximus and its role in running. *Journal of Experimental Biology* **209**, 2143-2155.

McMahon, T. A., Valiant, G. and Frederick, E. C. (1987). Groucho Running. *Journal of Applied Physiology* **62**, 2326-2337.

Roberts, T. J., Marsh, R. L., Weyand, P. G. and Taylor, C. R. (1997). Muscular force in running turkeys: the economy of minimizing work. *Science* **275**, 1113-1115.

Rodman, P. S. and McHenry, H. M. (1980). Bioenergetics and the origin of human bipedalism. *American Journal of Physical Anthropology* **52**, 103-106.

Rolian, C., Lieberman, D. E., Hamill, J., Scott, J. W. and Werbel, W. (2009). Walking, running and the evolution of short toes in humans. *Journal of Experimental Biology* **212**, 713-721.

Rose, M. (1984). A hominine hip bone, KNM-ER 3228, from East Lake Turkana, Kenya. *American Journal of Physical Anthropology* **63**, 371-378.

Sockol, M., Raichlen, D. and Pontzer, H. (2007). Chimpanzee locomotion energetics and the origin of human bipedalism. *Proceedings of the National Academy of Sciences* **104**, 12265-12269.

Taylor, C. R. and Rowntree, V. J. (1973). Running on two or on four legs: which consumes more energy? *Science (Washington D.C.)* **179**, 186-187.

Thorpe, S. K. S., Holder, R. L. and Crompton, R. H. (2007). Origin of human bipedalism as an adaptation for locomotion on flexible branches. *Science* **316**, 1328-1331.

Wheeler, P. (1984). The evolution of bipedality and loss of functional body hair in hominids. *Journal of Human Evolution* **13**, 91-98.

Chapter 1: Directional differences in the biaxial material properties of fascia lata and the implications for fascia function

Published as **Eng, C. M., Pancheri, F. Q., Lieberman, D. E., Biewener, A. A. and Dorfmann, L.** (2014). Directional differences in the biaxial material properties of fascia lata and the implications for fascia function. *Annals of Biomedical Engineering* **42**, 1224-1237.

Abstract

Fascia is a highly organized collagenous tissue that is ubiquitous in the body, but whose function is not well understood. Because fascia has a sheet-like structure attaching to muscles and bones at multiple sites, it is exposed to different states of multi- or biaxial strain. In order to measure how biaxial strain affects fascia material behavior, planar biaxial tests with strain control were performed on longitudinal and transversely oriented samples of goat fascia lata (FL). Cruciform samples were cycled to multiple strain levels while the perpendicular direction was held at a constant strain. Structural differences among FL layers were examined using histology and SEM. Results show that FL stiffness, hysteresis, and strain energy density are greater in the longitudinal versus transverse direction. Increased stiffness in the longitudinal layer is likely due to its greater thickness and greater average fibril diameter compared to the transverse layer(s). Perpendicular strain did not affect FL material behavior. Differential loading in the longitudinal versus transverse directions may lead to structural changes, enhancing the ability of the longitudinal FL to transmit force, store energy, or stabilize the limb during locomotion. The relative compliance of the transverse fibers may allow expansion of underlying muscles when they contract.

Introduction

Fascia is a multilayered collagenous tissue found throughout the body that is intimately connected with muscles but whose function during movement is not well understood. Various functional roles have been hypothesized for fascia. Because fascia attaches to and envelops many limb muscles, it is often hypothesized that it broadens the insertion of muscles, distributing or redirecting muscle force transmission (Mozan and Keagy, 1969; Garfin et al., 1981; Huijing and Baan, 2001; Huijing et al., 2003). Several studies have shown that disrupting the fascia between or around muscles decreases the muscle's force output (Garfin et al., 1981; Huijing and Baan, 2001; Huijing et al., 2003). Fascial continuity among limb segments and between the limbs and the trunk have led others to posit that fascia plays a role in transferring load and coordinating movement among limb segments and body regions (Dubiel and Wigren, 1974; Barker et al., 2004; Stahl, 2010). A recent investigation found increased variability in non-sagittal plane movement in the lower limb kinematics of cats after fasciotomy, suggesting that fascia stabilizes the limb by limiting non-sagittal plane movement during locomotion (Stahl, 2010). Finally, an elastic energy storage role has been hypothesized for fascia, wherein energy stored in the fascia during stance phase is recovered to propel the limb forward during swing (Bennett, 1989; Stahl, 2010; Eng et al., 2012).

Fascia's ability to serve these functions depends on its stiffness and resiliency, but these material properties have not been sufficiently characterized. As a multilayered, planar tissue attaching to muscles and bones at multiple sites, fascia is exposed to different states of multiaxial strain. Its functional potential is therefore best captured using biaxial testing protocols, rather than uniaxial tests. The purpose of this

study was to measure the biaxial material behavior of goat fascia lata (FL) in order to evaluate its potential mechanical functions during movement. We used scanning electron microscopy (SEM) and histology to characterize the structure of the multiple collagen layers in the FL and provide a basis for understanding its material behavior.

Data on the relative independence of the multiple collagen layers within fascia is important for understanding its function *in vivo.* In general, the alignment of collagen fibers differs among layers in fascia (Benjamin, 2009; Stecco et al., 2011), a structure which maintains fascial strength when loaded in multiple directions. If the collagen layers are loaded simultaneously in different directions, how does strain in one layer of collagen fibers influence tissue properties in the other layer(s)? Histological studies characterize the collagen layers in fascia as discrete and separated by layers of loose connective tissue, a structural organization which is thought to allow the collagen layers to move independently (Stecco et al., 2011). However, studies describing the biaxial material properties of other biological tissues including skin, aponeurosis, tendon, and aortic tissue have shown that tissue properties vary substantially when strained uniaxially versus biaxially. For instance, stiffness of rabbit skin and human aortic tissue is greater in biaxial versus uniaxial tests (Lanir and Fung, 1974; Vande Geest et al., 2006) and stiffness in the collagen fiber direction increases with strain in the orthogonal direction in turkey aponeurosis and shark skin (Wainwright et al., 1978; Azizi and Roberts, 2009). Whether the same is true for fascia has not been investigated. The potential for biaxial strain to modulate fascia stiffness is particularly important for a tissue that may play such diverse functional roles. For example, during a movement, fascia's stiffness may be modulated depending on its role in limb stability versus energy

storage. Planar biaxial testing with strain control provides an opportunity to investigate if fascia stiffness can be modulated by different biaxial strain conditions.

Finally, data on the relative independence of collagen layers in fascia are important for creating musculoskeletal models that are sufficiently accurate to explain fascia function. In commonly used multi-segment musculoskeletal models (Neptune et al., 2001; Arnold et al., 2010), muscles are represented as independent muscle-tendon units that attach to bones at discrete points proximally and distally. These models do not consider the three-dimensional strain environment that may occur in tissues when multiple muscles insert in a single connective tissue, when muscles attach to connective tissues both proximally and anteriorly or posteriorly, or when forces are transmitted both longitudinally and transversely. Data on the effect of biaxial strains on fascia material behavior will indicate whether the 3D strain environment of planar connective tissues can be accurately characterized using discrete and independent muscle-connective tissue units. Recent 3D finite element models of muscle incorporate the complex 3D architecture of muscle fibers and connective tissue (Blemker et al., 2005; Teran et al., 2005; Chi et al., 2010; Rehorn and Blemker, 2010). While these models may more accurately model the 3D strain environment of fascia and provide important insight into fascia function at the muscle level, connective tissues in these models are assumed to have the same stiffness as tendon (Blemker et al., 2005; Teran et al., 2005; Chi et al., 2010; Rehorn and Blemker, 2010), which may be inaccurate for fascia.

Here we focus on the fascia lata, which is found on the lateral side of the thigh of mammals. In goats, the gluteobiceps (GB) and tensor fascia lata (TFL) muscles insert into the FL. These muscles are knee extensors and antagonists at the hip joint (GB

extends and TFL flexes the hip). The goat FL is composed of two primary orientations of parallel-aligned collagen fibers (assemblies of collagen fibrils and considered here to be synonymous with collagen fascicles), which are visible both microscopically and macroscopically (Figure 1.1). The collagen fibers in the longitudinal layer(s) run approximately parallel with the femur and are parallel with the muscle fibers of TFL, while the collagen fibers in the transverse layer(s) are at a 67-80° angle to the longitudinal fibers (Pancheri et al., 2014) and are parallel with the inserting GB muscle fibers. Our histological analysis of the FL will reveal whether there is more than one layer of tissue within each primary collagen orientation. The FL is thickened relative to other limb fascia, suggesting that it has the potential to play a role in limb stability, force transmission, and/or energy storage. As with other fascia, however, the function of the FL during movement has not been well explored.

Based on the anatomy and hypothesized function of the FL and biaxial behavior of other connective tissues, we propose five hypotheses relating the biaxial material behavior of the goat FL to its functional role during movement. Although the attachments and inserting muscles load the fascia lata biaxially, goat locomotor kinematics occur primarily in the sagittal plane, likely creating larger longitudinal than transverse loads in the tissue. We therefore hypothesize that larger longitudinal loads necessitate greater longitudinal stiffness (H1). We hypothesize that perpendicular strain increases the stiffness of the FL in its primary, longitudinal loading axis (H2), consistent with prior studies of other connective tissues. We hypothesize that increased perpendicular strain preloads the FL, decreasing the length of the toe and heel region of the stress-strain curve (H3). We also hypothesize that the increase in tissue stiffness

with perpendicular strain increases the strain energy stored in the FL at a given strain (H4). Finally, we hypothesize that differences in material behavior between longitudinal and transverse samples are due to differences in collagen layer thickness and collagen fibril size (H5).

Materials and Methods

FL samples were obtained from hindlimbs of five adult goats (mean ± SD: 35.1 ± 7.3 kg) from Blood Farm (Groton, MA). The FL was dissected from the hindlimb within two hours and all tests were performed within 48 hours of sacrifice. The FL was removed from the skinned hindlimb, wrapped in saline-soaked gauze, and stored at 4°C prior to testing and between tests. Two samples were cut from each FL (for a total of ten samples from five goats), one oriented parallel to the longitudinal fibers while the other was oriented parallel to the transverse fibers (Figure 1.2). Samples were cut using a custom-made cruciform-shaped die with a central gage region measuring 12 mm x 12 mm. The die was aligned visually with the fiber orientation of one family of fibers (i.e., longitudinal or transverse fibers) and cut using pressure evenly distributed over the die. Because the two families of fibers are not orthogonal, the perpendicular arms of the die could not be aligned with both fiber directions in a single sample. Sample thickness was measured at several points in the central gage region and averaged across regions using a dial thickness gage accurate to 0.01 mm (Mitutoyo, Sakato, Japan). The thickness gauge contacted the sample with a flat anvil creating a distributed load and the spring-loaded spindle exerted a constant measuring force across samples ensuring that thickness measurements were accurate and repeatable. Gage marks were

arranged to correspond to each of the four arms of the cruciform sample (Figure 1.3) and were attached to the gage region using biocompatible glue (Loctite, Westlake, OH). A distance of 7-10 mm separated opposing pairs of gage marks. Each arm was secured in custom-made extension platens covered in fine grit sand paper (Figure 1.3A).

Biaxial testing

Biaxial tests with strain control were performed using a custom built Zwick/Roell planar biaxial testing system (Ulm, Germany) (Pancheri and Dorfmann, 2013). The sample was attached to the four linear independently controlled actuators via rigid pincer type grips (Figure 1.3B). The tissue was maintained at 39°C during testing via a temperature-controlled chamber filled with phosphate buffered saline (PBS). All tests were performed using simultaneous non-contact strain controlled measurements using a video extensometer rigidly fixed to the machine's frame. Images of the sample were recorded prior to testing to measure specimen width in the gage region, which was subsequently used with the thickness measure to calculate sample cross-sectional area.

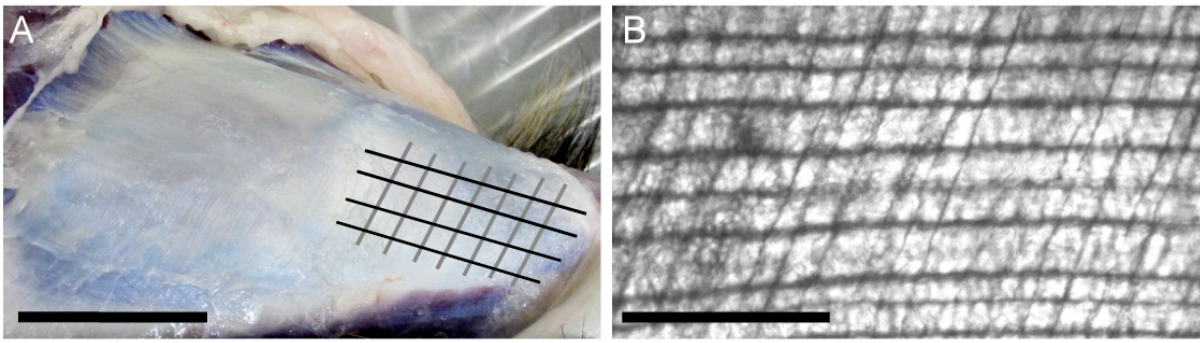

Figure 1.1. The transverse and longitudinal collagen layers in the fascia lata are each composed of highly aligned collagen fibers that are visible without (A) and with magnification (B). Gray and black lines in (A) represent the orientation of the transverse and longitudinal collagen fiber families, respectively. The sample in (B) was dehydrated in methanol, cleared in Benzyl Alcohol: Benzyl Benzoate (3:1) and imaged using differential interference contrast microscopy. Scale bar is 40 mm in (A) and 0.5 mm in (B).

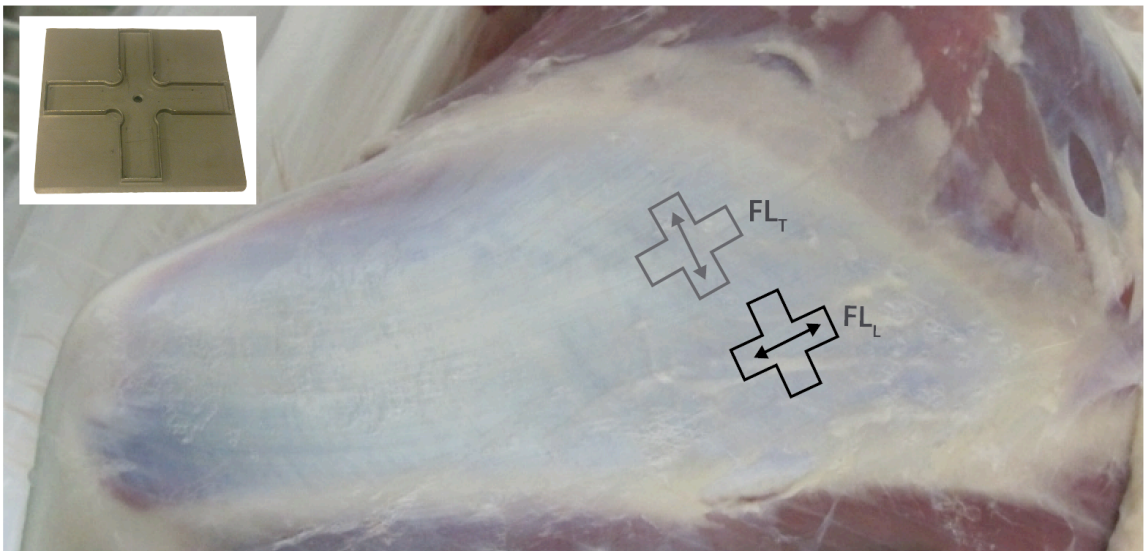

Figure 1.2. Longitudinal (FL_L) and transverse (FL_T) samples were cut from the fascia lata of each goat using a custom cruciform die (inset).

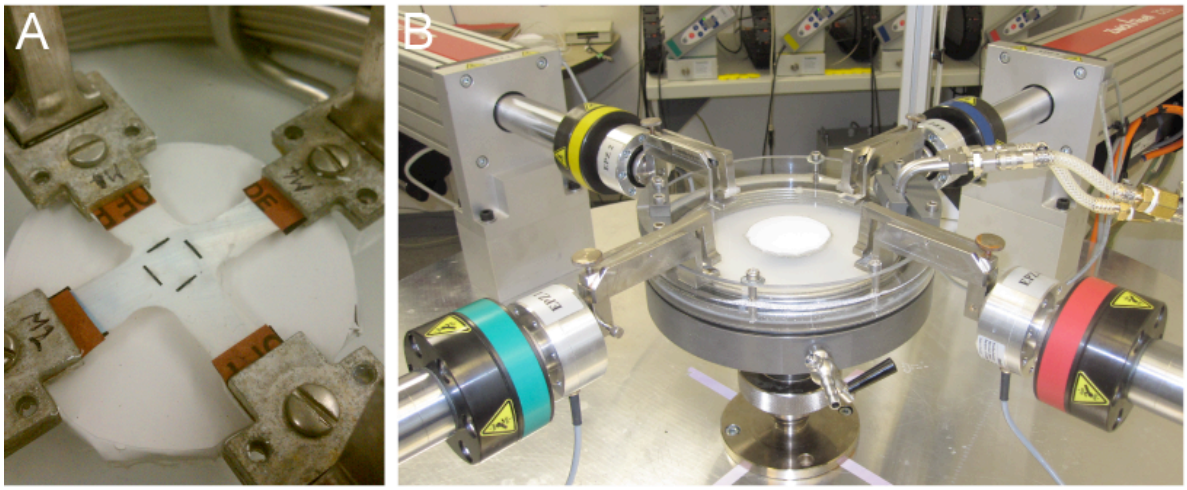

Figure 1.3. Gage marks were attached to each arm of the cruciform fascia lata sample and samples were mounted in extension platens with fine grit sand paper (A). Tests were performed in a Zwick/Roell biaxial testing system (B), which consisted of four independent actuators as described in Pancheri and Dorfmann (2013).

In the testing procedure, the perpendicular strain (ε_P; strain exerted on the tissue arms perpendicular to the arms aligned with one fiber family) was set at a pre-determined strain of 0% or 3% and held constant while the tissue was cycled five times each to cycling strains (ε_C) of 2%, 4%, 6%, and 8%. The tissue was returned to the initial length in the cycling direction ($L_{0,C}$) at the end of each cycle. A 180-second rest period was applied after each cycling strain. The testing protocol is summarized in Table 1.1 and was the same for both longitudinally and transversely-oriented samples. At each cycling strain level, ε_P was first set to 0% while ε_C was cycled and then 3% while ε_C was cycled again to the same strain. The sample's initial reference configuration was established as the length in the cycling and perpendicular directions when a nominal load of 80 mN was reached in each direction. A load of 80 mN was the minimum force required to remove visible slack from the tissue. Prior to testing, the sample was pre-conditioned by performing the described protocol to ε_C of 2% while holding ε_P at 0% then 3%. The sample reference configuration was re-determined after pre-conditioning. All tests were performed at a strain rate of 0.15%/s and recorded at 12.5 Hz. Data were expressed as engineering stress and strain, which were calculated using the sample cross-sectional area and $L_{0,C}$, respectively.

The stress-strain curves for each sample were used to calculate initial stress, maximum stress, initial stiffness, transition strain, stiffness, strain energy density, and hysteresis using custom Matlab code (MathWorks, Natick, MA). These parameters were calculated and averaged over cycles 2-5 at a strain of 6%. A strain of 6% was chosen for data analysis because it included both the nonlinear and linear portions of the stress-strain curve and damage often occurred at the greater cycling strain of 8%.

Table 1.1. Testing protocols consisted of a preconditioning sequence followed by cyclic strain testing sequences, in which perpendicular strain (ε_P) was initially set and held constant at 0% then 3% while cycling strain (ε_C) was cycled to each level.

	Preload (N)	**Testing sequence**	**Perpendicular strain (ε_P)**	**Cycling strain (ε_C)**
Initial reference configuration set	0.08			
		Preconditioning sequence	0%	2%
			3%	2%
Reference configuration reset	0.08			
		Testing sequence 1	0%	2%
			3%	2%
		Testing sequence 2	0%	4%
			3%	4%
		Testing sequence 3	0%	6%
			3%	6%
		Testing sequence 4	0%	8%
			3%	8%

Initial stress was determined as the stress in the cycling direction at a strain of 0% after the perpendicular strain was set at 0% or 3%. We expect initial stress to be greater than zero because the reference configuration was set at a preload of 80 mN. Maximum stress was determined as the stress at 6% strain. Initial stiffness was calculated by determining the derivative of a linear polynomial fit to the stress-strain data between a cycling strain of 0% and 1.25%. To find the transition point where the stress-strain curve became linear, a linear polynomial equation was incrementally fit to the stress-strain curve for successive overlapping increments of 1.25% cycling strain using a least-squares curve fit. Increments of stress-strain data starting at every data point and spanning the stress-strain data from the strain of that initial data point to a strain greater by 1.25% were determined. A linear polynomial equation was fit to the stress-strain data in each increment using a least squares fit and the R^2 and slope of the linear fit were recorded. From the recorded R^2 and slope values, the transition point was determined to occur in the increment that had an R^2 greater than 0.997 and a slope greater than 70% of the maximum slope calculated over all increments for that stress-strain curve. The initial strain value of that increment was determined to be the transition strain. The slope of the linear fit of the stress-strain data in that increment was determined to be the sample's stiffness. Figure 1.4 includes a representative stress-strain curve during loading and unloading of the FL and shows transition strain, initial stress, maximum stress, and the derivatives of linear polynomials fit to the loading data used to calculate stiffness and initial stiffness for those data. Strain energy density was calculated as the integral of the loading stress-strain curve from 0% to 6% strain. Hysteresis was calculated as the percent difference in loading and unloading work, which were

calculated as the integrals of the loading and unloading stress-strain curves, respectively.

Fascia structure

After removing samples for testing, four 1 cm x 1 cm samples were cut from the remaining fascia. For each of the two imaging techniques (histology and SEM), one sample was cut normal to the longitudinal fibers while a second sample was cut normal to the transverse fibers. All samples were obtained from the mid-region of each fascia lata, pinned to polystyrene, and covered with fine plastic mesh to keep the sample flat during fixation.

Samples used for SEM were fixed in 4% paraformaldehyde overnight, washed with 1x PBS, and serially dehydrated to 100% ethanol. Samples were critical point dried (Tousimis Autosamdri-815, Rockville, MD), mounted on an aluminum stub, and sputter coated with platinum-palladium (Cressington 208HR, Watford, UK). Imaging was performed using a field emission scanning electron microscope (Zeiss Supra55VP, Jena, Germany) at an accelerating voltage of 3.0 kV. The diameter of collagen fibrils was measured using ImageJ (NIH, Bethesda, MD).

Samples used for histological sectioning and staining were fixed in neutral-buffered formalin overnight, washed with 1x PBS, dehydrated, cleared with xylene, and infiltrated with Paraplast (Structure Probe Inc., West Chester, PA). Samples were oriented perpendicular to the face of the embedding block and embedded in Paraplast. All paraffin-embedding procedures were performed using a Tissue-Tek VIP tissue processor (MilesCo Scientific, Princeton, MN). From the paraffin-embedded samples, 6-8 μm sections were obtained and stained using Mallory's trichrome. Samples were

imaged with a Leica DMR microscope (Solms, Germany) equipped with a QImaging Retiga 2000r camera (Surrey, Canada). The thickness of the collagen layer(s) normal to the section plane was measured using ImageJ and averaged across sections.

Statistics

A multivariate linear mixed model fit by maximum likelihood was used to examine the effect of perpendicular strain on tissue properties including initial stress, initial stiffness, transition strain, stiffness, strain energy, and dissipation and to compare properties between the longitudinal and transverse tissue samples. This model accounts for repeated measures made on non-independent parameters and was implemented using R statistical software (R Core Team, 2012). Prior to fitting the model, parameters were transformed to a common log scale and then transformed to z-scores.

In the model, fixed effects included fascia orientation, perpendicular strain, and the parameters calculated from the stress-strain curve, and the random effects included random intercepts for cycle number nested within subject. The model included a first order autoregressive moving average correlation structure for the residuals to account for the correlation between the parameters and cycle number. Log-transformed residuals were examined to validate the model's assumption of normality and planned pair-wise comparisons were made using the model's contrast matrix with a sequential Bonferroni correction to generate adjusted p-values based on the number of comparisons (Holm, 1979). Structural measures were compared between orientations using a paired samples t-test. All results were considered significant at a level of $p < 0.05$ and are reported as mean ± standard error of sample mean (s.e.m.).

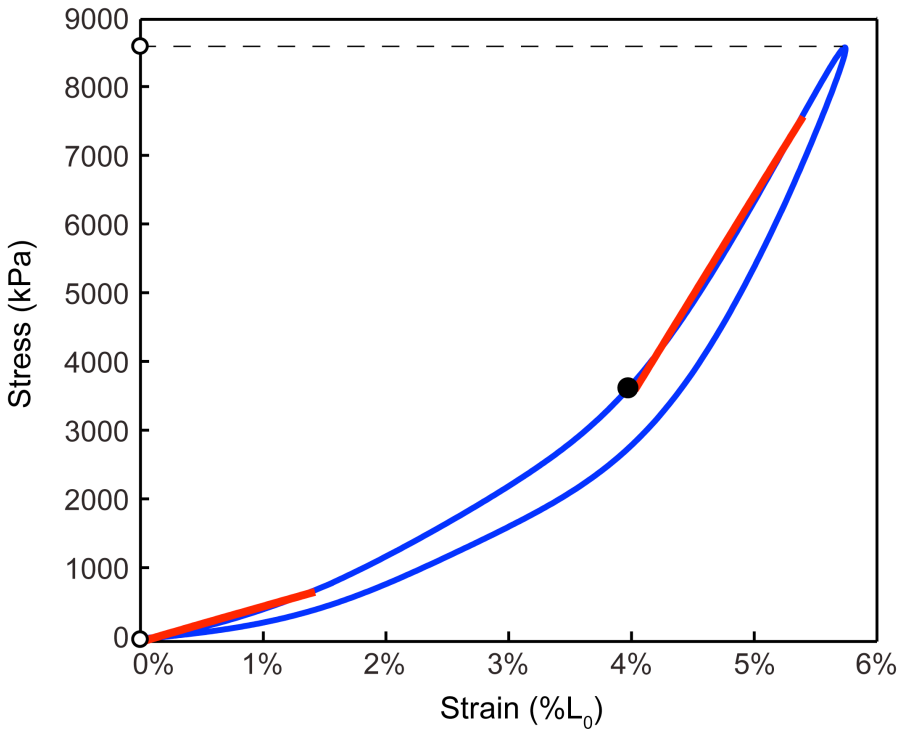

Figure 1.4. A representative loading and unloading curve showing the derivatives of linear polynomials fit to the loading data that were used to calculate stiffness and initial stiffness. The filled circle on the curve indicates transition strain, while the open circles on the y-axis indicate initial and maximum stress.

Results

Representative stress-strain curves for longitudinally and transversely oriented samples in Figure 1.5 show behavior characteristic of collagenous tissues with toe, heel, and linear regions of increasing stiffness. The tissue also demonstrated moderate hysteresis in both orientations. Lower stress in the tissue for a given strain in the transverse orientation compared to the longitudinal orientation indicates greater compliance in the transverse versus longitudinal orientation. Substantial decreases in stress with subsequent cycles at 8% strain in the longitudinal orientation likely indicate more extensive tissue damage at this strain level (Figure 1.5A).

The effect of sample orientation (longitudinal versus transverse) had a greater influence on material behavior than perpendicular strain (0% versus 3%), as demonstrated by the multivariate linear mixed model illustrated in Figure 1.6. The two-way interaction between orientation and perpendicular strain was not significant and a multivariate model that included this interaction term was not a significantly better fit than a simpler, more parsimonious model that excluded it. Therefore, the latter model was chosen to analyze these data. The non-significant interaction between orientation and perpendicular strain indicates that the effect of perpendicular strain does not depend on whether the sample was longitudinal or transversely oriented. Note that while we present means for comparison across orientation and perpendicular strain, the statistical model compared orientation and perpendicular strain within individual animals and lumped these comparisons across animals.

Effect of sample orientation on material behavior

Between longitudinal and transverse orientations there was a significant difference in most variables describing the shape of the stress-strain curve except transition strain (Table 1.2). Initial stiffness was significantly greater in the longitudinal versus transverse orientation (45.8 ± 14.8 MPa vs. 12.1 ± 3.5 MPa; $p<0.001$). Initial stress and maximum stress were also significantly greater in the longitudinal versus transverse orientation (Initial stress: 307.7 ± 206.5 kPa vs. 75.6 ± 61.6 kPa; $p<0.05$ and maximum stress: 9357.1 ± 1106.3 kPa vs. 1947.5 ± 254.0 kPa; $p<0.001$). The transition strain was 3.3 ± 0.3% in the longitudinal orientation and 3.1± 0.3% in the transverse orientation and was not significantly different between orientations. Stiffness was significantly greater in the longitudinal versus transverse orientation (263.5 ± 16.3 MPa vs. 52.2 ± 4.7 MPa; $p<0.001$). Across individuals, longitudinally oriented samples had on average a 4.4 times greater stiffness than transverse samples. Strain energy density was also significantly greater in the longitudinal than transverse orientation (197.2 ± 38.2 mJ/m^3 vs. 39.7 ± 9.1 mJ/m^3; $p<0.001$). Hysteresis was also significantly greater in the longitudinal than transverse orientation (14.8 ± 1.6% vs. 10.1 ± 1.3%; $p<0.001$).

Effect of perpendicular strain on material behavior

Although tissue orientation had a large effect on FL material behavior, an increase in perpendicular strain did not significantly alter the stress-strain curve in either longitudinal or transverse orientations (Figure 1.7; Table 1.3). The parameters describing the shape of the stress-strain curve including initial stiffness, transition strain, and stiffness did not significantly change when perpendicular strain was increased from 0% to 3% ($p>0.05$). Perpendicular strain also did not have a significant effect on hysteresis or strain energy density. While initial stress significantly increased as

perpendicular strain increased from 0% to 3% in the longitudinal (104.5 ± 118.1 kPa vs. 511.0 ± 396.5 kPa; $p<0.001$) and transverse orientations (11.2 ± 7.2 kPa vs. 140.0 ± 122.3 kPa; $p<0.001$), maximum stress did not significantly change ($p>0.05$).

Fascia structure

The average total thickness of fascia lata samples was 0.32 ± 0.02 mm. As figure 1.8 illustrates, histology revealed that there was only one layer of longitudinal collagen fibers, while many fascia samples had two layers of transverse collagen fibers. The thickness of the longitudinal layer of collagen fibers was significantly greater than the transverse layer(s) (218.0 ± 22.7 vs. 94.7 ± 6.5 μm; $p<0.05$). Across samples, the average ratio of longitudinal to transverse layer thickness was 2.4 ± 0.3 (Figure 1.8; Table 1.4). The collagen fibrils in the longitudinal layer were significantly larger compared to those in the transverse layer(s) (Figure 1.8; Table 1.4). The average diameter of the longitudinal fibrils was 127.0 ± 9.2 nm, while the average diameter of the transverse fibrils was 94.9 ± 8.9 nm ($p<0.05$).

Table 1.2. Goat fascia lata biaxial material properties of longitudinally (long.) and transversely (trans.) oriented samples.

Sample orientation	Stiffness (MPa)	Hysteresis (%)	Strain energy (mJ/m^3)	Transition strain (%)	Initial stiffness (MPa)	Initial stress (kPa)	Maximum stress (kPa)
Long.	263.5 ± 16.3	14.8 ±1.6	197.2 ± 38.2	3.3 ± 0.3	45.8 ± 14.8	307.7 ± 206.5	9357.1 ± 1106.3
Trans.	52.2 ± 4.7	10.1 ± 1.3	39.7 ± 9.1	3.1 ± 0.3	12.1 ± 3.5	75.6 ± 61.6	1947.5 ± 254.0
P-value	*<0.001*	*<0.001*	*<0.001*	1.00	*<0.001*	*0.034*	*<0.001*

Data are expressed as mean ± s.e.m.
Significant pair-wise comparisons are italicized ($p < 0.05$).
For each orientation, properties calculated for perpendicular strains of 0% and 3% are averaged.

Table 1.3. Goat fascia lata biaxial material properties at 0% versus 3% perpendicular strain for longitudinally (long.) and transversely (trans.) oriented samples.

Perpendicular strain		Stiffness (MPa)	Hysteresis (%)	Strain energy (mJ/m^3)	Transition strain (%)	Initial stiffness (MPa)	Initial Stress (kPa)	Maximum stress (kPa)
Long.	0%	261.6 ± 28.9	15.2 ± 3.0	178.4 ± 49.7	3.4 ± 0.5	39.7 ± 15.7	104.5 ± 118.1	9215.7 ± 1835.3
	3%	265.4 ± 18.8	14.4 ± 1.3	216.0 ± 62.7	3.2 ± 0.5	51.9 ± 26.9	511.0 ± 396.5	9498.5 ± 1459.2
Trans.	0%	49.5 ± 6.9	10.5 ± 1.7	30.1 ± 9.8	3.0 ± 0.4	10.0 ± 4.2	11.2 ± 7.2	1661.0 ± 318.5
	3%	54.9 ± 6.9	9.7 ± 2.2	49.3 ± 15.3	3.3 ± 0.4	14.3 ± 5.8	140.0 ± 122.3	2234.1 ± 384.4
P-value		1.00	1.00	0.858	1.00	1.00	*<0.001*	0.86

Data are expressed as mean ± s.e.m.
Significant pair-wise comparisons are italicized ($p < 0.05$).

Table 1.4. Structural properties of longitudinal and transverse collagen layers of goat fascia lata.

	Collagen layer thickness (μm)	Collagen fibril diameter (nm)
Longitudinal	218.0 ± 22.7	127.0 ± 9.2
Transverse	94.7 ± 6.5	94.9 ± 8.9
p-value	*0.007*	*0.038*

Data are expressed as mean ± s.e.m.
Significant pair-wise comparisons are italicized ($p < 0.05$).

Table 1.5. Material properties of goat fascia lata compared to other connective tissues.

Tissue	Orientation	Stiffness (MPa)	Hysteresis (%)
Goat fascia lata	Longitudinal	263.5 ± 16.3	14.8 ±1.6
	Transverse	52.2 ± 4.7	10.1 ± 1.3
Dog fascia lata[1]	Longitudinal	390	11 ± 2
Human fascia lata[2]		397.5 ± 17.1	
Turkey aponeurosis[3]	Longitudinal	744.4 ± 51.6	11.1 ± 0.7
	Transverse	115.7 ± 16.1	15.7 ± 0.9
Tendon	--	305.5-612.8[2]	
		800-2000[4]	6-10
		1270-1590[5]	

Data are expressed as mean ± s.e.m.
[1]Bennett et al. (1989)
[2]Butler et al. (1984)
[3]Azizi et al. (2009)
[4]Pollock and Shadwick (1994)
[5]Bennett et al. (1986)

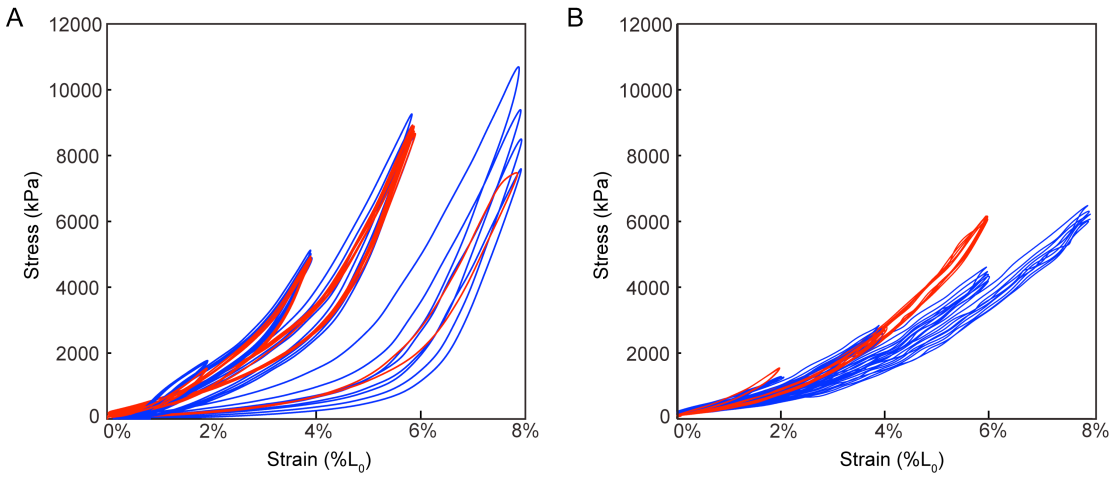

Figure 1.5. Representative data from longitudinally (A) and transversely (B) oriented fascia lata samples. Data shown are from cycles 2-5 at each strain level (2%, 4%, 6%, and 8%) for a perpendicular strain of 0% (blue) and 3% (red). The transverse sample failed at a perpendicular strain of 3% and cycling strain of 8% so no data are shown. The longitudinal sample failed after a single cycle at a perpendicular strain of 3% and cycling strain of 8%.

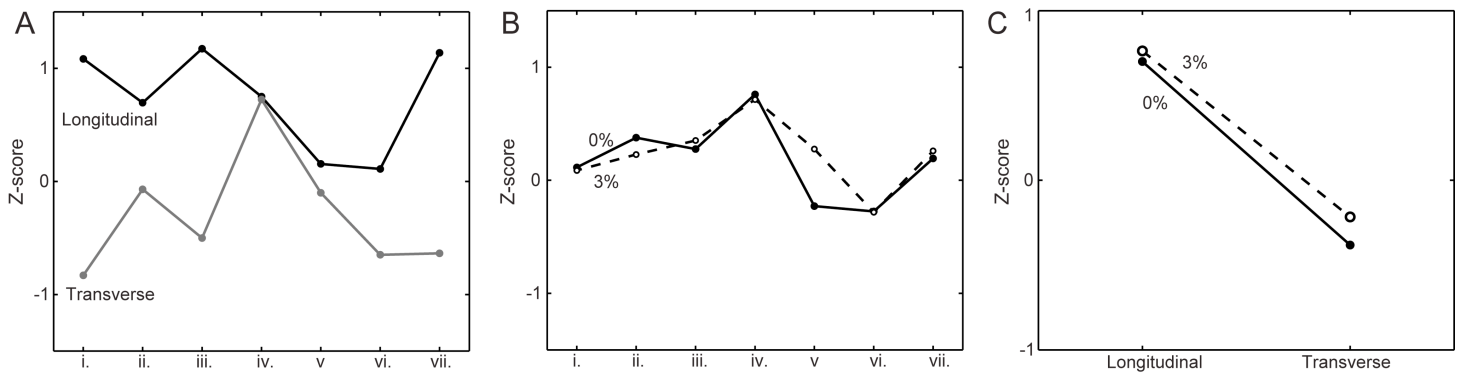

Figure 1.6. Plots of z-scores for sample orientation (A) and perpendicular strain (B) demonstrate that there is an effect of orientation but not perpendicular strain for most material property measures including stiffness (i), dissipation (ii), strain energy density (iii), initial stiffness (v), initial stress (vi), and maximum stress (vii). Transition strain (iv) does not vary between longitudinal and transverse samples (A). A plot showing the interaction between orientation and perpendicular strain (C) demonstrates that the effect of perpendicular strain is the same for longitudinal and transverse samples (i.e., there is no interaction between sample orientation and perpendicular strain).

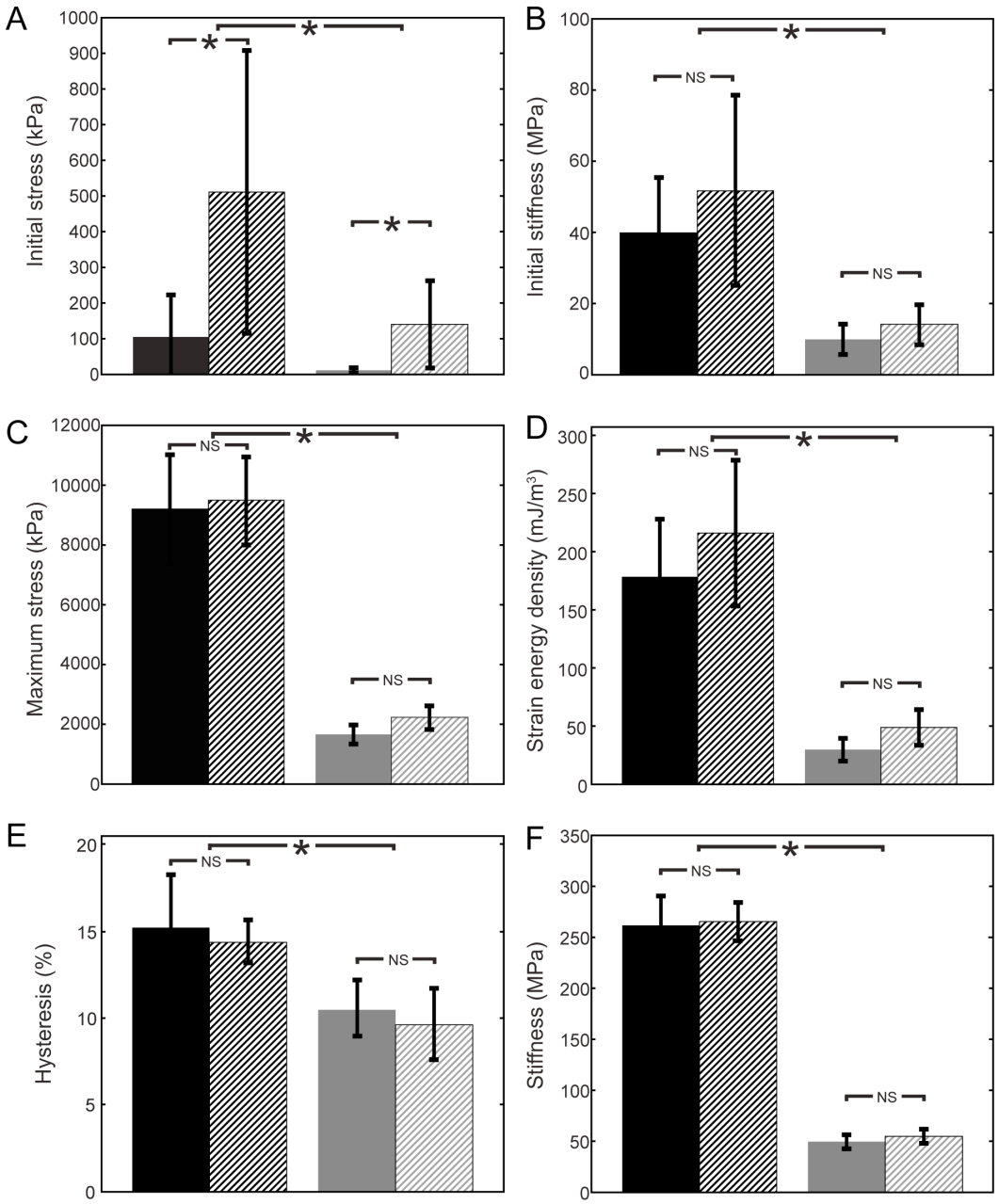

Figure 1.7. Initial stress was greater in longitudinal (black) than transverse (gray) samples and increased from 0% (solid) to 3% (crosshatch) perpendicular strain (A). Initial stiffness (B), maximum stress (C), strain energy density (D), hysteresis (E), and stiffness were greater in longitudinal versus transverse samples but did not change with perpendicular strain (see text for details). The asterisks denote a significant difference ($p < 0.05$) while non-significant differences are indicated as “NS.”

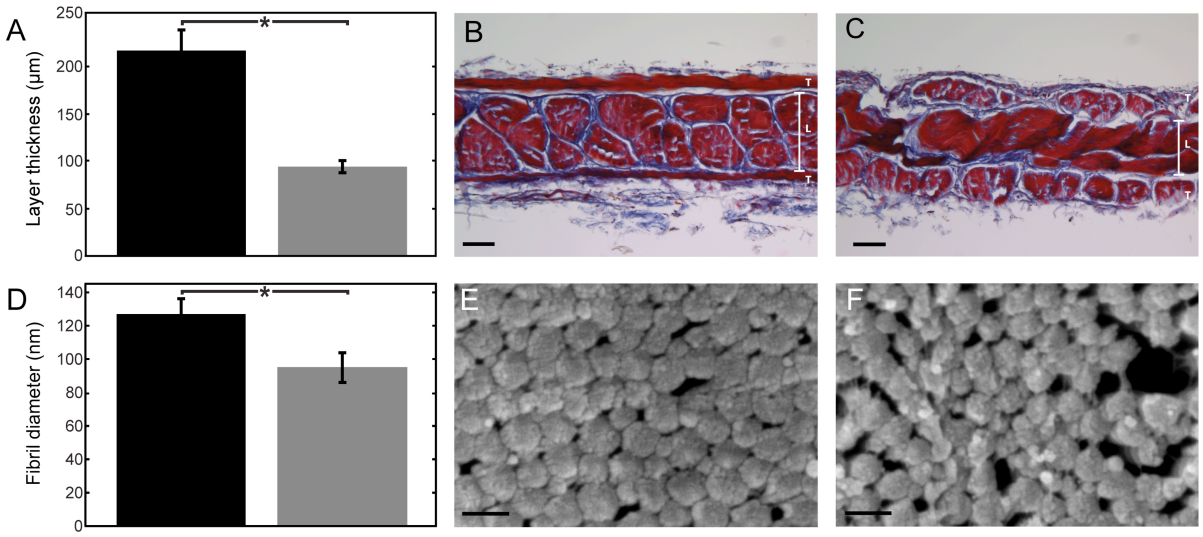

Figure 1.8. The longitudinal layer of collagen fibers is on average, 2.4 times thicker than the transverse layer(s) of fibers (A). Histological sections of the fascia lata sectioned normal to the longitudinal (B) and transverse (C) planes show that collagen layer thickness is greater in the longitudinal (L) than transverse (T) orientation. Many samples, including the ones shown, had two layers of transverse collagen fibers. The diameter of the longitudinal collagen fibrils is on average, 39% larger than the transverse fibrils (D). Scanning electron microscopy images demonstrate that the diameter of collagen fibrils is larger in the longitudinal (E) than transverse (F) layer. Scale bar is 80 μm in (B) and (C) and 200 nm in (E) and (F). The asterisks in (A) and (D) demonstrate a significant difference between orientations ($p < 0.05$).

Discussion

Effect of perpendicular strain and sample orientation on material behavior

We found that an increase in perpendicular strain from 0% to 3% did not greatly alter the biaxial material behavior of FL. Contrary to Hypothesis 2, stiffness did not increase with increased perpendicular strain, and strain energy density also did not increase with perpendicular strain as hypothesized (H4). We hypothesized that increased perpendicular strain would preload the tissue and decrease transition strain in the cycling direction (H3), yet transition strain did not change with perpendicular strain. However preloading from perpendicular strain did cause a significant increase in initial stress. Because deformation of biological tissues is isovolumetric (Qiu and Pence, 1997), when the FL was strained perpendicularly prior to cycling, the tissue in the cycling direction must contract. Since our protocol maintained the tissue in the cycling direction at a constant strain as initial deformation occurred in the perpendicular direction, initial stress must increase. Interestingly, although this was the case (Table 1.3), maximum stress did not significantly increase, indicating that perpendicular strain does not merely cause the stress-strain curve to shift upwards leading to higher stresses at all strain values.

While there was little effect of perpendicular strain on tissue properties, a large influence of tissue orientation on biaxial material behavior was observed. Compared to the transversely oriented tissue, the tissue samples cut and cycled in the longitudinal direction had significantly greater initial stress, initial stiffness, maximum stress, hysteresis, and strain energy density (Figure 1.7). Transition strain did not differ

between orientations. As hypothesized, stiffness was significantly greater in the longitudinal direction (H1).

Structural differences and their influence on material behavior

Differences in material behavior between the longitudinal and transverse orientations can largely be explained by differences in tissue structure as hypothesized (H5). The more than two-fold greater thickness in the longitudinal layer compared to the transverse layer(s) likely played a role in the longitudinal samples' greater stiffness. Histological sections revealed that two transverse layers often flanked a single longitudinal layer. Cross-links within and between collagen molecules are important for determining the stiffness of collagen (Davison, 1989; Puxkandl et al., 2002). The discontinuity between transverse layers and subsequent increase in surface area to volume ratio in the transverse layer(s) likely decreases the number of cross-links forming in the transverse layer, which may contribute to the decreased transverse stiffness we observed.

Because the discrepancy in longitudinal versus transverse layer thickness is only detectable using microscopy, the sample cross-sectional areas used to estimate tissue stress did not take this difference into account. Therefore the longitudinal and transverse layers of fascia lata are not mechanically equivalent and our stress calculations likely overestimate the actual load-bearing component of the tissue, especially in the transverse orientation. Nevertheless, although we may underestimate the intrinsic strength of the collagen in the transverse layer(s), our calculations capture the functionally relevant characteristics of the fascia's biaxial response as it would respond *in vivo*. Under a given muscle load transmitted to the FL, the FL will undergo

larger strains in its transverse versus longitudinal orientation because of structural differences including greater thickness in FL's longitudinal orientation. Pancheri et al. (2014) present a material model of the FL that accounts for its multilayered structure.

Differences in material behavior with respect to fascia orientation are also likely due to differences in collagen fibril size. Electron microscopy results showed that the collagen fibrils in the longitudinal layer have a larger average diameter than the fibrils in the transverse layer(s). Previous research has shown that collagen fibril size correlates with increased tensile strength and stiffness in connective tissues (Parry, 1988; Robinson et al., 2004). Together, these structural differences between the longitudinal and transverse orientations explain the tissue's greater stiffness, initial and maximum stress, and strain energy density in the longitudinal versus transverse orientation.

Finally, collagen fiber alignment is another factor that potentially contributes to the greater initial stiffness in longitudinal versus transverse fascial orientations. More highly aligned fibers in the longitudinal orientation could explain the increased initial stiffness in the longitudinally oriented samples. Tissues with more aligned collagen fibrils are stiffer, and imaging of tissue during mechanical testing shows that fibers re-orient in the direction of loading under tension (Tower et al., 2002; Sellaro et al., 2007; Lake et al., 2009; Szczesny et al., 2012). Fiber re-alignment in the transverse orientation may also lead to increased hysteresis. Hysteresis would also be expected to be greater in the transverse orientation due to smaller fibril size with higher surface area-to-volume ratio, increasing shear stresses that result from interactions between the fibrils and the matrix components (Parry, 1988; Puxkandl et al., 2002). However, greater hysteresis was observed in the longitudinal direction. A possible explanation for this

result is that hysteresis was compared for cycles 2-5, but re-alignment may have occurred in the first cycle. Consistent with this, when cycling to 6% strain, hysteresis was 131% higher in the first cycle relative to subsequent cycles in the transversely oriented samples, while hysteresis is only 30% higher in the first cycle for samples cycled in the longitudinal direction. The greater energy loss in the first cycle relative to subsequent cycles in the transverse samples indicates that the FL's transverse layer(s) have lower collagen fiber alignment causing substantial realignment during testing.

Comparisons with other studies

Contrary to previous findings that an increase in perpendicular strain causes an increase in stiffness in other connective tissues including aponeurosis (Azizi and Roberts, 2009) and shark skin (Wainwright et al., 1978), our results demonstrate that the stiffness of goat FL does not change with increased perpendicular strain. One reason for the discrepancy in our results may be that higher perpendicular strains of up to 10% were reached in the aponeurosis, while we imposed a maximum perpendicular strain of 3%. Additionally, Wainwright and co-authors may have imposed higher perpendicular strains on the shark skin than the 3% strain used here but their study only reports perpendicular stresses.

The material properties of fascia described here are relatively consistent with results from other studies describing material properties of connective tissues including fascia, tendon, and aponeurosis (Table 1.5). Our measure of longitudinal stiffness (263.5 ± 16.3 MPa) is lower than measures of fascia lata stiffness from dogs (390 MPa) (Bennett, 1989) and humans (397.5 ± 17.1 MPa) (Butler et al., 1984). One reason for the difference compared with dog fascia is that Bennett et al. (1989) described peak

stiffness whereas the stiffness reported here is was based on the initial linear portion of the stress-strain curve and peak stiffness values can be higher. Additionally, Bennett et al. measured strain using grip-to-grip separation, while in our study and in Butler et al. (1984), true strain was measured by tracking fiducial markers in the sample gage region. The lower stiffness values in our study may also be due to interspecific differences in tissue properties.

Our stiffness values for the longitudinal and transverse FL are also lower than measures of longitudinal and transverse stiffness in turkey aponeurosis (Azizi et al., 2009). The lower transverse FL stiffness compared to aponeurosis is particularly puzzling because our FL tests were performed in alignment with a layer of collagen fibers in the transversely oriented FL and these collagen fibers are absent from aponeurosis. While our results show that the goat FL is less stiff than tendon, which has stiffness values ranging from 300-2000 MPa (Butler et al., 1984; Bennett et al., 1986; Pollock and Shadwick, 1994), hysteresis in FL and tendon is similar, suggesting that fascia has similar resiliency compared to tendon (Table 1.5).

Fascia function

The biaxial properties of FL measured here have implications for inferring its *in vivo* function. In order to play an appreciable role in elastic energy storage, force transmission, or limb stability, the fascia must be relatively stiff when loaded by muscle or stretched by joint motion. Because the GB and TFL muscle fibers insert orthogonally in the FL, nearly orthogonal collagen fiber families allow the FL to transmit loads from both muscles. The increased tissue stiffness achieved by reinforcement with the transverse fibers may play another role in fascia function. Studies exploring the role of

fascia in mediating muscle force output show that fascia may play a role in maintaining intramuscular pressure (Mozan and Keagy, 1969; Garfin et al., 1981). However, fascia often covers or envelops muscles, and thus must be sufficiently compliant to allow underlying muscles to expand during contraction. By expanding circumferentially, muscles will stretch the fascia transversely. The relatively low transverse stiffness observed here would allow this expansion. The transverse layer of FL fibers may provide adequate tissue stiffness to transmit muscle forces and maintain intramuscular pressure, while their relative compliance would facilitate expansion of underlying muscles during contractions.

To sum up, the data presented here provide an important first step in understanding the function of the myriad planar collagenous tissues found throughout the body. Unexpectedly, our results indicate that fascia material behavior is not strongly influenced by its biaxial strain environment, suggesting that muscle-connective tissue complexes can be accurately modeled as a collection of independent, proximal-to-distal units in which muscles generate forces in series with connective tissue. Furthermore, our results provide fascia-specific bidirectional material properties, which may allow the connective tissue material properties assumed in musculoskeletal models to be further refined. Three-dimensional finite element muscle models are important for understanding fascia's function at the muscle level (Blemker et al., 2005; Teran et al., 2005; Chi et al., 2010; Rehorn and Blemker, 2010), but few 3D muscle models incorporate multiple limb segments and thus are less informative for exploring fascia's role in locomotion. Multi-segment models are necessary for understanding fascia's role in intersegmental force transmission and elastic energy storage during walking and

running. In this context, further refining musculoskeletal models such as Arnold et al. (2010) will likely be important for understanding the function of fascial tissues such as the human iliotibial band, which is difficult to measure and not well understood. Combining our biaxial results with a musculoskeletal model of the human lower extremity may provide new insights into how the iliotibial band stabilizes limb segments, stores elastic energy from inserting muscles, or transmits muscle force between limb segments.

Potential limitations

While our results have implications for the function of fascia, they also have some limitations. Materials testing was performed at a low strain rate of 0.15%/s, likely much lower than *in vivo* loading rates. Previous studies, however, have shown that strain rate has little effect on the stiffness of other connective tissues (Ker, 1981; Dorfmann et al., 2008). Nonetheless, future experiments incorporating higher strain rates may capture FL's *in vivo* material behavior more accurately. Although thickness measurements were not validated using the volumetric approach, measures made with a thickness gauge are repeatable and accurate (O'Leary et al., 2013) and thus are unlikely to be a large source of error in our stress calculations. The maximum perpendicular strain of 3% used here may be too low to see a significant effect on FL material behavior. However, when we used higher perpendicular strains, the FL samples failed before reaching cycling strains of 6%. Additionally, the testing protocol used here was performed with a non-randomized order of strains increasing from cyclic strains of 2% to 8%, with perpendicular strains of 0% and subsequently 3% strain in order to avoid causing tissue damage. Even so, we did observe evidence of damage in

the tissue at or above 3% perpendicular strain. Longitudinal and transverse tests both exhibited evidence of stress softening at increasing strains (Figure 1.5), indicating disruption of matrix components leading to a loss of stiffness and increased extensibility (Dorfmann et al., 2007; Peña, 2011). Although tissue samples were loaded in primary alignment with collagen fiber directions, substantial *in situ* curvature of fibers exists in the fascia lata. This fiber curvature was more apparent in the transverse orientation and may be partially responsible for the differences in stiffness observed between the transverse and longitudinal sample orientations if the collagen fibers in the transverse orientation did not always extend from grip to grip. Finally, because the longitudinal and transverse collagen layers in the fascia lata are not orthogonal or mechanically equivalent, the deformations are not purely homogeneous and an in-plane shear stress would be needed to achieve pure homogeneous deformation. Pancheri et al. (2014) developed a material model of goat fascia lata and used a series of images captured during testing to show that in-plane shear deformation is small and thus their assumption of pure homogenous strain may be justified.

To summarize, a strain controlled planar biaxial protocol was applied to goat FL samples. These results demonstrate that although the collagen layers in the goat FL are not entirely independent, they do not appear to strongly influence one another's material behavior when loaded in opposing directions during biaxial testing. Directional differences in tissue properties are likely due to structural differences between transverse versus longitudinal layer(s) of the FL including layer thickness and collagen fibril size. The differing material behavior observed between the longitudinal and transverse orientations suggest that differential loading in these directions during growth

and development may lead to these structural changes, enhancing the ability of the longitudinal FL to transmit force, store energy, and/or stabilize the goat limb. These data are important for generating more accurate musculoskeletal models of fascia function.

Acknowledgements

The authors gratefully acknowledge Richard Blood at Blood Farm for help in procuring goat hindlimbs. We are grateful to Steven Worthington and Simo Goshev of the research consulting team at Harvard's Institute for Quantitative Social Sciences for their assistance with statistical analysis. We thank Zachary Lewis and James Weaver for their help with tissue imaging techniques. The comments of three anonymous reviewers significantly improved this manuscript. This work was performed in part at the Harvard University Center for Nanoscale Systems, which is supported by the National Science Foundation under award no. ECS-0335765.

Abbreviations

FL	Fascia lata
SEM	Scanning electron microscopy
GB	Gluteobiceps
TFL	Tensor fascia lata
$L_{0,C}$	Initial length in the cycling direction
$L_{0,P}$	Initial length in the perpendicular direction
ε_P	Perpendicular strain
ε_C	Cycling strain
PBS	Phosphate-buffered saline

References

Arnold, E. M., Ward, S. R., Lieber, R. L. and Delp, S. L. (2010). A model of the lower limb for analysis of human movement. *Annals of Biomedical Engineering* **38**, 269-279.

Azizi, E., Halenda, G. M. and Roberts, T. J. (2009). Mechanical properties of the gastrocnemius aponeurosis in wild turkeys. *Integrative and Comparative Biology* **49**, 51-58.

Azizi, E. and Roberts, T. J. (2009). Biaxial strain and variable stiffness in aponeuroses. *The Journal of physiology* **587**, 4309-4318.

Barker, P. J., Briggs, C. A. and Bogeski, G. (2004). Tensile transmission across the lumbar fasciae in unembalmed cadavers: effects of tension to various muscular attachments. *Spine* **29**, 129-138.

Benjamin, M. (2009). The fascia of the limbs and back--a review. *Journal of Anatomy* **214**, 1-18.

Bennett, M. B. (1989). A possible energy-saving role for the major fascia of the thigh in running quadrupedal mammals. *Journal of Zoology* **219**, 221-230.

Bennett, M. B., Ker, R. F., Dimery, N. J. and Alexander, R. M. (1986). Mechanical properties of various mammalian tendons. *Journal of Zoology* **209**, 537-548.

Blemker, S. S., Pinsky, P. M. and Delp, S. L. (2005). A 3D model of muscle reveals the causes of nonuniform strains in the biceps brachii. *Journal of Biomechanics* **38**, 657-665.

Butler, D. L., Grood, E. S., Noyes, F. R., Zernicke, R. F. and Brackett, K. (1984). Effects of structure and strain measurement technique on the material properties of young human tendons and fascia. *Journal of Biomechanics* **17**, 579-596.

Chi, S.-W., Hodgson, J., Chen, J.-S., Reggie Edgerton, V., Shin, D. D., Roiz, R. A. and Sinha, S. (2010). Finite element modeling reveals complex strain mechanics in the aponeuroses of contracting skeletal muscle. *Journal of Biomechanics* **43**, 1243-1250.

Davison, P. F. (1989). The contribution of labile crosslinks to the tensile behavior of tendons. *Connective Tissue Research* **18**, 293-305.

Dorfmann, A. L., Trimmer, B. A. and Woods, W. A. (2007). A constitutive model for muscle properties in a soft bodied arthropod. *Journal of the Royal Society Interface* **4**, 257-269.

Dorfmann, A. L., Trimmer, B. A. and Woods, W. A. (2008). Muscle performance in a soft-bodied terrestrial crawler: Constitutive modeling of strain-rate dependency. *Journal of the Royal Society Interface* **5**, 349-362.

Dubiel, W. T. and Wigren, A. (1974). Functional Status of the Lower Extremity After Resection of Fascia Lata: A Clinical and Physiological Follow-up Study in Patients with Fascia Lata Heart Valve Replacement. *Acta Orthopaedica* **45**, 599-613.

Eng, C. M., Lieberman, D. E. and Biewener, A. A. (2012). In vivo strain patterns indicate different functions in the proximal and distal fascia lata of the goat. In *Society for Integrative and Comparative Biology Annual Meeting*. Charleston, S.C.

Garfin, S. R., Tipton, C. M., Mubarak, S. J., Woo, S. L., Hargens, A. R. and Akeson, W. H. (1981). Role of fascia in maintenance of muscle tension and pressure. *Journal of Applied Physiology* **51**, 317-320.

Holm, S. (1979). A simple sequentially rejective multiple test procedure. *Scandinavian Journal of Statistics* **6**, 65-70.

Huijing, P. A. and Baan, G. C. (2001). Myofascial force transmission causes interaction between adjacent muscles and connective tissue: effects of blunt dissection and compartmental fasciotomy on length force characteristics of rat extensor digitorum longus muscle. *Archives of Physiology and Biochemistry* **109**, 97-109.

Huijing, P. A., Maas, H. and Baan, G. C. (2003). Compartmental fasciotomy and isolating a muscle from neighboring muscles interfere with myofascial force transmission within the rat anterior crural compartment. *Journal of Morphology* **256**, 306-321.

Ker, R. F. (1981). Dynamic tensile properties of the plantaris tendon of sheep (Ovis aries). *Journal of Experimental Biology* **93**, 283-302.

Lake, S. P., Miller, K. S., Elliott, D. M. and Soslowsky, L. J. (2009). Effect of fiber distribution and realignment on the nonlinear and inhomogeneous mechanical properties of human supraspinatus tendon under longitudinal tensile loading. *Journal of Orthopaedic Research* **27**, 1596-1602.

Lanir, Y. and Fung, Y. (1974). Two-dimensional mechanical properties of rabbit skin—II. Experimental results. *Journal of Biomechanics* **7**, 171-182.

Mozan, L. C. and Keagy, R. D. (1969). Muscle relationships in functional fascia: a preliminary study. *Clinical Orthopaedics and Related Research* **67**, 225-230.

Neptune, R. R., Kautz, S. and Zajac, F. (2001). Contributions of the individual ankle plantar flexors to support, forward progression and swing initiation during walking. *Journal of Biomechanics* **34**, 1387-1398.

O'Leary, S. A., Doyle, B. J. and McGloughlin, T. M. (2013). Comparison of methods used to measure the thickness of soft tissues and their influence on the evaluation of tensile stress. *Journal of Biomechanics* **46**, 1955-1960.

Pancheri, F. Q. and Dorfmann, A. L. (2013). Strain controlled biaxial tension of natural rubber: New experimental data. *Rubber Chemistry and Technology*, **In press**.

Pancheri, F. Q., Eng, C. M., Lieberman, D. E., Biewener, A. A. and Dorfmann, L. (2014). A constitutive description of the anisotropic response of the fascia lata. *Journal of the Mechanical Behavior of Biomedical Materials* **30**, 306-323.

Parry, D. A. D. (1988). The molecular and fibrillar structure of collagen and its relationship to the mechanical properties of connective tissue. *Biophysical Chemistry* **29**, 195-209.

Peña, E. (2011). Prediction of the softening and damage effects with permanent set in fibrous biological materials. *Journal of the Mechanics and Physics of Solids* **59**, 1808-1822.

Pollock, C. M. and Shadwick, R. E. (1994). Allometry of muscle, tendon, and elastic energy storage capacity in mammals. *American Journal of Physiology* **266**, R1022-1031.

Puxkandl, R., Zizak, I., Paris, O., Keckes, J., Tesch, W., Bernstorff, S., Purslow, P. and Fratzl, P. (2002). Viscoelastic properties of collagen: synchrotron radiation investigations and structural model. *Philosophical Transactions of the Royal Society of London. Series B: Biological Sciences* **357**, 191-197.

Qiu, G. and Pence, T. (1997). Remarks on the behavior of simple directionally reinforced incompressible nonlinearly elastic solids. *Journal of Elasticity* **49**, 1-30.

R Core Team. (2012). R: A language and environment for statistical computing. Vienna, Austria: R Foundation for Statistical Computing.

Rehorn, M. R. and Blemker, S. S. (2010). The effects of aponeurosis geometry on strain injury susceptibility explored with a 3D muscle model. *Journal of Biomechanics* **43**, 2574-2581.

Robinson, P. S., Lin, T. W., Jawad, A. F., Iozzo, R. V. and Soslowsky, L. J. (2004). Investigating tendon fascicle structure–function relationships in a transgenic-age mouse model using multiple regression models. *Annals of Biomedical Engineering* **32**, 924-931.

Sellaro, T. L., Hildebrand, D., Lu, Q., Vyavahare, N., Scott, M. and Sacks, M. S. (2007). Effects of collagen fiber orientation on the response of biologically derived

soft tissue biomaterials to cyclic loading. *Journal of Biomedical Materials Research Part A* **80**, 194-205.

Stahl, V. A. (2010). A biomechanical analysis of the the role of the crural fascia in the cat hindlimb. In *Biomedical Engineering*, vol. Doctor of Philosophy: Georgia Institute of Technology and Emory University.

Stecco, C., Macchi, V., Porzionato, A., Duparc, F. and De Caro, R. (2011). The fascia: the forgotten structure. *Italian Journal of Anatomy and Embryology* **116**, 127-138.

Szczesny, S. E., Peloquin, J. M., Cortes, D. H., Kadlowec, J. A., Soslowsky, L. J. and Elliott, D. M. (2012). Biaxial tensile testing and constitutive modeling of human supraspinatus tendon. *Journal of Biomedical Engineering* **134**, 021004.1-021004.9.

Teran, J., Sifakis, E., Blemker, S. S., Ng-Thow-Hing, V., Lau, C. and Fedkiw, R. (2005). Creating and simulating skeletal muscle from the visible human data set. *Visualization and Computer Graphics, IEEE Transactions on* **11**, 317-328.

Tower, T. T., Neidert, M. R. and Tranquillo, R. T. (2002). Fiber alignment imaging during mechanical testing of soft tissues. *Annals of Biomedical Engineering* **30**, 1221-1233.

Vande Geest, J. P., Sacks, M. S. and Vorp, D. A. (2006). The effects of aneurysm on the biaxial mechanical behavior of human abdominal aorta. *Journal of Biomechanics* **39**, 1324-1334.

Wainwright, S. A., Vosburgh, F. and Hebrank, J. H. (1978). Shark skin: function in locomotion. *Science* **202**, 747-749.

Chapter 2: The potential for elastic energy storage in the goat fascia lata during walking and trotting on different grades

Abstract

This study estimated the amount of elastic energy stored in the goat fascia lata (FL) during walking and trotting from direct *in vivo* measures of strain in the FL and inserting muscles. Additionally, we examined whether FL energy storage varied when goats walked or trotted on the incline, decline, and level to investigate whether elastic energy recovered from the FL contributes to the increased work required to swing the limb faster during incline locomotion. To estimate biaxial strains, sonomicrometry crystals were implanted in the proximal and distal FL and were aligned with longitudinal and transverse collagen fiber directions. We also examined, via sonomicrometry and electromyography (EMG), how the tensor fascia lata muscle (TFL) contracts to transmit force via the proximal FL and how the gluteobiceps (GB) contracts to transmit force via the distal FL. Our results show that both the proximal and distal FL stretch in the longitudinal direction during stance phase, storing energy that can be recovered in swing phase. The distal FL stretches as GB actively shortens, indicating that the distal FL is stretched by active GB contraction. The proximal FL is stretched as the hip extends in late stance, and it is further stretched when the TFL muscle is active in early swing. During walking, increased lengthening and shortening strain in the distal FL on the incline compared to the level suggests that energy recovered from the distal FL may

contribute to the increased mechanical work required to swing the limb faster during incline walking.

Introduction

Fascia is ubiquitous in the limbs of vertebrates, and intimate connections with muscles suggest that fascia plays an important role in muscle-tendon mechanics. However, its function is not well understood. Many hypothesized functions for fascia have been proposed, but few have been directly tested in animals. Fascia serves as the insertion site for many muscles, and thus it may broaden the insertion of muscles or re-direct the forces generated by muscles (Wood Jones, 1944; Mozan and Keagy, 1969; Garfin et al., 1981; Kalin and Hirsch, 1987; Huijing and Baan, 2001; Huijing et al., 2003; Smeulders et al., 2006). Fascia also envelops muscles and may increase intramuscular pressure to facilitate muscle force output (Mozan and Keagy, 1969; Garfin et al., 1981; Aspden, 1990). Finally, fascia is continuous among limb segments indicating that it may transfer loads and coordinate movements among limb segments and body regions (Wood Jones, 1944; Dubiel and Wigren, 1974; Vleeming et al., 1995; Barker et al., 2004; Myers, 2008; Benjamin, 2009; Stahl, 2010). For example, increased variability in the hip ab/adduction angles of cats who have had a fasciotomy suggests that fascia helps to stabilize the lower limb during locomotion (Stahl, 2010). An additional hypothesis, tested here in goats, is that fascia stretches during locomotion to store elastic energy, and this energy helps propel the limb forward during swing phase.

Storing and recovering energy from elastic structures such as fascia may decrease the cost of locomotion. An important determinant of locomotor cost is the

mechanical work done to move the body relative to the environment (increasing the *body's* kinetic and potential energy, KE and PE) plus the additional work done to move the limbs relative to the body (increasing *limb* KE and PE, or internal energy) (Cavagna et al., 1964). Additional energy is dissipated when active muscles stretch to decelerate the limbs. While previous studies have shown that the body's KE and PE are absorbed and released from the Achilles tendon during stance phase of running (Ker et al., 1987; Biewener and Roberts, 2000), elastic energy storage and recovery of the limb's KE and PE is not well studied (Wilson et al., 2003). During the swing phase of a stride, muscle-tendon forces act to decelerate the limb (thereby decreasing the limb's KE) and to re-accelerate the limb (thereby increasing the limb's KE). To decelerate the limb and decrease the limb's KE, energy can either be dissipated or stored in stretched elastic tissues. To re-accelerate the limb and increase the limb's KE, forces are required. The required forces can either come from active muscles or from elastic tissues that have previously been stretched. Using cadaveric dog hindlimbs, Bennett (1989) estimated the joint positions at which the dog fascia lata (FL) is stretched. By combining these data along with FL material properties and the measured kinematics and muscle activity patterns of dogs during galloping, Bennett estimated that the dog FL could store and recover 17-25% of the limb's maximum kinetic energy during the swing phase of a galloping stride. This potential savings in energy via the mammalian FL is substantial, but such estimates have never been validated in vivo.

Therefore, the goals of this study were to directly measure strains in the goat fascia lata, gluteobiceps, and TFL muscles during locomotion and to estimate energy storage *in vivo*. Additionally, we examined whether energy storage in the FL is

modulated to meet the varying mechanical demands of trotting uphill. The FL is found on the lateral aspect of the thigh of mammals. In goats, the gluteobiceps (GB) and tensor fascia lata (TFL) muscles insert into the FL (Figure 2.1A). These muscles are agonist knee extensors and antagonists at the hip joint (GB extends and TFL flexes the hip). When animals run at steady speeds on the level, net mechanical work on the COM is zero. When animals run on an incline, muscles must do additional work to increase the body's PE with each stride. Conversely, when animals run on a decline, muscles must absorb energy to accommodate a decrease in the body's PE with each stride. Limb KE also increases on an incline compared to level locomotion. On an incline, goats increase stride frequency and duty factor (McGuigan et al., 2009), both of which would cause the limb to oscillate faster during swing phase on the incline compared to the level. During human running, increases in stride frequency with speed and incline were found to mirror increases in internal work (Minetti et al., 1994). Furthermore, using blood flow measurements to estimate muscle metabolic activity, Rubenson et al. (2006) showed that swing phase muscles of guinea fowl contributed 30% of the increase in energy use with speed and 11% of the increase in energy use during incline versus level locomotion. Thus, increased work is required to move both the body and the limbs in incline versus level locomotion.

While previous studies in other animals have shown that distal muscles increase net shortening strain when running on an incline (Roberts et al., 1997; Daley and Biewener, 2003; Gabaldón et al., 2004), McGuigan and colleagues (2009) found that goat distal hindlimb muscles contribute only 3% of the total work required to locomote uphill and thus, a large contribution must come from the proximal hindlimb muscles.

Arnold et al. (2013) suggest that goat proximal hip extensors including the GB muscle generate greater forces and perform substantially more work during uphill versus level locomotion. Because of its insertion in the fascia lata, GB work may contribute to both the work required to move the body and the limbs. We, therefore, ask whether increased force in GB increases the elastic energy storage in the FL and whether the increased work requirements to move the body and limbs during incline locomotion can be met in part by storing and recovering energy in the FL? The observation that tendon elastic energy recovery increases on an incline compared to level, as well as being greater on the level versus decline, in goat distal limb muscle-tendon units (McGuigan et al., 2009), suggests that more proximal connective tissues, such as the FL, may also contribute to energy savings.

We use sonomicrometry and electromyography (EMG) to measure patterns of strain and activation in gluteobiceps (GB) and tensor fascia lata (TFL) in relation to strain patterns in the goat fascia lata. By measuring muscle and FL mechanical function at different grades, we investigated whether fascia lata energy storage and recovery is capable of contributing to the increased work required during incline locomotion. These data are used to test the following hypotheses: that the goat FL stretches to store energy during the second half of stance and shortens and recovers energy in initial swing (H1); that GB and TFL muscles contract isometrically during stance while the FL stretches, indicating that active muscle contraction stretches the FL (H2); and that muscle shortening and FL energy storage and recovery both increase on an incline compared to level (H3) to raise the body's COM and swing the limbs faster.

Materials and methods

Five adult African pygmy goats (*Capra hircus* L.; 2 male and 3 female, mass: 26.5 ± 3.3 kg*)* were obtained from the breeding colony at Harvard University's Concord Field Station. All animals were housed in outdoor enclosures and fed available foliage supplemented with goat pellets. Goats were trained to walk and trot on the level, incline and decline for two weeks prior to each experiment. All training and experiments were performed on a large motorized treadmill (belt length x width: 2.50 m x 0.75 m), which was elevated and supported with struts at an angle of 15° during the incline and decline trials. The goat's direction of travel was reversed for decline locomotion. All procedures for working with goats were approved by Harvard's IACUC.

Surgical procedures

Goats were sedated with ketamine and xylazine (8 and 0.5 mg per mg/kg body mass) administered via the jugular (IV). After sedation, the goats were intubated and maintained at an appropriate level anesthesia on 0.5-1.0% vaporized isoflurane. The instrumented limb was shaved and prepped for surgery. Three incisions were made on the lateral thigh over the proximal and distal fascia lata. Prior to surgery, electromyography and sonomicrometry lead wires were soldered to female connectors and chemically sterilized. Lead wires were passed subcutaneously through an additional small incision over the ilium to each of the three incision sites.

Following Biewener et al. (1998), 2.0 mm sonomicrometry crystals (Sonometrics, London, Canada) were implanted in the distal gluteobiceps (GB) and tensor fascia lata (TFL) muscles near their insertion in the fascia lata (FL; Figure 2.1). Crystal pairs were placed in small incisions made approximately 15 mm apart and oriented along the

muscle fiber direction. Crystals were aligned until their signals were optimized using an oscilloscope, and then muscle incisions were closed using 4-0 silk suture. Fine-wire electromyography (EMG) electrodes were implanted in the TFL and GB muscles to measure muscle activity (Loeb and Gans, 1986). Offset twist-hook bipolar silver fine-wire electrodes (0.1 mm, California Fine Wire Inc., Grover Beach, CA) with tips bared of insulation (0.5 mm bared with 2 mm between electrodes) were inserted in the distal belly of each muscle adjacent to the sonomicrometry crystals using a 21-gauge hypodermic needle and then anchored to the muscle surface using 4-0 silk suture.

One or two additional sonomicrometry crystal pairs were implanted in both the proximal and distal FL near where the muscle fibers implanted with sonomicrometry crystals inserted into the fascia to measure uniaxial or biaxial FL strains (Figure 2.1A). At each site in the FL, one pair of crystals was oriented with the FL's longitudinal collagen fibers and the second pair of crystals was aligned with FL's transverse collagen fibers. To anchor each crystal to the FL and to minimize its rotation during the experiment, a 5 mm piece of plastic tubing was threaded on to the lead wire and adhered to the base of the crystal using waterproof epoxy (Figure 2.1C inset). A 3 mm incision was made in the fascia with 4-0 silk suture threaded through the incision. The crystal was placed in the opening and the 4-0 suture secured at the junction between the crystal and plastic tubing to the fascia. The crystal was also sutured to the fascia at the base of the plastic tubing to anchor it into place. The width of the FL was recorded for later cross-sectional area calculations. Incisions were closed using 3-0 vicryl, which was also used to attach the connector to the skin over the ilium. An intramuscular

injection of flunixin meglumine (1 mg/kg body mass) was administered post-operatively and every 12 hours thereafter for a 48 hr period.

Data collection

In vivo measures were made 24 hours after surgery. The data collected for each goat are described in table 2.1. White, non-toxic paint was used to mark the centers of rotation of the hip, knee, ankle, and metatarsophalangeal joints and the hooves of both limbs to facilitate kinematic measurements. The instrumented limb was videotaped during the level and incline trials, and the contralateral limb was videotaped during the decline trials. A shielded cable was connected to the recording amplifiers. EMG signals were amplified (x1000) and filtered (60 Hz notch and 100-3000 Hz bandpass) using a Grass P511 amplifier (Grass Technologies, Warwick, RI). Sonomicrometry signals were processed using a Triton Technology Inc., unit (San Diego, CA). All data were digitized at 2.5 kHz using a 16-channel A/D data acquisition system (Biopac Systems Inc., Goleta, CA).

Recordings were made while the goats walked at 1.1 m/s and trotted at 2.1 (n=3) or 2.6 m/s (n=2) on the incline, level and decline treadmill. Two trials each consisting of 6-8 strides of steady locomotion were recorded for each goat for each gait and grade. A lateral view of the goat was recorded with high-speed video (Photron USA Inc., San Diego, CA) at 125 Hz and synchronized with EMG and sonomicrometry recordings using a voltage trigger pulse. Videos were calibrated using a length scale on the treadmill. On the day following data collection, all EMG wires and sonomicrometry crystals were removed under anesthesia as per the initial surgery and the goat was allowed to recover.

Data analysis

For each goat, stance and stride times were determined from high-speed video recordings. Two-dimensional coordinates of limb markers were digitized using DLTdv5 custom MATLAB software (The MathWorks, Natick, MA, USA) (Hedrick, 2008) and used to calculate hip and knee angles during stance and swing. EMG and sonomicrometry data were analyzed relative to stance and swing times for 3-4 strides per gait and grade. Stride frequency was calculated as the inverse of stride time in seconds. Duty factor was calculated as the proportion of the stride in which the instrumented limb was in contact with the treadmill.

EMG data were analyzed to obtain onset time, offset time, and signal intensity of TFL and GB activity. EMG intensity was computed as the average spike amplitude of the rectified signal over the activation period and normalized to the maximum average amplitude recorded for that electrode.

Prior to muscle and fascia strain analysis, the sonomicrometry signals were corrected for a 5 ms delay introduced by the Triton sonomicrometry amplifier filter, and adjusted by 2.7% to account for the speed of sound in muscle. A 0.82 mm length correction was added to account for the faster speed of sound through the epoxy lens of the 2.0 mm crystal. Fascia lata and muscle fiber strains were calculated as the length change relative to the initial length (L_0), which was measured as the average length over several strides during an initial walking trial. Total lengthening, shortening and net (lengthening-shortening) strains were calculated over the entire stride for GB and TFL. Fascia lengthening strains were calculated during stance phase and shortening strains

were calculated during swing phase in the longitudinal and transverse, distal and proximal FL.

Strain values were used, together with FL stiffness values of 263.5 MPa (longitudinal) and 52.2 (transverse) (Chapter 1) to estimate FL stress during walking and trotting. Stress values were used, together with our estimate of the FL cross-sectional area, to calculate FL force. Cross-sectional area was estimated as FL width measured in surgery multiplied by the average FL thickness of 0.32 mm reported in Chapter 1 and was used to calculate force (F_{FL}) from stress values.

Energy stored in the FL (E_{FL}) was calculated when the FL stretched (positive strain), and energy recovered was calculated when the FL shortened (negative strains):

$$E_{FL} = \tfrac{1}{2} F_{FL} \Delta L_{FL} \quad (1)$$

where ΔL_{FL} is fascia length change relative to L_0.

Lower limb internal energy (E_{int}), which includes translational and rotational components of kinetic energy as well as potential energy, was calculated as the sum of the energies of the four limb segments (thigh, shank, tarsus, and hoof) as:

$$E_{\text{int}} = \sum_{s=1}^{4} \tfrac{1}{2} m_s v_s^2 + \tfrac{1}{2} \mathrm{I}_s \omega_s^2 + m_s g h_s \quad (2)$$

where m_s is limb segment mass, v_s is limb segment linear velocity relative to the body's center of mass, I_s is limb segment mass moment of inertia, ω_s is limb segment rotational velocity, g is acceleration due to gravity (9.8 m/s^2), and h_s is the height of the segment above the treadmill (Fedak et al., 1982). Velocity terms were calculated from digitized coordinates of joint markers. Goat hindlimb segment masses and mass moments of inertia were measured on a representative individual and scaled to each individual using body mass (A Arnold-Rife, unpublished data). E_{int} was calculated at each time point and

total internal work (W_{int}) was calculated as the cumulative change in E_{int} during the swing phase.

Statistical analysis

Data from 3-4 strides in each gait and grade for each goat were averaged and then these individual goat means were averaged across goats to obtain a mean ± s.e.m. A two-way, mixed model ANOVA was used to examine the effect of grade (incline, decline, level) and gait (walk and trot) on the dependent variables. The model's fixed effects included grade and gait while random effects included stride number nested within the goat individual. Pair-wise comparisons were made with a paired t-test using a *post hoc* sequential Bonferroni correction. Significance was set at $p < 0.05$.

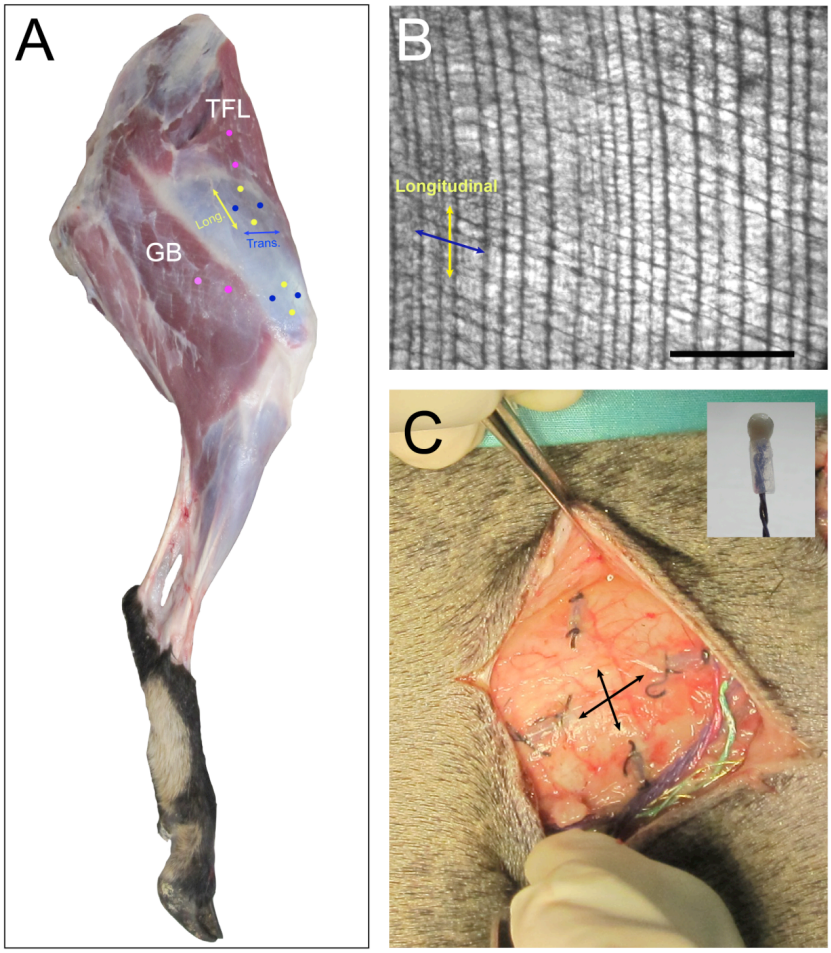

Figure 2.1. A: Sonomicrometry crystals were implanted in the tensor fascia lata (TFL) and gluteobiceps (GB) muscles. Two sonomicrometry crystal pairs were implanted in the proximal and distal FL near where the muscle fibers implanted with sonomicrometry crystals inserted into the fascia. At each site in the FL, one crystal pair was aligned with the primary, longitudinal orientation of the collagen fibers in the FL and the other pair was aligned with the second set of transverse collagen fibers. B: The longitudinal collagen fibers are approximately parallel to the long axis of the femur and the transverse fibers are approximately 70° from the longitudinal fibers. The sample in (B) was dehydrated in methanol, cleared in Benzyl Alcohol: Benzyl Benzoate (3:1) and imaged using differential interference contrast microscopy. Scale bar is 0.5 mm. C: Image of two pairs of crystals implanted in the fascia lata in surgery. Inset: plastic tubing was placed around the base of the sonomicrometry crystal to prevent crystal rotation.

Results

Stride parameters

Goats lengthened their stance times and shortened their swing times when walking and trotting on the incline. Duty factor significantly increased from decline to level and again from level to incline in walking (decline: 0.49 ± 0.09 strides/s; level: 0.62 ± 0.01 strides/s; incline: 0.65 ± 0.01; $p < 0.05$); when trotting, duty factor was significantly greater on the decline and incline compared to level (decline: 0.51 ± 0.01 strides/s; level: 0.45 ± 0.02 strides/s; incline: 0.53± 0.01). Stride frequency increased significantly from decline to level and incline for walking (decline: 1.30 ± 0.23 strides/s; level: 1.65 ± 0.08 strides/s; incline: 1.75 ± 0.07; $p < 0.05$) and trotting (decline: 2.15 ± 0.11 strides/s; level: 2.53 ± 0.06 strides/s; incline: 2.54 ± 0.07), but did not differ significantly between level and incline.

Muscle activity and strain

Gluteobiceps muscle strain and EMG activity in a representative individual during level walking demonstrated that GB is active from late swing to mid to late stance phase and is coincident with the period of GB muscle shortening during stance phase (Figure 2.2A). Tensor fascia lata was active from midstance to midswing and began to shorten in early swing, indicating a period of isometric contraction at the end of stance phase before the muscle shortens during swing phase (Figure 2.2B).

As predicted, the magnitude of GB and TFL shortening increased on the incline compared to level and increased on the level compared to decline (Figure 2.3; Table 2.2). GB shortening strains were significantly greater on the incline than on the level, and were greater on the level than on the decline for walking (incline: 44.3% ± 0.06%;

level: 33.0% ± 0.04%; decline: 18.3% ± 0.04%; $p < 0.05$) and trotting (incline: 35.1% ± 0.10%; level: 28.8% ± 0.05%; decline: 25.3% ± 0.01%; $p<0.05$)(Figure 2.3A,C). During walking, TFL shortening strains were significantly greater on the incline compared to level (incline: 36.5% ± 0.04%; level: 28.7% ± 0.02%; decline: 25.0% ± 0.05%; $p<0.05$), with the increase in shortening strain on the level versus decline approaching significance ($p=0.095$)(Figure 2.3B). During trotting, TFL shortening strains were significantly greater on the incline and level compared to decline (incline: 28.7% ± 0.06%; level: 27.9% ± 0.02%; decline: 25.8% ± 0.03%; $p<0.05$), with the increased shortening strain on the incline versus level approaching significance ($p=0.054$)(Figure 2.3D).

The relative EMG intensity of GB and TFL increased on the incline compared to level in walking and trotting (Fig 2.4A,C). When walking and trotting, the duration of GB and TFL EMG activity was significantly greater on the level versus decline ($p<0.05$) but did not vary significantly between the level and incline ($p>0.05$; Figure 2.4B,D).

Fascia lata strain

GB and distal FL strain patterns in the representative individual during level and incline walking demonstrate that the longitudinal distal fascia lata (distal FL_{long}) stretches during stance phase and reaches peak stretch in initial swing when GB is at its shortest length (Figure 2.5A-B,E-F). The increase in GB strains on incline compared to level were matched by increased distal FL_{long} strains (Figure 2.5E-F). In this individual shown in figure 2.5, the distal FL stretched transversely during swing phase and shortened during stance phase (Figure 2.5C,G).

Both the TFL and proximal FL stretched during stance phase and shortened in swing (Figure 2.6). The increased FL strains in level versus incline walking were met by increased strains in both the longitudinal and transverse proximal FL. In this individual, longitudinal and transverse strain patterns were similar in early stance phase, but the longitudinal FL continued to stretch until initial swing (Figure 2.6B,E) while the transverse FL shortened in midstance (Figure 2.6C,F).

When averaged across goats, the distal FL lengthening strains during stance phase of walking are increased on the incline compared to on the level (Figure 2.7; Table 2.3). Distal lengthening strains were significantly greater on the incline than on the level, in both the longitudinal (incline: 20.6% ± 8.7%; level: 6.8% ± 2.0; $p<0.05$) and transverse (incline: 18.6 ± 8.2; level: 6.4 ± 1.3; $p<0.05$) directions. Swing phase shortening strains during walking were also significantly greater on the incline compared to level in both the longitudinal and transverse distal FL (Figure 2.7A-B; Table 2.3).

Differences in distal FL lengthening and shortening strains across grades were less pronounced during trotting compared to walking because of increased strain variability. Longitudinal lengthening and shortening strains in the distal FL were not significantly different among grades in trotting ($p>0.05$; Figure 2.8C).

Proximal FL longitudinal and transverse lengthening strains during stance did not significantly differ with grade (Table 2.3). This is likely due, in part, to the high variability in proximal FL strains among individuals. During walking, longitudinal proximal FL shortening strains were significantly greater on the incline compared to level (incline: 8.9% ± 7.8%; level: 3.1% ± 2.9%; $p<0.05$) but did not significantly differ between level and decline.

GB and TFL muscle strain and proximal and distal longitudinal FL strain patterns demonstrate that muscle strain patterns are more consistent among goats than FL strain (Figure 2.8). Although transverse strain patterns were generally more variable among goats than longitudinal FL strains (data not shown here), when averaged across goats, muscle and fascia strains generally increased on the incline compared to level.

FL elastic energy and hindlimb internal energy

The internal energy of the hindlimb increased on the incline compared to level walking, with the increased work requirement potentially met, in part, by increased energy recovered from FL (Figure 2.9). During walking, peak hindlimb internal energy was significantly greater on the incline compared to level and on the level compared to decline (incline: 3.6 ± 0.6 J; level: 3.0 ± 0.6 J; decline: 2.0 ± 0.3 J; $p<0.05$). During trotting, peak hindlimb energy was significantly increased on the incline and level compared to the decline (incline: 4.2 ± 0.9 J; level: 3.6 ± 0.4 J; decline: 2.4 ± 0.2 J; $p<0.05$), but peak hindlimb internal energy did not differ significantly between level and incline. Peak elastic energy stored in the distal FL during walking was significantly greater on the incline compared to level in the longitudinal distal FL (Figure 2.9; Table 2.3). In walking, peak energy in the transverse distal FL was significantly greater on the incline compared to level and level compared to decline (incline: 2.1 ± 1.0 J; level: 0.7 ± 0.2 J; decline: 0.4 ± 0.3 J; $p<0.05$). Peak elastic energy did not differ significantly among grades during walking and trotting in both longitudinal and transverse directions of the proximal FL.

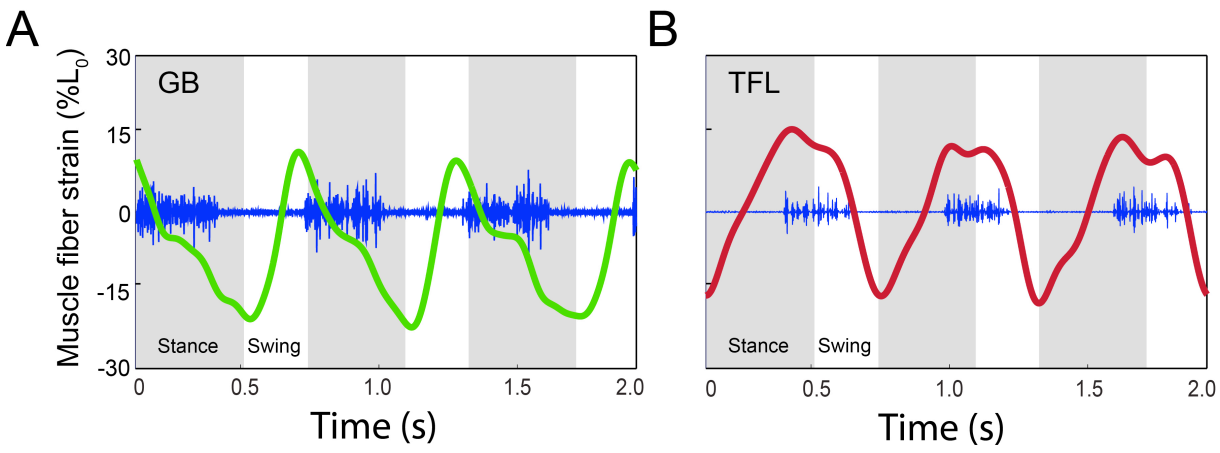

Figure 2.2. A: GB muscle fiber strain and EMG activity from a single individual (goat 5) during level walking. B: TFL muscle fiber strain and EMG activity from the same individual (goat 5) during level walking.

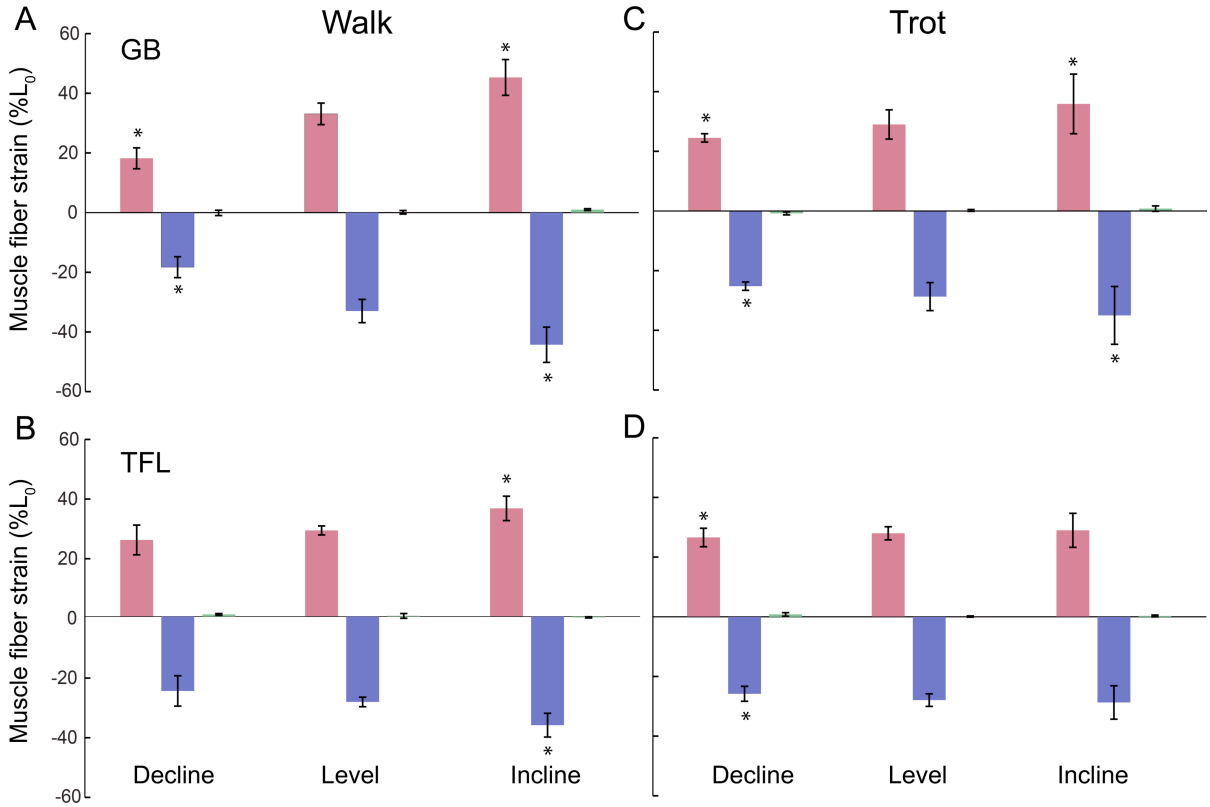

Figure 2.3. A: Lengthening, shortening, and net gluteobiceps (GB) muscle fiber strain for decline, level, and incline walking. B: Tensor fascia lata (TFL) lengthening, shortening, and net strain for decline, level, and incline walking. C: GB strains during decline, level, and incline trotting. D: TFL strains for decline, level, and incline trotting. The asterisk indicates significantly different from level in *post hoc* tests ($p<0.05$).

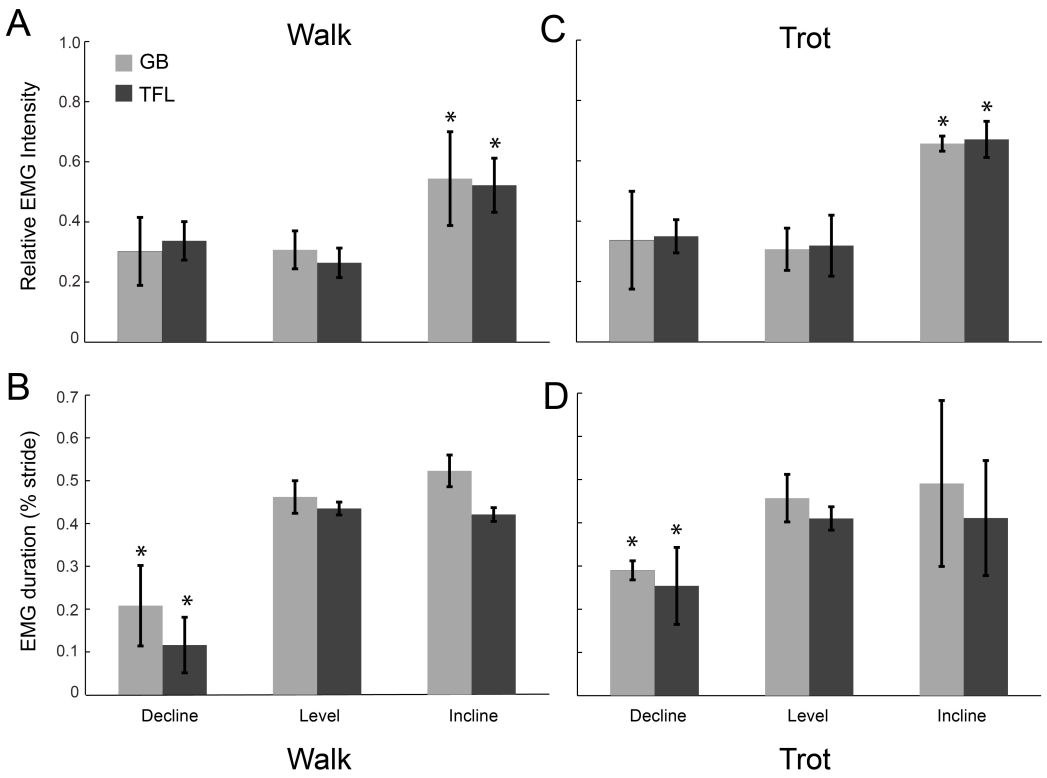

Figure 2.4. A: GB and TFL relative EMG intensity during walking on decline, level, and incline. B: GB and TFL EMG duration (calculated as a % of stride) during decline, level, and incline walking. C: GB and TFL relative EMG intensity during trotting on decline, level, and incline. D: GB and TFL EMG duration (calculated as a % of stride) during decline, level, and incline trotting. The asterisk indicates significantly different from level in *post hoc* tests ($p<0.05$).

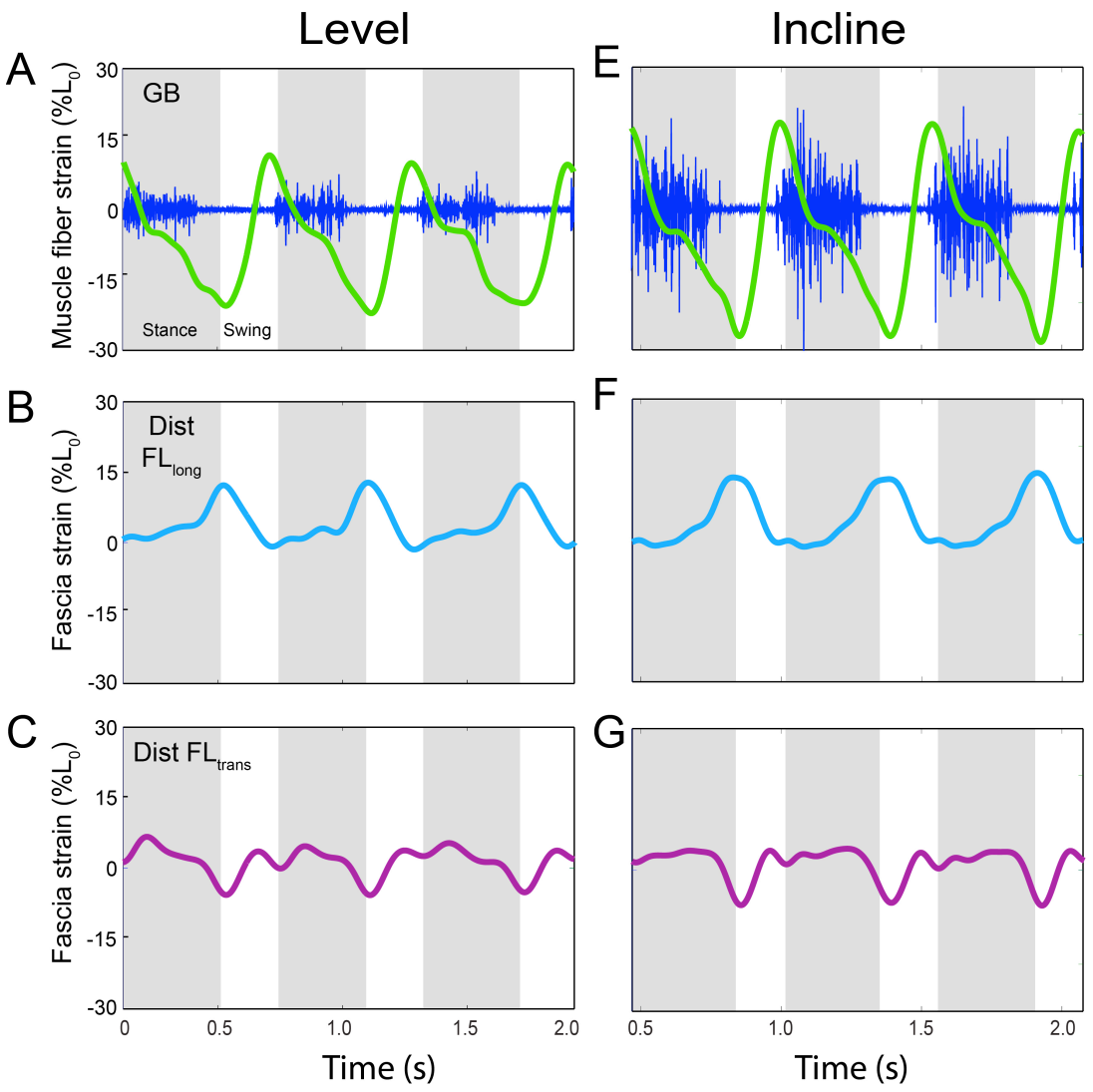

Figure 2.5. A: GB muscle strain and EMG activity from a representative individual (goat 5) during level walking. B: Longitudinal strains in the distal FL (distal FL_{long}) during level walking. C: Transverse strains in the distal FL (distal FL_{trans}) during level walking. E-G: GB muscle activity and strain and distal FL_{trans} and distal FL_{long} strains during incline walking.

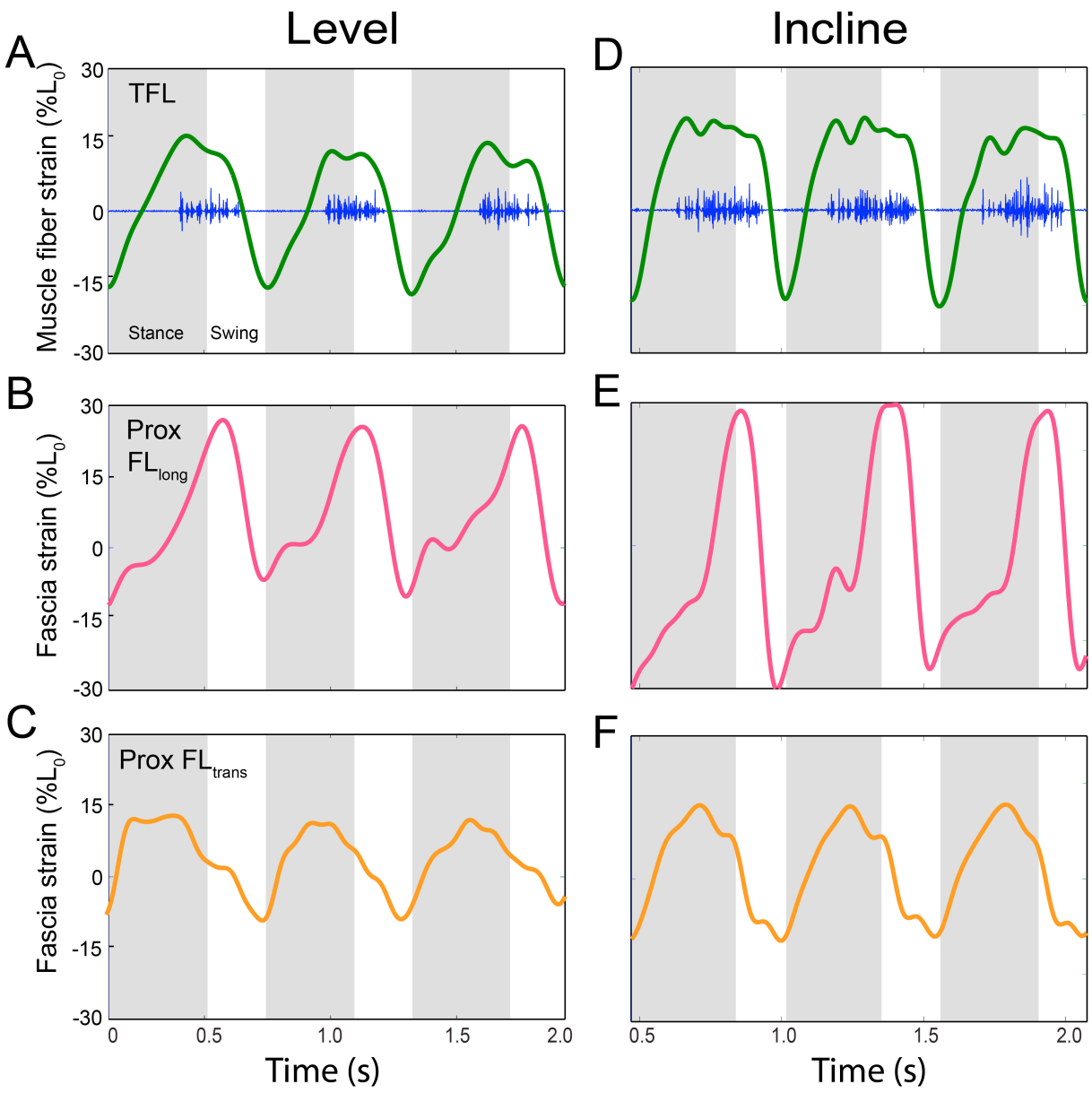

Figure 2.6. A: TFL muscle strain and EMG activity from a representative individual (goat 5) during level walking. B: Longitudinal strains in the proximal FL (proximal FL_{long}) during level walking. C: Transverse strains in the proximal FL (proximal FL_{trans}) during level walking. E-G: TFL muscle activity and strain and distal FL_{trans} and proximal FL_{trans} strains during incline walking.

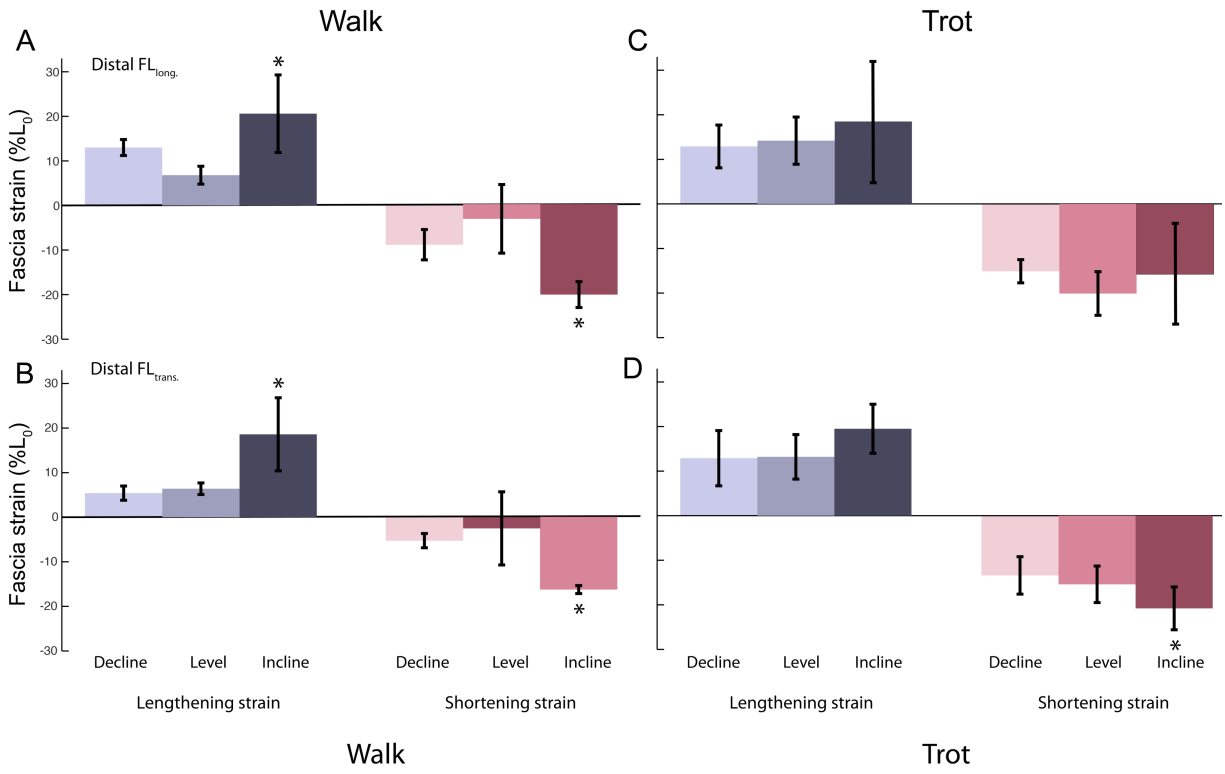

Figure 2.7. A: Distal FL_{long} lengthening strain during stance phase and shortening strain during swing phase in decline, level, and incline walking. B: Distal FL_{trans} lengthening strain during stance phase and shortening strain during swing phase in decline, level, and incline walking. C: Distal FL_{long} lengthening strain during stance phase and shortening strain during swing phase in decline, level, and incline trotting. D: Distal FL_{trans} lengthening strain during stance phase and shortening strain during swing phase in decline, level, and incline trotting. The asterisk indicates significantly different from level in *post hoc* tests ($p<0.05$).

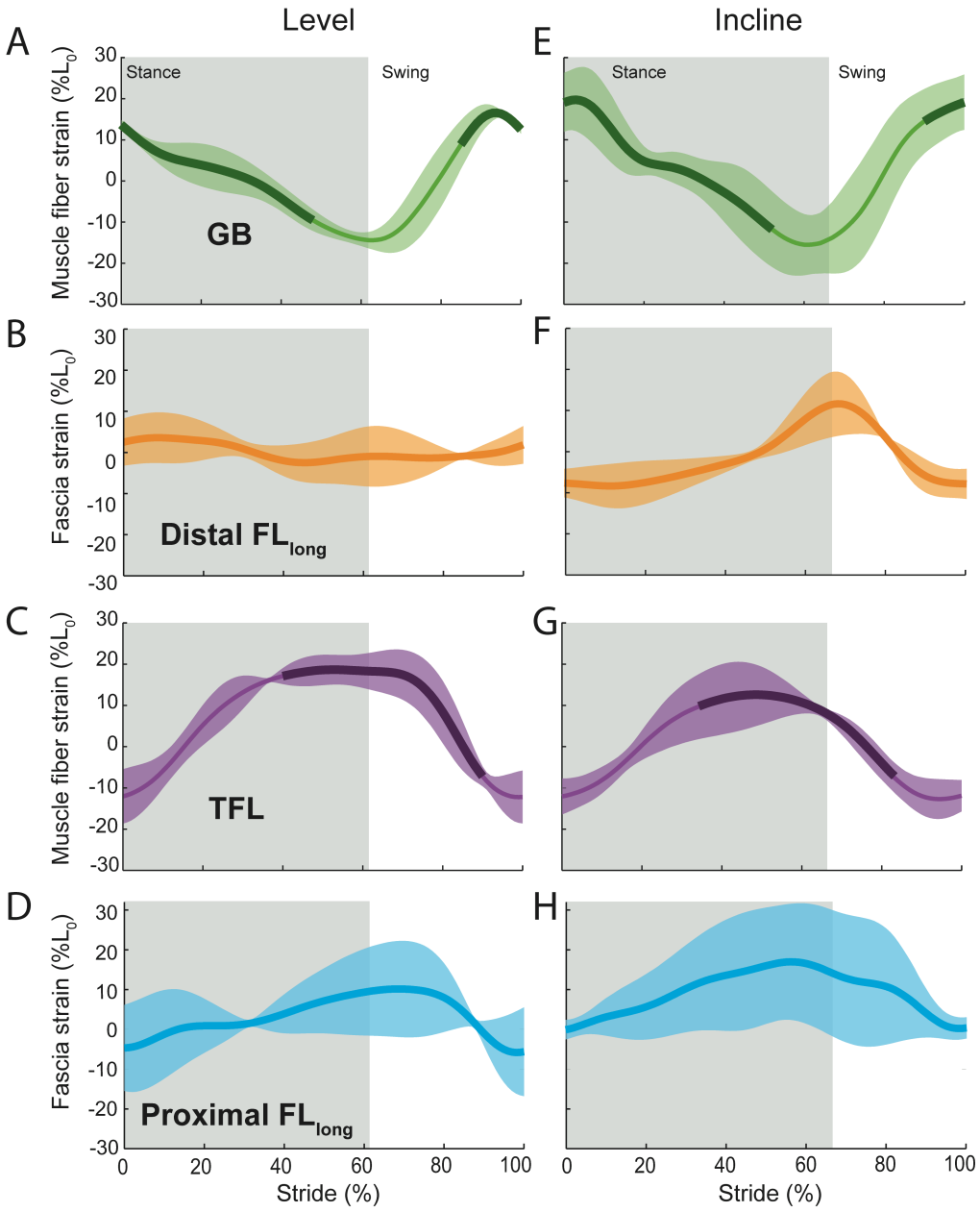

Figure 2.8. A: GB muscle strain averaged across goats for level walking. GB shortens in stance phase, stretching the distal FL. B: Variability among goats leads to low average strains in the distal FL_{long}. C: TFL muscle strain during level walking. TFL may contract isometrically at the end of stance phase. D: Proximal FL_{long} strains coincide with TFL stretch in stance. E: GB muscle strain during incline walking. The magnitude of GB stretch increases on the incline versus level. F: TFL muscle strain during incline walking. G: Proximal FL_{long} stretches during stance phase of incline walking. H: Distal FL_{long} stretches in stance phase during level walking. Typical muscle activity measured in the goats is shown with the thickened portion of the muscle curves.

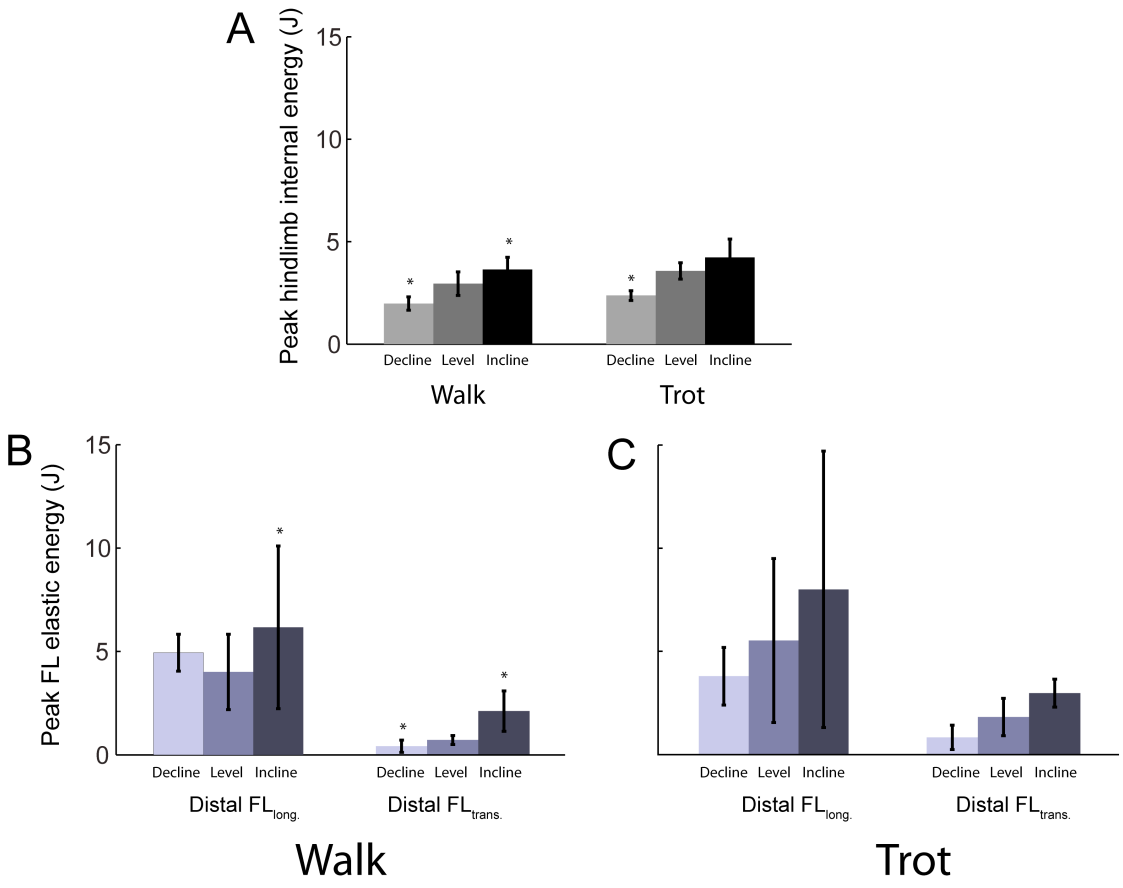

Figure 2.9. A: Peak hindlimb internal energy during swing phase in decline, level, and incline walking and trotting. B: Peak elastic energy stored in the longitudinal and transverse distal FL in swing phase for level, incline, and decline walking. C: Peak distal FL_{long} and distal FL_{trans} elastic energy during decline, level, and incline trotting. The asterisk indicates significantly different from level in *post hoc* tests ($p<0.05$).

Table 2.1. The recordings of gluteobiceps (GB) and tensor fascia lata (TFL) muscle activity, muscle strain, and uniaxial and biaxial strains in the proximal and distal fascia lata (FL) of five goats.

	GB		TFL		FL strain			
					Proximal		Distal	
Individual	**EMG**	**Strain**	**EMG**	**Strain**	**Uniaxial**	**Biaxial**	**Uniaxial**	**Biaxial**
Goat 1	X	X	X	X	O	X	X	O
Goat 2	X	X	X	X	O	X	O	X
Goat 3	X	X	X	X	O	X	X	O
Goat 4	X	X	X	X	X	O	X	O
Goat 5	X	X	X	X	X	O	O	X

Table 2.2. Gluteobiceps (GB) and tensor fascia lata (TFL) lengthening and shortening strains and EMG intensity and duration during decline, level, and incline walking and trotting.

		Walk (1.1 m/s)			**Trot (2.1 or 2.6 m/s)**		
		Decline	**Level**	**Incline**	**Decline**	**Level**	**Incline**
GB	Lengthening strain ($\%L_0$)	18.2 ± 3.5*	33.1 ± 3.6	45.3 ± 6.0*	24.4 ± 1.4	28.9 ± 4.9	35.8 ± 10.0
	Shortening strain ($\%L_0$)	18.3 ± 3.5*	33.0 ± 3.9	44.3 ± 5.9*	25.3 ± 1.4	28.8 ± 4.7	35.1 ± 9.7
	Relative EMG intensity (% max)	0.30 ± 0.11	0.31 ± 0.06	0.54 ± 0.16	0.34 ± 0.16	0.31 ± 0.05	0.65 ± 0.08
	EMG duration (% stride)	20.8 ± 9.4	46.2 ± 3.8	52.3 ± 3.7	29.0 ± 2.2	45.7 ± 5.5	49.1 ± 19.2
	Onset time (% stride)	95.1 ± 1.7	86.1 ± 4.7	95.6 ± 1.0	81.9 ± 11.9	80.0 ± 3.9	88.9 ± 6.1
	Offset time (% stride)	17.9 ± 6.4	54.2 ± 1.7	48.5 ± 2.8	30.2 ± 2.1	25.6 ± 3.5	40.3 ± 10.4
TFL	Lengthening strain ($\%L_0$)	25.7 ± 5.0	28.9 ± 1.5	36.3 ± 4.1	26.6 ± 3.1	28.0 ± 2.2	29.0 ± 5.7
	Shortening strain ($\%L_0$)	25.0 ± 5.1	28.7 ± 1.6	36.5 ± 4.0	25.8 ± 2.5	27.9 ± 2.1	28.7 ± 5.6
	Relative EMG intensity (%max)	0.35 ± 0.06	0.26 ± 0.05	0.52 ± 0.09	0.35 ± 0.10	0.32 ± 0.03	0.67 ± 0.06
	EMG duration (%stride)	11.6 ± 6.5	43.5 ± 1.5	42.1 ± 1.6	25.4 ± 8.9	41.0 ± 2.7	41.1 ± 13.3
	Onset time (% stride)	44.5 ± 2.6	44.2 ± 2.8	41.6 ± 2.1	54.3 ± 14.0	27.2 ± 2.6	31.9 ± 7.1
	Offset time (% stride)	59.2 ± 4.5	86.4 ± 3.5	83.6 ± 2.1	44.0 ± 11.0	67.0 ± 2.8	71.4 ± 7.0

Values are mean ± s.e.m. Values in **bold** indicate significant differences from level in *post hoc* tests ($p<0.05$).

Table 2.3. Stance phase lengthening strains, swing phase shortening strains, and peak elastic energy in the proximal and distal FL during walking and trotting.

		Walk (1.1 m/s)			Trot (2.1-2.6 m/s)		
		Decline	**Level**	**Incline**	**Decline**	**Level**	**Incline**
Proximal FL_{long}	Lengthening strain (%L_0)	4.3 ± 0.8	7.7 ± 1.1	11.6 ± 8.5	10.2 ± 2.9	15.2 ± 5.8	4.9 ± 0.2
	Shortening strain (%L_0)	5.2 ± 2.9	3.1 ± 2.9	**8.9 ± 7.8**	10.0 ± 1.8	15.7 ± 7.2	16.5 ± 10.4
	Peak elastic energy (J)	2.2 ± 0.4	6.0 ± 5.3	4.9 ± 4.0	2.7 ± 0.4	8.2 ± 3.6	5.5 ± 4.5
Proximal FL_{trans}	Lengthening strain (%L_0)	7.5 ± 2.0	9.7 ± 4.7	11.2 ± 5.2	9.1 ± 3.1	6.4 ± 2.9	3.7 ± 0.9
	Shortening strain (%L_0)	6.2 ± 2.9	5.8 ± 2.9	8.9 ± 1.4	8.4 ± 2.0	8.7 ± 2.5	5.3 ± 3.1
	Peak elastic energy (J)	**0.3 ± 0.2**	1.1 ± 0.7	0.7 ± 0.2	0.5 ± 0.2	1.1 ± 0.5	0.5 ± 0.3
Distal FL_{long}	Lengthening strain (%L_0)	13.0 ± 1.8	6.8 ± 2.0	**20.6 ± 8.7**	12.9 ± 4.8	14.2 ± 5.3	18.5 ± 13.6
	Shortening strain (%L_0)	9.1 ± 3.4	3.3 ± 2.9	**20.3 ± 7.7**	15.1 ± 2.6	15.8 ± 4.9	20.1 ± 11.3
	Peak elastic energy (J)	4.9 ± 0.9	4.0 ± 1.8	**6.2 ± 3.9**	3.8 ± 1.4	5.5 ± 4.0	8.0 ± 6.7
Distal FL_{trans}	Lengthening strain (%L_0)	5.4 ± 1.6	6.4 ± 1.3	**18.6 ± 8.2**	12.9 ± 6.2	13.2 ± 5.0	19.5 ± 5.5
	Shortening strain (%L_0)	5.5 ± 1.6	2.5 ± 0.9	**16.3 ± 8.2**	13.4 ± 4.2	15.4 ± 4.1	**20.8 ± 4.8**
	Peak elastic energy (J)	**0.4 ± 0.3**	0.7 ± 0.2	**2.1 ± 1.0**	0.8 ± 0.6	1.8 ± 0.9	3.0 ± 0.7

Values are mean ± s.e.m. Values in **bold** indicate significant differences from level in *post hoc* tests ($p<0.05$).

Discussion

The results presented above indicate that the goat fascia lata has the potential to store elastic energy during the stance phase of walking and trotting, which may be recovered in swing phase. As hypothesized, the FL stretched in stance phase and shortened in swing phase (H1). This length change pattern was consistent across goats for longitudinal strains in the proximal and distal FL. However, transverse strains were more variable among goats. The distal FL was stretched by active gluteobiceps muscle contraction during stance phase. However, during both incline and level walking and trotting, GB contracted concentrically and not isometrically as hypothesized (H2). The proximal FL also stretched during stance phase, but was stretched passively by hip extension (i.e., the in series tensor fascia lata muscle was not electrically active) and was coincident with passive stretch in the inserting TFL muscle fibers. Muscle recordings indicated that additional proximal FL stretch may have occurred in late stance when TFL contracted isometrically. In some goats (including goat 5 shown in figure 2.6), the proximal FL continued to stretch along its longitudinal axis after the TFL began to shorten or contract isometrically indicating that the proximal FL may be stretched both passively by joint motion in early stance and actively by muscle contraction in late stance phase. If stretched passively, the proximal FL may be more sensitive to kinematic differences among strides and between goats, resulting in the greater variability in proximal FL strains seen here. Our results support the hypothesis that muscle shortening increased during incline versus level walking and trotting in GB (H3). Increased GB shortening strains during stance may have resulted in the increased

distal FL strains on the incline versus the level. During walking, peak energy storage in the distal FL also increased on the incline compared to level as hypothesized.

These results provide the first *in vivo* evidence of fascia energy storage during locomotion. In the goats, the FL stretched during walking and trotting and suggests that the fascia was stretched by hip extension and by active shortening of in series muscles. Increased stretch on the incline compared to level suggests that the FL may contribute to the increased mechanical work required to swing the limb faster during incline versus level walking.

Various sources of error likely underlie the variability of fascia strains recorded among goats. When recording FL strains, we attempted to align the sonomicrometry crystals with the longitudinal and transverse collagen fiber families of the FL, which are visible without a microscope. However, visibility can be limited in the surgical field and incisions were small. Any variation in crystal placement relative to the collagen fibers would have led to variability in measured strains as crystal rotation and off-axis strains may occur because the collagen fiber families in the goat FL are not orthogonal (Pancheri et al., 2014).

These data have implications for human ITB function. Many convergent features exist between the human ITB and goat FL, suggesting that both fascias have similar functions. As with the human ITB, the goat's TFL and GB muscles insert on the FL (Getty, 1975). The human ITB and goat FL are thick and tendinous and are further thickened in the regions where the GMax/GB and TFL muscles insert (Getty, 1975; Gray et al., 1995). Similar to the human TFL, increased TFL size is seen in cursorial quadrupeds compared to their non-cursorial ancestors (Jayes and Alexander, 1982).

Finally, the human ITB and goat FL are both composed of multiple layers of collagen fibers (Getty, 1975). The primary collagen layer in both the human ITB and goat FL runs parallel to the femur, while the secondary layer runs perpendicular (Paré et al., 1981; Bennett, 1989; Gray et al., 1995). These similarities suggest that the goat FL may be a good model for the human ITB.

The human ITB is traditionally considered to play a primary role in providing stability to the pelvis in the lateral plane (Inman, 1947; Kaplan, 1958; Gottschalk et al., 1989; Fredericson et al., 2000). A role in stability requires that the ITB acts like a stiff strut, transmitting muscle forces directly to the bone with minimal length change. However, the data shown here demonstrates that a similar fascial structure, the goat FL, changes length during locomotion and thus acts as a spring, suggesting that the human ITB may have a similar spring-like function. There are many elastic tendons in the human lower limb that play a role in elastic energy storage and recovery during running (see Bramble and Lieberman, 2004 for review) and the human ITB may be an additional example of a lower limb spring. To test this hypothesis, I will use a human lower limb model to examine the capacity of the human ITB to store and recover elastic energy in chapter 3. Furthermore, by comparing human ITB function to the chimp FL, I can test whether the energy storage function of the ITB is a uniquely derived trait in humans (chapter 4).

References

Arnold, A. S., Lee, D. V. and Biewener, A. A. (2013). Modulation of joint moments and work in the goat hindlimb with locomotor speed and surface grade. *The Journal of experimental biology* **216**, 2201-2212.

Aspden, R. (1990). Constraining the lateral dimensions of uniaxially loaded materials increases the calculated strength and stiffness: application to muscle and bone. *Journal of Materials Science: Materials in Medicine* **1**, 100-104.

Barker, P. J., Briggs, C. A. and Bogeski, G. (2004). Tensile transmission across the lumbar fasciae in unembalmed cadavers: effects of tension to various muscular attachments. *Spine* **29**, 129-138.

Benjamin, M. (2009). The fascia of the limbs and back--a review. *Journal of Anatomy* **214**, 1-18.

Bennett, M. B. (1989). A possible energy-saving role for the major fascia of the thigh in running quadrupedal mammals. *Journal of Zoology* **219**, 221-230.

Biewener, A., Konieczynski, D. and Baudinette, R. (1998). In vivo muscle force-length behavior during steady-speed hopping in tammar wallabies. *Journal of Experimental Biology* **201**, 1681-1694.

Biewener, A. and Roberts, T. (2000). Muscle and tendon contributions to force, work, and elastic energy savings: a comparative perspective. *Exercise and Sport Sciences Reviews* **28**, 99-107.

Bramble, D. and Lieberman, D. (2004). Endurance running and the evolution of *Homo*. *Nature* **432**, 345-352.

Cavagna, G., Saibene, F. and Margaria, R. (1964). Mechanical work in running. *Journal of Applied Physiology* **19**, 249-256.

Daley, M. A. and Biewener, A. A. (2003). Muscle force-length dynamics during level *versus* incline locomotion: a comparison of *in vivo* performance of two guinea fowl ankle extensors. *Journal of Experimental Biology* **206**, 2941-2958.

Dubiel, W. T. and Wigren, A. (1974). Functional Status of the Lower Extremity After Resection of Fascia Lata: A Clinical and Physiological Follow-up Study in Patients with Fascia Lata Heart Valve Replacement. *Acta Orthopaedica* **45**, 599-613.

Fedak, M. A., Heglund, N. C. and Taylor, C. R. (1982). Energetics and mechanics of terrestrial locomotion. II. Kinetic energy changes of the limbs and body as a function of speed and body size in birds and mammals. *Journal of Experimental Biology* **79**, 23-40.

Fredericson, M., Cookingham, C., Chaudhari, A., Dowdell, B., Oestreicher, N. and Sahrmann, S. (2000). Hip abductor weakness in distance runners with iliotibial band syndrome. *Clinical Journal of Sport Medicine* **10**, 169-175.

Gabaldón, A. M., Nelson, F. E. and Roberts, T. J. (2004). Mechanical function of two ankle extensors in wild turkeys: shifts from energy production to energy absorption during incline *versus* decline running. *Journal of Experimental Biology* **207**, 2277-2288.

Garfin, S. R., Tipton, C. M., Mubarak, S. J., Woo, S. L., Hargens, A. R. and Akeson, W. H. (1981). Role of fascia in maintenance of muscle tension and pressure. *Journal of Applied Physiology* **51**, 317-320.

Getty, R. (1975). Sisson and Grossman's The anatomy of the domestic animals, fifth edition. Philadelphia: W.B. Saunders Company.

Gottschalk, F., Kourosh, S. and Leveau, B. (1989). The functional anatomy of tensor fasciae latae and gluteus medius and minimus. *Journal of Anatomy* **166**, 179-189.

Gray, H., Williams, P. L. and Bannister, L. H. (1995). Gray's anatomy: the anatomical basis of medicine and surgery. Edinburgh: Churchill Livingstone.

Hedrick, T. L. (2008). Software techniques for two-and three-dimensional kinematic measurements of biological and biomimetic systems. *Bioinspiration & Biomimetics* **3**, 034001.

Huijing, P. A. and Baan, G. C. (2001). Myofascial force transmission causes interaction between adjacent muscles and connective tissue: effects of blunt dissection and compartmental fasciotomy on length force characteristics of rat extensor digitorum longus muscle. *Archives of Physiology and Biochemistry* **109**, 97-109.

Huijing, P. A., Maas, H. and Baan, G. C. (2003). Compartmental fasciotomy and isolating a muscle from neighboring muscles interfere with myofascial force transmission within the rat anterior crural compartment. *Journal of Morphology* **256**, 306-321.

Inman, V. T. (1947). Functional aspects of the abductor muscles of the hip. *The Journal of Bone and Joint Surgery* **29**, 607-619.

Jayes, A. and Alexander, R. (1982). Estimates of mechanical stresses in leg muscles of galloping Greyhounds (Canis familiaris. *Journal of Zoology* **198**, 315-328.

Kalin, P. J. and Hirsch, B. E. (1987). The origins and function of the interosseous muscles of the foot. *Journal of Anatomy* **152**, 83-91.

Kaplan, E. B. (1958). The iliotibial tract: Clinical and morphological significance. *The Journal of Bone and Joint Surgery* **40**, 817-832.

Ker, R. F., Bennett, M. B., Bibby, S. R., Kester, R. C. and Alexander, R. M. (1987). The spring in the arch of the human foot. *Nature* **325**, 147-149.

Loeb, G. E. and Gans, C. (1986). Electromyography for Experimentalists. Chicago: University of Chicago Press.

McGuigan, M. P., Yoo, E., Lee, D. V. and Biewener, A. A. (2009). Dynamics of goat distal hind limb muscle–tendon function in response to locomotor grade. *Journal of Experimental Biology* **212**, 2092-2104.

Minetti, A., Ardigo, L. and Saibene, F. (1994). Mechanical determinants of the minimum energy cost of gradient running in humans. *Journal of Experimental Biology* **195**, 211-225.

Mozan, L. C. and Keagy, R. D. (1969). Muscle relationships in functional fascia: a preliminary study. *Clinical Orthopaedics and Related Research* **67**, 225-230.

Myers, T. W. (2008). Anatomy trains: myofascial meridians for manual and movement therapists. New York: Churchill Livingstone.

Pancheri, F. Q., Eng, C. M., Lieberman, D. E., Biewener, A. A. and Dorfmann, L. (2014). A constitutive description of the anisotropic response of the fascia lata. *Journal of the Mechanical Behavior of Biomedical Materials* **30**, 306-323.

Paré, E., Stern, J. and Schwartz, J. (1981). Functional differentiation within the tensor fasciae latae. *The Journal of Bone and Joint Surgery* **63**, 1457-1471.

Roberts, T. J., Marsh, R. L., Weyand, P. G. and Taylor, C. R. (1997). Muscular force in running turkeys: the economy of minimizing work. *Science* **275**, 1113-1115.

Rubenson, J., Henry, H. T., Dimoulas, P. M. and Marsh, R. L. (2006). The cost of running uphill: linking organismal and muscle energy use in guinea fowl (Numida meleagris). *Journal of Experimental Biology* **209**, 2395-2408.

Smeulders, M. J., Kreulen, M., Joris Hage, J., Baan, G. C. and Huijing, P. A. (2006). Progressive surgical dissection for tendon transposition affects length−force characteristics of rat flexor carpi ulnaris muscle. *Journal of Orthopaedic Research* **20**, 863-868.

Stahl, V. A. (2010). A biomechanical analysis of the the role of the crural fascia in the cat hindlimb. In *Biomedical Engineering*, vol. Doctor of Philosophy: Georgia Institute of Technology and Emory University.

Vleeming, A., Pool-Goudzwaard, A. L., Stoeckart, R., van Wingerden, J.-P. and Snijders, C. J. (1995). The posterior layer of the thoracolumbar fascia. Its function in load transfer from spine to legs. *Spine* **20**, 753.

Wilson, A. M., Watson, J. C. and Lichtwark, G. A. (2003). Biomechanics: a catapult action for rapid limb protraction. *Nature* **421**, 35-36.

Wood Jones, F. (1944). Structure and Function as Seen in the Foot. London: Baillière, Tindall, and Cox.

Chapter 3: The capacity of the human tensor fascia lata and gluteus maximus muscles to stretch the iliotibial band during walking and running

Abstract

The human iliotibial band (ITB) is fascial structure whose function is not well understood, but which may have evolved as an adaptation for bipedal locomotion, particularly endurance running. This study evaluated the capacity of the human ITB to store and release elastic energy during locomotion using a musculoskeletal model of the human lower limb that includes 3D skeletal geometry and the attachments and force-length properties of the ITB, tensor fascia lata (TFL), and gluteus maximus (GMax). The model was based on detailed analyses of the muscle architecture, dissections of the 3D anatomy, and measurements of the muscles' hip and knee moment arms in cadaveric specimens. The model was used, in combination with measured joint kinematics and published EMG recordings, to examine the capacity of the ITB to store elastic energy during walking, running, and sprinting. We found that forces generated by the TFL and GMax muscles potentially stretch the ITB during walking and running, resulting in ITB energy storage in both gaits. The anterior and posterior ITB have distinct length change patterns and periods of predicted elastic energy storage because of different MAs. The anterior ITB potentially stores energy in stance phase, which may be recovered in swing phase. Estimates of posterior ITB energy storage are greater than anterior ITB energy storage because of larger maximum muscle forces. The potential for ITB energy storage is eight times greater in

running than in walking, suggesting that selection for reduced locomotor costs during running may have selected for traits increasing ITB energy storage in *Homo*.

Introduction

Habitual bipedalism is a major derived feature of hominins (species more closely related to humans than chimpanzees), suggesting that many distinctive features of the human spine and lower extremity are adaptations to improve bipedal locomotor performance. Many of these features appear early in hominin evolution including a downwardly-oriented foramen magnum, lordosis of the lumbar spine, reorientation of the ilium into the parasagittal plane, and an increase in the size of lower extremity joints (see Aiello and Dean, 1990). Other derived features appearing later in the genus *Homo* may reflect selection for endurance running and include a stabilized sacroiliac joint, an expanded attachment of gluteus maximus on the ilium, and shorter toes (Bramble and Lieberman, 2004; Lieberman et al., 2006; Rolian et al., 2009), but the hypothesis that humans are specialized for endurance running remains controversial. If selection for distance running was indeed a driving force in the evolution of the human form, then we should be able to identify derived features, unique to humans among apes, that decrease locomotor cost. Long compliant tendons that store and recover elastic energy have been linked to locomotor economy in other species (Ker et al., 1987; Roberts, 2002; Biewener, 2003). However, the role of elastic mechanisms in the evolution of bipedal locomotion remains unknown.

The human iliotibial band (ITB) is an interesting example of a fascial structure, unique to humans, whose function is not well understood, but which may have evolved

as an adaptation for bipedal locomotion, particularly endurance running. The ITB is a complex thickening of the lateral fascia of the thigh that originates on the pelvis and inserts on the tibia; it receives muscle fibers from the tensor fascia lata (TFL) anteriorly, and from the gluteus maximus (GMax) posteriorly (Ober, 1936; Kaplan, 1958; Gottschalk et al., 1989; Gray et al., 1995; Birnbaum et al., 2004; Cruells Vieira et al., 2007). The ITB has traditionally been considered to function as a "strut" during locomotion, stabilizing the hip in the coronal plane when tensed by the inserting muscles (Inman, 1947; Fredericson et al., 2000). However, the compliance of the ITB (Gratz, 1931; Butler et al., 1984; Derwin et al., 2008), the fact that it crosses the knee and the presence of in-series muscles suggest that the ITB may play additional roles. If the ITB stretches substantially with hip or knee motion while transmitting muscle forces, thereby storing elastic strain energy, then it may decrease the metabolic cost of walking and running. Studies have estimated that energy stored and recovered from the Achilles tendon in late stance can reduce muscle work by as much as 6% during walking (Maganaris and Paul, 2002) and 35% during running (Alexander and Bennet-Clark, 1977; Ker et al., 1987). However, whether energy storage in the ITB also contributes to locomotor economy is not known.

This study evaluated the capacity of the human ITB to store and release elastic energy during locomotion. In particular, we hypothesized that forces generated by TFL and GMax stretch the ITB during walking and running, storing elastic energy that is released later in the stride. We further predicted that the ITB stores more energy (i.e., undergoes greater strains while transmitting larger forces) during running than walking,

suggesting that the ITB is another derived feature of the human lower limb specialized for endurance running.

We tested these hypotheses by developing a musculoskeletal model of the ITB and inserting muscles. Our model characterizes the 3D skeletal geometry, the hip and knee kinematics, and the attachments and force-length properties of the ITB, TFL and GMax for an average-sized adult male. Because existing representations of TFL and GMax were not sufficiently accurate for our study, we determined the muscles' force-generating capacity based on detailed analyses of the muscle architecture, dissections of the 3D anatomy, and measurements of the muscles' hip and knee moment arms in cadaveric specimens. TFL has largely been neglected in studies of muscle architecture (e.g., Wickiewicz et al., 1983; Ward et al., 2009) and locomotor function (e.g., Sasaki and Neptune, 2006; Dorn et al., 2012), despite the fact that TFL is active during running (Paré et al., 1981; Mann et al., 1986; Montgomery et al., 1994; Andersson et al., 1997) and presumably plays a role. GMax is routinely modeled as a uniarticular hip extensor that inserts on the femur, despite evidence that a substantial portion of GMax inserts on the ITB (Stern, 1972; Gray et al., 1995). Overcoming the limitations of previous models was an important aim of our study, and our refined model is available on SimTK (simtk.org). Using this refined model, we estimated the forces transmitted to anterior and posterior portions of the ITB at body positions corresponding to walking and running, predicted the length changes of the ITB, and calculated the corresponding ITB strain energies based on published measurements of the tissue's elastic modulus (Gratz, 1931; Derwin et al., 2008).

Materials and methods

Muscle architecture measurements

We characterized the isometric force-generating capacity of TFL and GMax based on measurements of muscle architecture in three formalin-fixed human cadavers (Table 3.1). Specimens were dissected and the muscles isolated and removed. Total mass (M) of each muscle was measured. GMax was separated into four superior-inferior regions, and the mass of each region measured. Muscle fascicles were carefully dissected from three regions of TFL and four regions of GMax, and the fascicle lengths (L_f') measured. Surface pennation angle between the fascicles and distal tendon was also measured. Under magnification, muscle fiber bundles were isolated from each fascicle and mounted on slides. Following Lieber et al. (1990), bundle sarcomere length (L_s') was determined by laser diffraction and used to calculate normalized fascicle length (L_f):

$$L_f = L_f' \left(\frac{2.7 \mu m}{L_s'} \right) \quad (1)$$

where 2.7 μm is the optimal sarcomere length for human muscle (Lieber et al., 1994). Physiological cross-sectional area (PCSA) was calculated from muscle mass and normalized fiber length (Powell et al., 1984):

$$PCSA = \frac{M}{\rho \cdot L_f} \quad (2)$$

where ρ is muscle density (1.056 g/cm^3; (Mendez and Keys, 1960). Our architecture data for GMax is consistent with data reported by Ward et al. (2009).

Muscle moment arm measurements

We characterized the 3D anatomy and moment arms of TFL-ITB and GMax-ITB muscle-tendon units (MTUs) in five fresh frozen cadaveric hemi-pelvises obtained from MedCure (Portland, OR). Moment arms (MAs) were determined for hip flex/extension, rotation, ab/adduction, and knee flex/extension using the tendon excursion method (Brand et al., 1975; An et al., 1984). We approximated the TFL-ITB MTU with two Kevlar thread paths (Figure 3.1A) and the GMax-ITB MTU with four paths (Figure 3.1B). We anchored each thread to a screw eye located at the MTU's insertion, routed the thread through plastic tubing to a screw eye located at the MTU's origin, and attached it to one of two cable-extension position transducers (PTX101, Celesco, Canoga Park, CA) that measured length changes with an accuracy of ±0.32 mm while applying a tension of 1.4 or 2.8 N. The plastic tubing ensured a repeatable path and decreased friction between the thread and underlying tissues.

Hip and knee angles were measured simultaneously with MTU length changes using a motion tracking system (Polhemus Fastrak, Colchester, VT) and custom software (LabView, National Instruments Corporation, Austin, TX). Receivers were rigidly attached to the pelvis, femur, and tibia to track the segments' positions and orientations. Coordinate systems, based on anatomical axes, were defined for each segment by digitizing bony landmarks and solving for the location of the hip center (Figure 3.2A). We digitized the 3D coordinates of each MTU's origin, insertion, and key "via" points (points through which a muscle is constrained to act) relative to the segment coordinate systems. We also tracked, using high-speed video, the locations of 9 marker pairs sutured in the ITB while moving the limb through its ranges of hip and knee

motion. These data were used to determine the hip and knee angles at which the anterior and posterior ITB began to stretch.

Each specimen was mounted in a custom frame (Figure 3.2B) that allowed independent control of hip flex/extension, rotation, ab/adduction, and knee flexion following Arnold et al. (2000). Alignment of the specimen in the frame comprised four main steps, each performed with real-time feedback to ensure that the pelvis, femur, and tibia were secured to within 5 mm and 2° of the desired alignment. First, the pelvis was aligned so that either its medial-lateral or anterior-posterior axis was perpendicular to the table, for measuring hip flex/extension or ab/adduction MAs, respectively. Second, for measuring hip rotation MAs, the femur was secured to the inner of two concentric rings so that its long axis (from the hip center to the midpoint of femoral epicondyles) was perpendicular to the plane of the rings and coincident with the center of the rings. Third, the cart was adjusted so that it rolled in an arc about the specimen's hip joint center. Fourth, the tibia was extended and secured to a locking hinge attached to the inner ring. When measuring knee MAs, the hinge was removed. To verify alignment, we monitored residual coupling of hip angular motion; hip adduction varied less than 2° and hip rotation less than 4° over a 75° range of hip flex/extension, and similar values were maintained over a 50° range of hip ab/adduction.

To determine muscle MAs, MTU excursion was recorded while slowly moving the specimen through a range of hip flex/extension, hip ab/adduction, hip rotation, or knee flexion. MTU excursion and joint angle data were sampled at 10 Hz (National Instruments BNC-2090 analog-to-digital converter). While MAs were measured about a given joint axis, the other axes were locked in a neutral position (hip flexion = 0°, hip

rotation = 5°, hip adduction = 0°, knee flexion = 0°). The lengthening excursion versus joint angle data were fit with a fourth order polynomial, and the polynomial derivative used to estimate the MA. A minimum of five trials was collected for each condition, with MAs averaged across trials.

After MA measurements were completed, muscles were dissected from the limb, cleaned of fat and connective tissue, and weighed (Table 3.2). In two specimens, the four regions of GMax were carefully dissected to determine the relative masses of the portions that insert on the ITB and those that insert on the femur. ITB thickness was measured in anterior and posterior regions and was found to be thicker posteriorly, ranging from 0.83 mm to 1.01 mm proximally and from 1.04 mm to 1.17 mm distally.

Model of TFL-ITB and Gmax-ITB MTUs

We modified paths of the TFL and GMax MTUs in the musculoskeletal model reported by Arnold et al. (2010) to match our digitized muscle attachments and moment arm data (Figure 3.3). Because I showed in chapter 1 (Eng et al., 2014) that the goat fascia lata's material properties are not strongly influenced by its biaxial strain environment despite its complex structure, we reasoned that the TFL- and GMax-ITB paths could be represented, for this analysis, as independent, proximal-to-distal MTUs. Using SIMM (*Software for Interactive Musculoskeletal Modeling*, v7.0, MusculoGraphics, Santa Rosa, CA), we created 2 paths for TFL and 8 paths for GMax (4 to the femur and 4 to the ITB). Because the muscles' MAs predicted by our model are extremely consistent with the MAs determined from our experiments (Figures 3.4&3.5), we are confident that the model accurately predicts length changes of the TFL-ITB and GMax-ITB MTUs over functional ranges of hip and knee motion. To estimate ITB strain

during walking and running, we created three additional MTU paths consistent with the three major paths of ITB force transmission as determined from our experiments (Figure 3.3B,C). One path accounts for the cumulative force transmitted by the anterior ITB when TFL1 and TFL2 are simultaneously activated (TFL-ITB_{ant}). The other paths account for the cumulative force transmitted by the posterior ITB when GMax1 and GMax2 are activated (GMax1,2-ITB_{post1}) or GMax3 and GMax4 are activated (GMax 3&4; GMax3,4-ITB_{post2}). Each path was adjusted to yield average MAs of the combined MTUs (Figures. 3.4&3.5).

We used a generic Hill-type muscle model (Zajac, 1989; Delp et al., 1990) to estimate isometric forces generated by TFL-ITB_{ant}, GMax1,2-$ITB_{post1,}$ and GMax3,4-ITB_{post2} at different levels of activation. Two parameters, maximum isometric force (F_{max}) and optimal fiber length (L_{opt}), scaled normalized active and passive force-length (F-L) curves to each muscle (Table 3.3). F_{max} and an additional parameter, tendon slack length (L_{TS}), scaled a normalized "tendon" F-L curve to each MTU. The generic tendon F-L curve in SIMM assumes 3% strain at maximum isometric muscle force, and thus assumes tendon cross-sectional area scales with muscle size. However, the ITB is more compliant than tendon (Butler et al., 1984; Derwin et al., 2008), and our thickness measurements show that the ITB has a relatively uniform anterior-posterior thickness, despite the fact that inserting muscles differ substantially in force-generating capacity. We therefore created new normalized F-L curves for each ITB MTU in the model (Figure 3.6) based on ITB stress-strain data reported in Derwin et al. (2008). We assessed the sensitivity of our ITB strain and energy storage calculations to these assumed ITB F-L properties by creating a set of additional, stiffer ITB MTUs based on

human Achilles tendon stress-strain data reported by Arya and Kulig (2010). Tendon slack lengths were chosen for each MTU such that the ITB began to stretch passively at hip and knee angles consistent with our experimental measurements. We verified that these L_{TS} values allow the muscles in our model to generate force over functional ranges of motion.

Assessment of ITB energy storage during walking and running

We used our model, in combination with measured joint kinematics and published EMG recordings, to examine the capacity of the ITB to store elastic energy during walking and running. First, we calculated the origin-to-insertion lengths of the MTUs at hip and knee angles corresponding to walking (S. Ounpuu, unpublished data from 10 healthy adults using methods described in Ounpuu et al., 1991) and running at speeds of 2, 3, 4, and 5 m/s (Hamner and Delp, 2013). We identified periods of the stride when TFL-ITB_{ant} was near maximum length and TFL was likely active (Paré et al., 1981; Montgomery et al., 1994), and periods when GMax1,2-$ITB_{post1,}$ and GMax3,4-ITB_{post2} were near maximum length and GMax was likely active (Jönhagen et al., 1996; Swanson and Caldwell, 2000; Bartlett et al., 2014), and we assumed that peak strains in the ITB_{ant} or ITB_{post} would occur at these times. Next, we separated the MTU lengths into ITB lengths and muscle fiber lengths by independently activating each MTU in the model and solving for the lengths at which the muscle force and ITB force were equivalent, accounting for pennation angle. We set each muscle's activation to 25% (of its maximum activation) to assess ITB strains during walking (Paré et al., 1981; Bartlett et al., 2014) and slow running at 2 m/s (Montgomery et al., 1994). We set each muscle's activation to 50%, 75%, or 100% to estimate ITB strains during faster running at 3, 4,

and 5 m/s, respectively (Paré et al., 1981; Montgomery et al., 1994; Jönhagen et al., 1996; Swanson and Caldwell, 2000). Lastly, we used ITB force and strain to estimate elastic energy (E):

$$E = \tfrac{1}{2} F_{ITB} \Delta L_{ITB} \quad (3)$$

following Alexander (1984). Length changes of the ITB were determined relative to the tendon slack length.

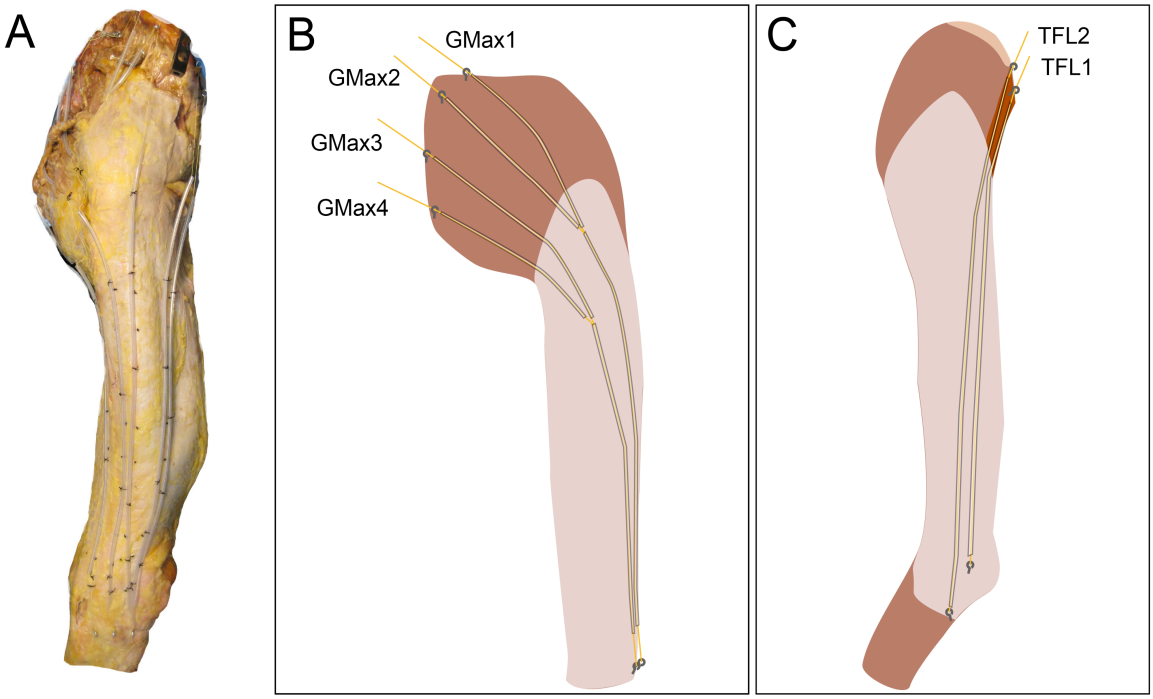

Figure 3.1. A: Anterolateral view of ITB showing the two TFL paths used for moment arm measurements. The anterior path (TFL1) originated on the iliac crest near the anterior superior iliac spine (ASIS) and the posterior path (TFL2) originated on the lateral iliac crest approximately 3 cm posterior to the ASIS. Screw eyes inserted in the ilium anchored the origins of thread paths to these locations. TFL1 muscle fibers were continuous with ITB fibers inserting in the distal femur approximately 3.0 cm anterior to the lateral epicondyle, so a screw eye was anchored at this location in the femur. TFL2 fibers were continuous with ITB fibers inserting on the tibia, so its insertion screw eye was placed in the lateral tibial condyle ~1.0 cm posterior to the most anterior point on the tibial tuberosity. B: Posterolateral view of the ITB showing four GMax paths used for moment arm measurements. The most superior path of GMax (GMax1) originated on the ilium 1.5 cm lateral and 2.5 cm superior to the posterior superior iliac spine (PSIS). The origin of GMax2 was 1.0 cm inferior to PSIS on the ilium. The GMax3 origin was placed 1.0 cm lateral to the midline of the sacrum at the level of the intervertebral disc between the second and third sacral vertebrae. The most inferior path of GMax (GMax4) originated 1.0 cm lateral to the coccygeal midline on the proximal coccyx. GMax1 and GMax2 shared a screw eye placed 2.5 cm posterior to the tibial tuberosity, while GMax3 and 4 shared a screw eye placed 4.0 cm posterior to the tibial tuberosity.

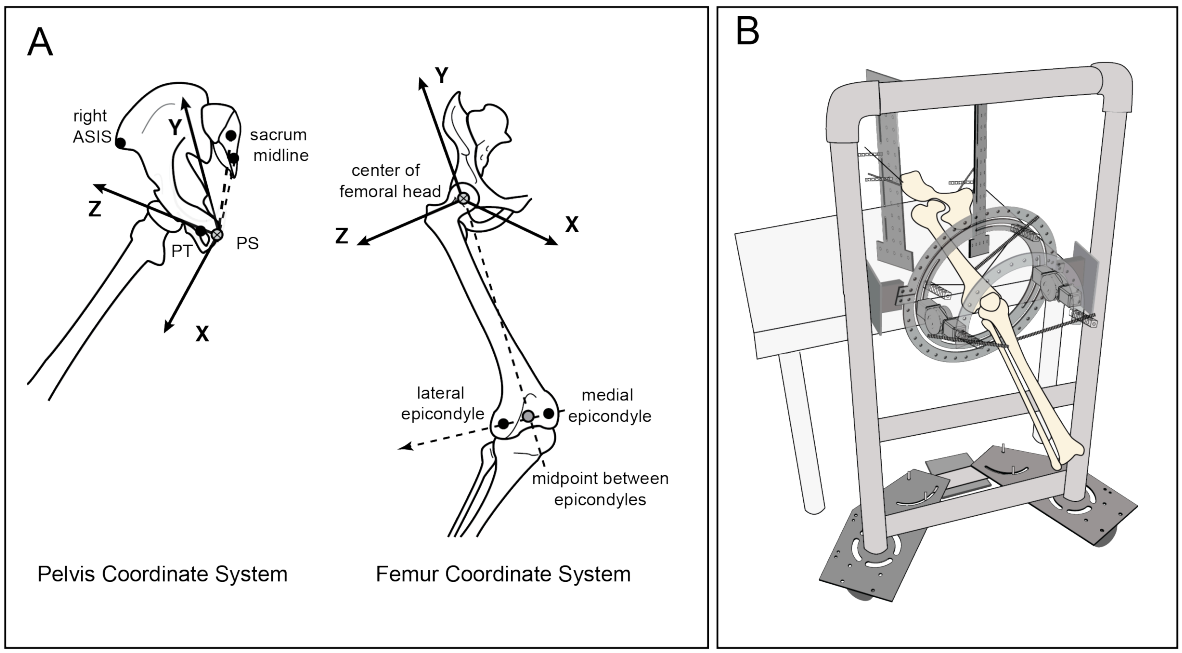

Figure 3.2. A: The pelvis and femur segment coordinate systems (CSs) were aligned with anatomical axes. For the pelvis CS, the medial-lateral plane was defined to be parallel to the plane formed by two vectors from the pubic symphysis to superior and inferior points on the sacral midline. The origin of the pelvis CS was located at the pubic symphysis. The right ASIS and pubic tubercle defined the frontal plane. For the femur, the superior-inferior axis was defined by the vector joining the midpoint between the medial and lateral epicondyles and the hip joint center (determined as described in the methods). The hip joint center was defined as the origin of the femur CS. The frontal plane of the femur CS was defined to be parallel to the vector between the lateral and medial epicondyles. The tibia CS was specified to be coincident with the femur CS when the knee was fully extended. B: The specimen was mounted in a custom frame, comprising a fixed table for securing the pelvis, a rotating cart for moving the femur through a range of hip flex/extension and ab/adduction angles, and a set of concentric rings for rotating the femur, following Arnold et al. (2000). The cart consisted of two vertical support posts each mounted on a wheeled baseplate with a ball caster mounted on a rod between them. The limb is shown here with its pelvis mounted for hip ab/adduction, which is achieved by rotating the cart.

Table 3.1. Muscle architecture of tensor fascia lata (TFL) and gluteus maximus (GMax*)

Muscle	Mass (g)	Normalized fascicle length (cm)	Pennation angle (degrees)	PCSA¥ (cm^2)
TFL	35.5 ± 9.6	101.3 ± 5.8	1.1 ± 1.1	3.4 ± 1.0
GMax1	124.2 ± 22.0	122.0 ± 1.0	37.5 ± 0.0	10.6 ± 2.4
GMax2	143.1 ± 8.9	140.8 ± 15.3	35.0 ± 2.5	10.3 ± 1.7
GMax3	66.4 ± 20.8	134.3 ± 21.9	19.2 ± 11.0	4.9 ± 1.5
GMax4	78.4 ± 29.8	157.8 ± 4.0	11.3 ± 3.8	5.7 ± 2.4

Data from 3 elderly cadaveric specimens (2 male, 1 female, ages unknown) are expressed as mean ± s.e.m.
*GMax1 is the most superior and GMax4 is the most inferior muscle region (see Figure 3.1B)
¥Pennation angle is not included in the PCSA calculation since our SIMM model multiplies PCSA, specific tension, and pennation angle to determine peak muscle-tendon force.

Table 3.2. Muscle regional masses of tensor fascia lata (TFL) and gluteus maximus (GMax)

Muscle	Total mass of region (g) (n=5)	Percentage of mass inserting on ITB (%) (n=2)
TFL1∞	26.4 ± 7.2	100%
TFL2	21.4 ± 5.5	100%
GMax1¥	110.6 ± 26.2	44.6 ± 4.9%
GMax2	109.4 ± 24.8	52.7 ± 7.8%
GMax3	121.9 ± 19.8	47.7 ± 11.3%
GMax4	104.7 ± 29.7	71.7 ± 28.3%

Data from 5 adult males (mean age: 62 ± 10 years) are expressed as mean ± s.e.m.
∞TFL was divided into two anterior-posterior regions based on origin and fascicle orientation.
¥GMax was separated into 4 superior-inferior regions.

Table 3.3. Muscle parameters used to scale generic muscle properties to each muscle-ITB path.

Muscle-ITB path	Maximum isometric force (N; F_{max})[¥]	Optimal fiber length (cm; L_{opt})	Pennation angle (degrees; θ)	Tendon slack length (mm; L_{TS})
TFL1,2-ITB_{ant}[$]	197.0	9.4	2.5	42.6
GMax1,2-ITB_{post1}[*]	452.5	15.2	21.9	40.3
GMax3,4-ITB_{post2}[*]	554.5	16.7	21.9	37.7

[$]TFL PCSA, L_{opt}, and θ from our measurements.
[*] GMax PCSA, L_{opt}, and θ from Ward et al. (2009).
[¥]Fmax calculated as the product of PCSA and muscle specific tension of 61 N/cm^2 used by Arnold et al. (2010).

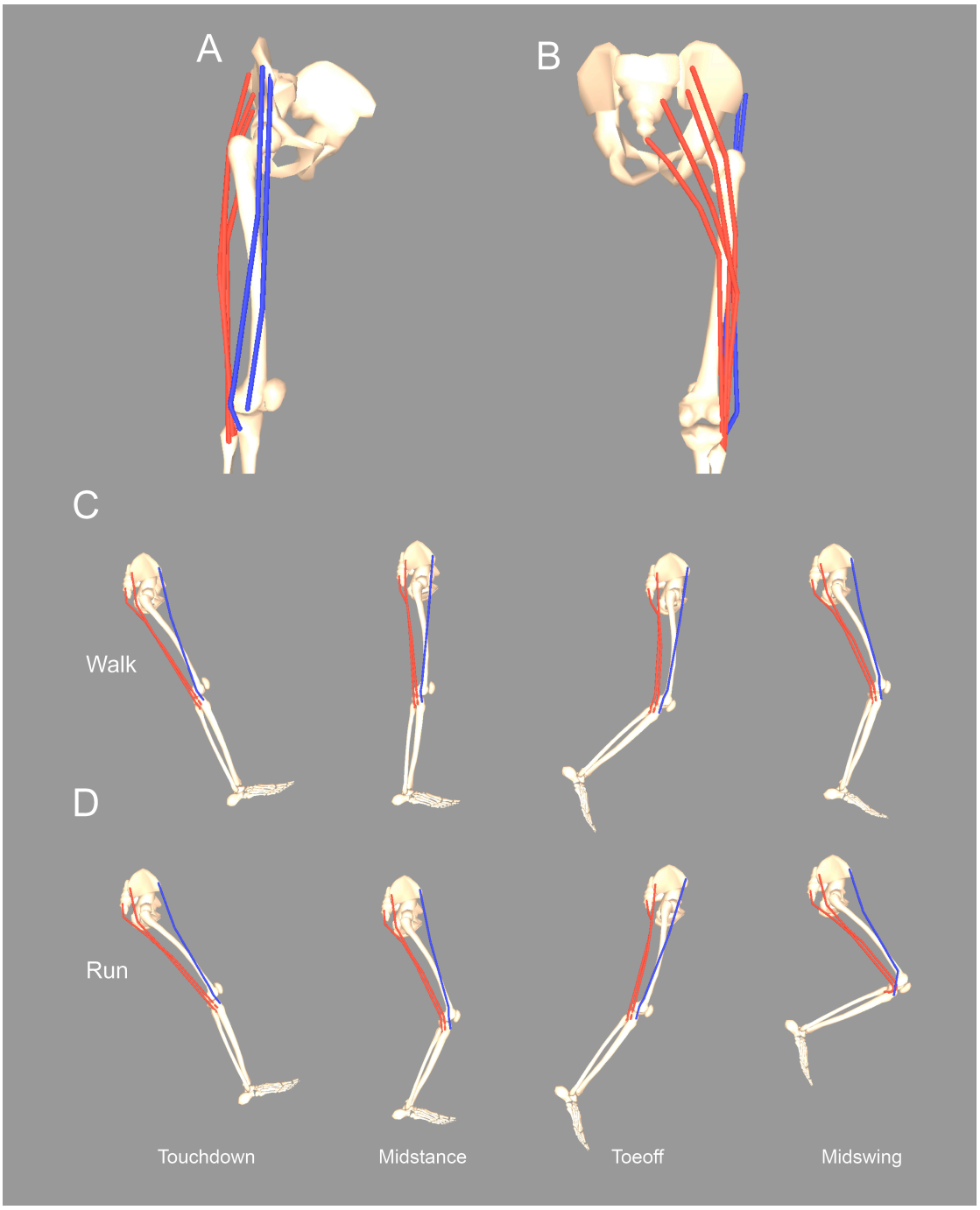

Figure 3.3. (**A**) Anterolateral view of the lower extremity model modified from Arnold et al. (2010) showing the TFL1- and TFL2-ITB$_{ant}$ MTU paths. (**B**) Posterolateral view of model with four GMax-ITB$_{post}$ MTU paths originating on the ilium, sacrum, and coccyx and inserting on the ITB. Model with combined TFL-ITB$_{ant}$, GMax1,2-ITB$_{post1}$, and GMax3,4-ITB$_{post2}$ MTU paths shown at the joint positions found at 25, 50, 75, and 100% of stride during walking (**C**) and running at 4 m/s (**D**). The TFL-ITB$_{ant}$ MTU is in its most stretched position at about 50% stride in walking and running. The GMax-ITB$_{post}$ MTUs are most stretched around 100% stride in both gaits.

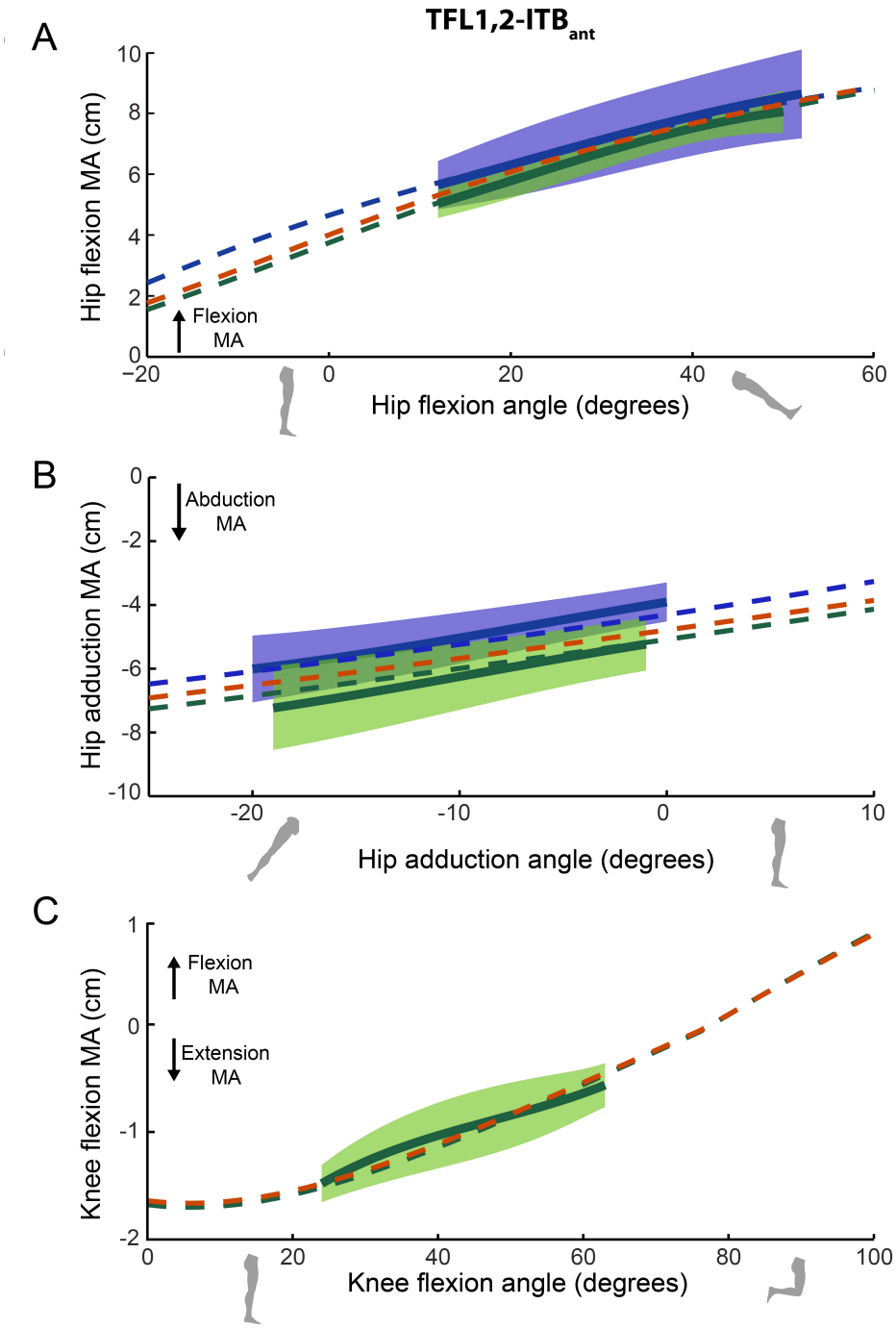

Figure 3.4. The TFL-ITB$_{ant}$ moment arms of the modified lower limb model are consistent with experimental MA measurements. A: TFL-ITB MTUs have similar hip flexion MAs that increase as the hip flexes. B: The hip abduction MAs of both TFL-ITB MTUs increase with hip abduction. C: The TFL2-ITB MTU knee extension MA decreases with knee flexion. Solid lines and shaded regions indicate mean and standard deviation of experimentally measured MAs from five cadaveric lower limbs. Dashed lines indicate modified model MAs. TFL1-ITB (blue), TFL2-ITB (green), and the combined TFL1,2-ITB$_{ant}$ (red).

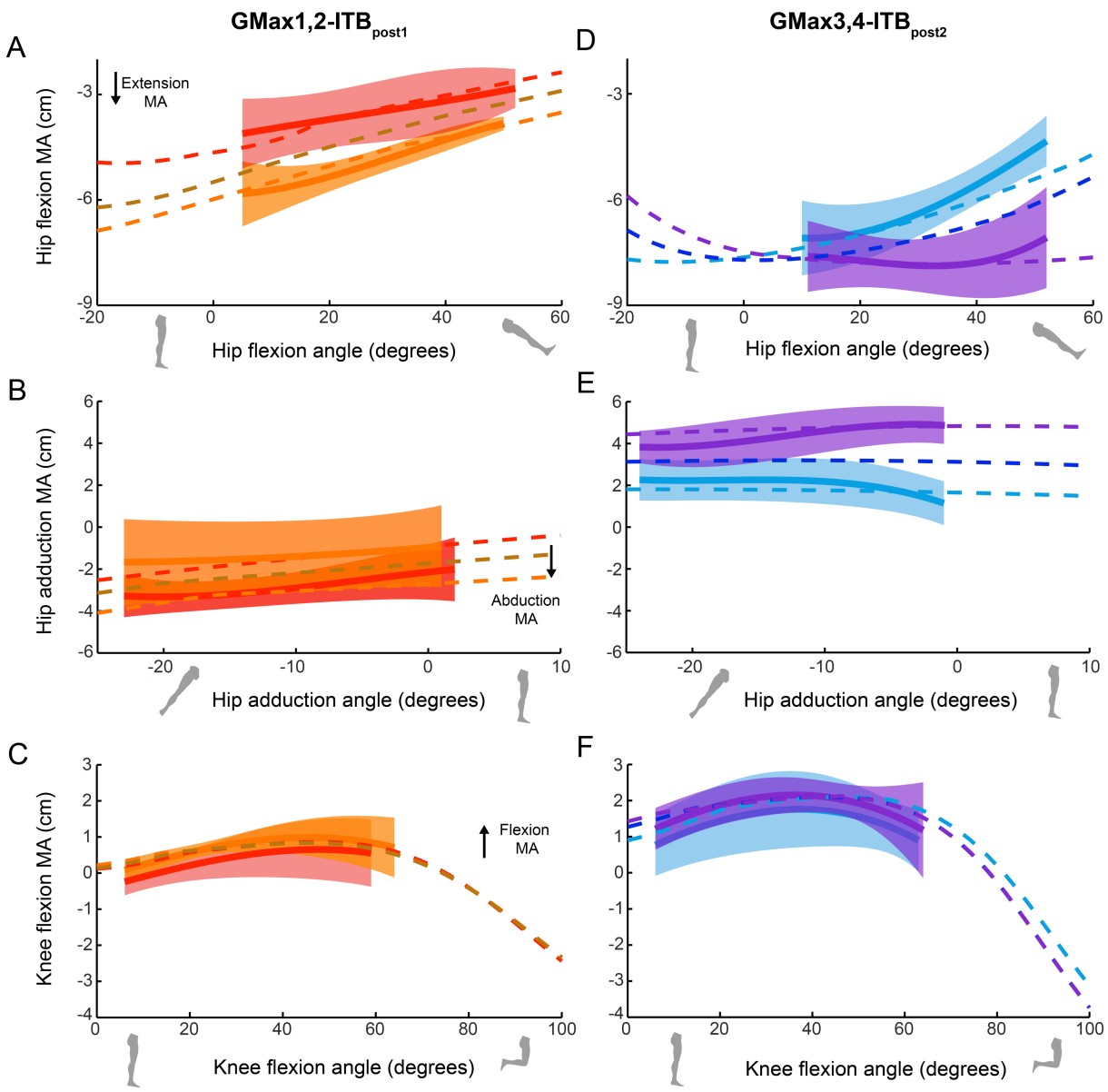

Figure 3.5. The GMax-ITB$_{post}$ moment arms of the modified lower limb model are consistent with experimental MA measurements. A,D: All GMax-ITB MTUs have hip extension MAs. B: GMax1-ITB and GMax2-ITB have hip abduction MAs. E: GMax3-ITB and GMax4-ITB have hip adduction MAs. C,F: With the knee extended, the GMax-ITB MTU have knee flexion MAs, which become knee extension MAs with the knee flexed. Solid lines and shaded regions indicate mean and standard deviation of experimental MAs from five cadaveric lower limbs. Dashed lines indicate modified model MAs. The four GMax regions from superior to inferior are GMax1 (red), GMax2 (orange), GMax3 (blue), and GMax4 (purple). MAs of the combined path for GMax1,2-ITB$_{post1}$ is shown in yellow (A-C) and GMax3,4-ITB$_{post2}$ in navy (D-F).

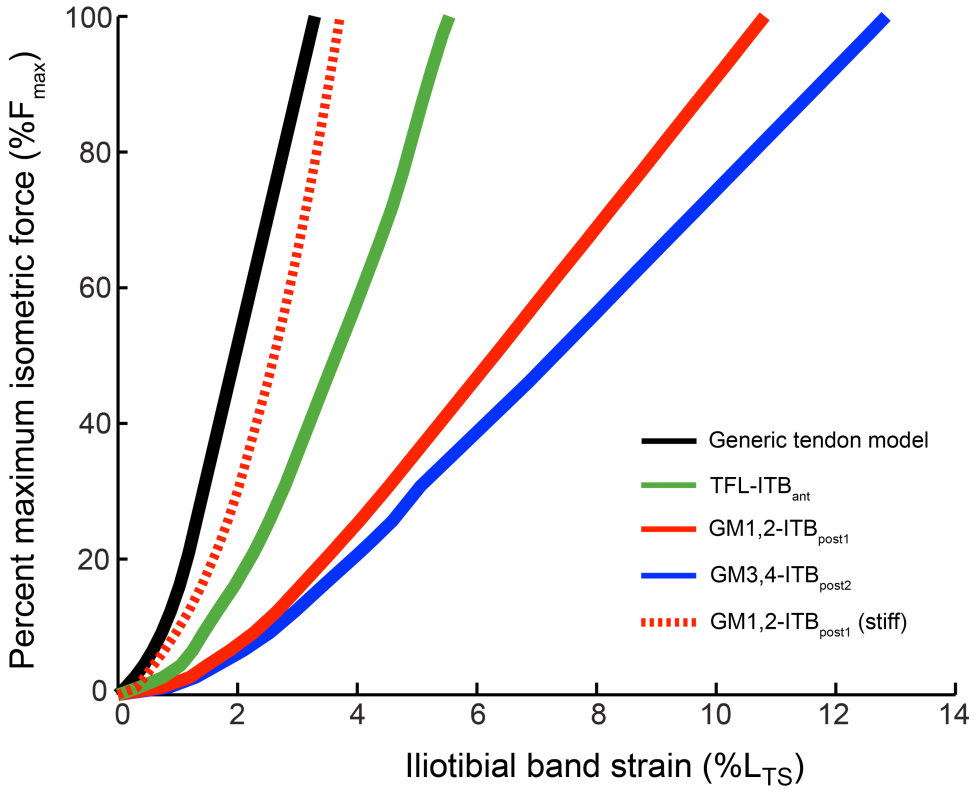

Figure 3.6. ITB force-length curves derived from Derwin et al. (2008) are shown with solid lines for GM1,2-ITB$_{post1}$ (red), GM3,4-ITB$_{post2}$ (blue), and TFL-ITB$_{ant}$ (green) and are substantially more compliant than the default tendon force-length curve (black) defined in the lower limb model from Arnold et al. (2010). The GM1,2-ITB$_{post1}$ stiff ITB force strain-curve (short dash) was defined based on Arya and Kulig (2010). Similar curves were derived for TFL-ITB$_{ant}$ and GM3,4-ITB$_{post2}$.

Results

The ITB MTUs in our model undergo substantial length changes during walking and running (Figure 3.7). With its hip flexion and knee extension MAs, TFL-ITB$_{ant}$ is maximally stretched during late stance (walking) and early swing (running) when the hip is extended and the knee is flexed (Figure 3.3C-D). EMG recordings show that TFL is active during this time (Figure 3.7) (Paré et al., 1981; Montgomery et al., 1994). With their hip extension and knee flexion MAs, GMax-ITB$_{post1}$ and GMax-ITB$_{post2}$ are maximally stretched during the late swing phase when the hip is flexed and the knee extended (Figure 3.3C-D). EMG recordings show that GMax is active during this time (Figure 3.7) (Jönhagen et al., 1996; Swanson and Caldwell, 2000; Bartlett et al., 2014). GMax3,4-ITB$_{post2}$ lengthens nearly 4% more than GMax1,2-ITB$_{post1}$ during walking and 7% more during running, due to its substantially larger hip extension MA when the hip is flexed. Length changes of all three ITB MTUs are 3.7-8% greater during running compared to walking because of the greater ranges of hip and knee motion during running.

Contraction of TFL and GMax during the late stance and swing phases, respectfully, substantially stretch the ITB in our model, storing elastic energy. In the anterior ITB, peak strains range from 2.5% during walking to 5.6% during sprinting, suggesting that the anterior ITB may store as much as 2.35 J of elastic energy in sprinting (Figure 3.8A). In the posterior ITB, peak strains range are 3.9% and 4.4% during walking in the GMax1,2 and Gmax3,4 MTUs respectively. During sprinting, peak strains of 10 and 12% suggest that the posterior ITB stores up to 12.1 J during sprinting (Figure 3.8B-C).

Energy storage is greater in the posterior ITB than the anterior ITB because GMax generates much larger forces than TFL (Table 3.3). Our estimates of energy storage are greater for sprinting than for slow running or walking (Figure 3.8) because we assumed, based on published EMG recordings, that TFL and GMax are activated more during sprinting.

Increasing the ITB's stiffness in our model decreased ITB strains, resulting in reduced elastic energy storage. In particular, with a nearly 3-fold stiffer anterior ITB, peak strains decreased by 1.4% during walking and 3.2% during sprinting (Figure 3.9A). The lower anterior ITB strains decreased peak anterior ITB energy storage by 67% and 57% during walking and sprinting, respectively. With increased stiffness, peak posterior ITB strains decreased by 2.4% during walking and 8% during sprinting (Figure 3.9B), resulting in 55% lower peak energy in walking and 66% lower peak energy in sprinting.

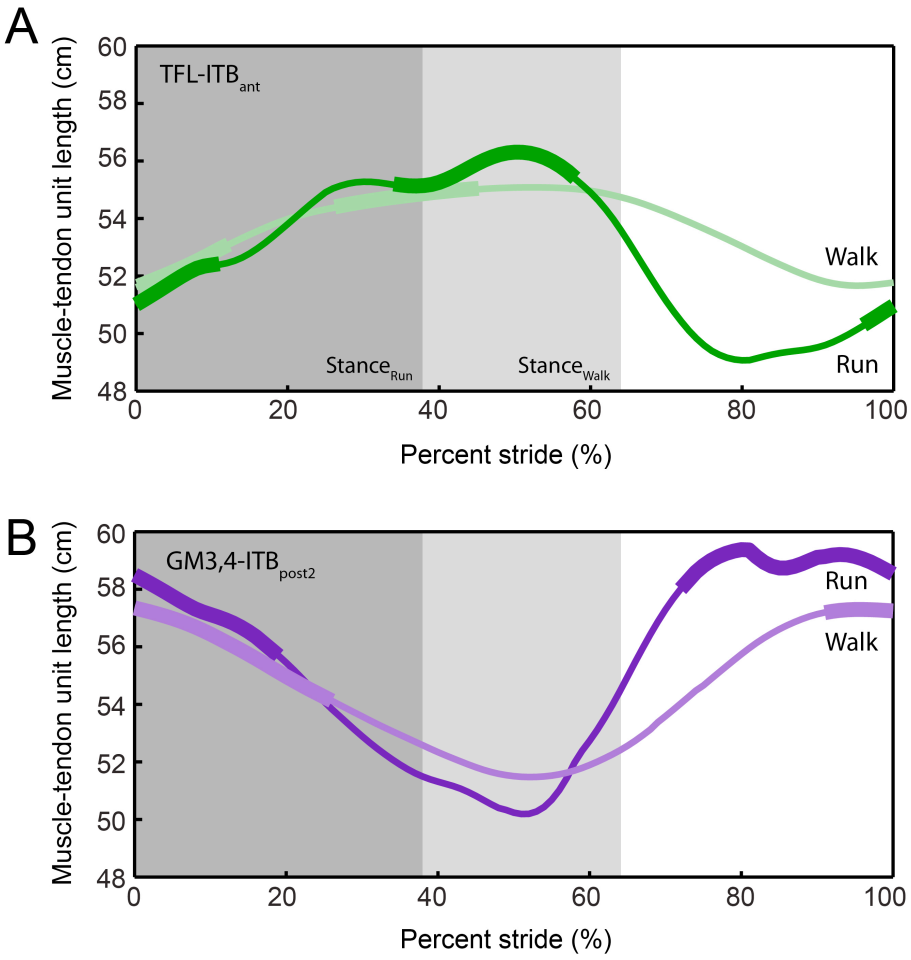

Figure 3.7. A: The TFL-ITB$_{ant}$ MTU stretches during stance phase in both walking and sprinting (5 m/s). The magnitude of TFL-ITB$_{ant}$ MTU length change is greater in sprinting. B: The GMax1,2-ITB$_{post1}$ (blue) and GMax3,4-ITB$_{post2}$ (purple) MTUs stretch during swing phase in both walking and sprinting. The magnitude of MTU length change is greater in GM3,4-ITB$_{post2}$ because of greater hip extension and knee flexion MAs. Regions of typical muscle activity (thickened portion of MTU length change pattern) demonstrate that the muscles are typically active during when the MTU is stretching or at maximum stretch.

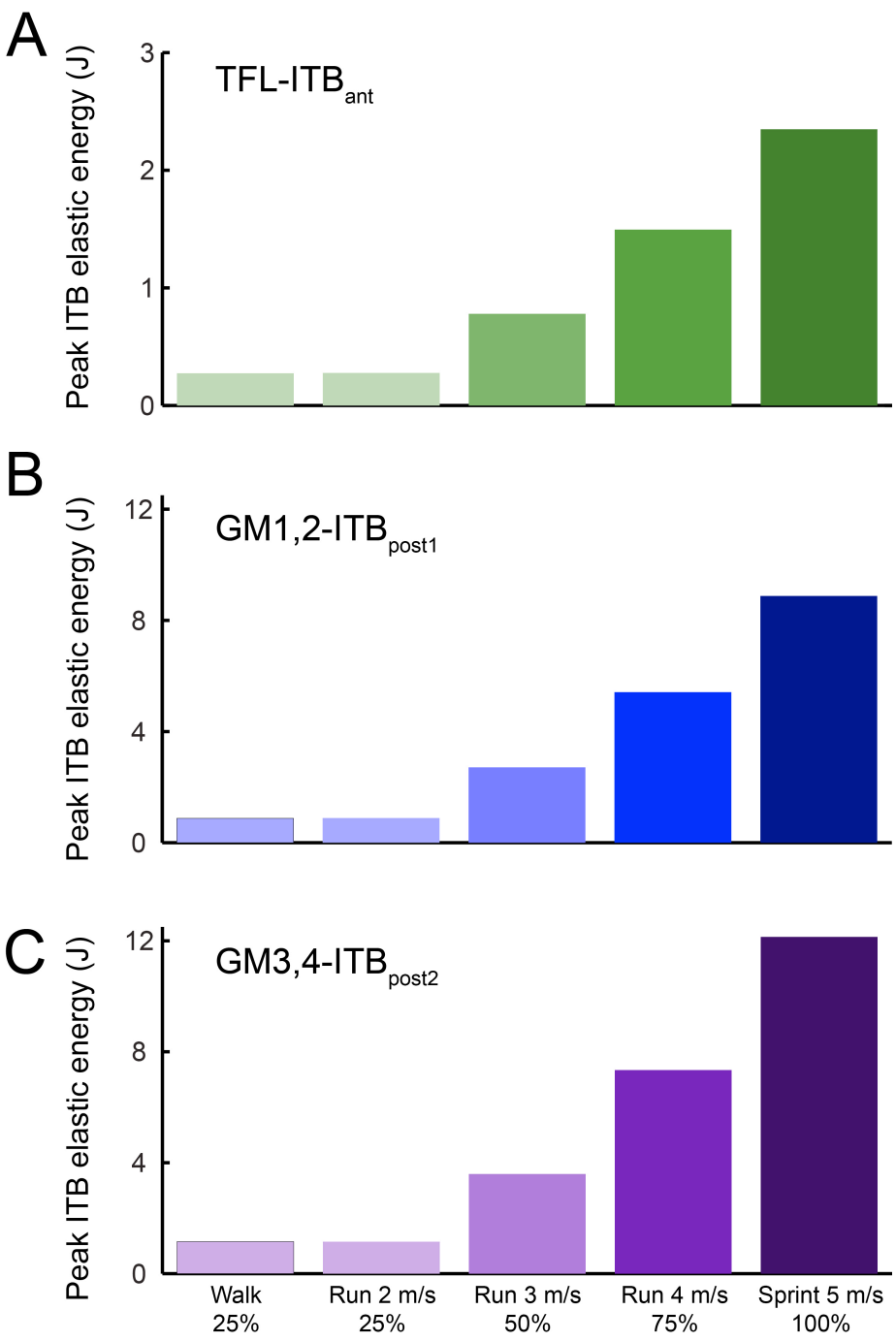

Figure 3.8. Peak ITB elastic energy during the period when the muscle is active in each gait and speed for TFL-ITB$_{ant}$ (**A**), GMax1,2-ITB$_{post1}$ (**B**), and GMax3,4-ITB$_{post2}$ (**C**). Muscle activations used for each muscle in each gait are shown. Peak energy is greater in the ITB MTUs during running compared to walking.

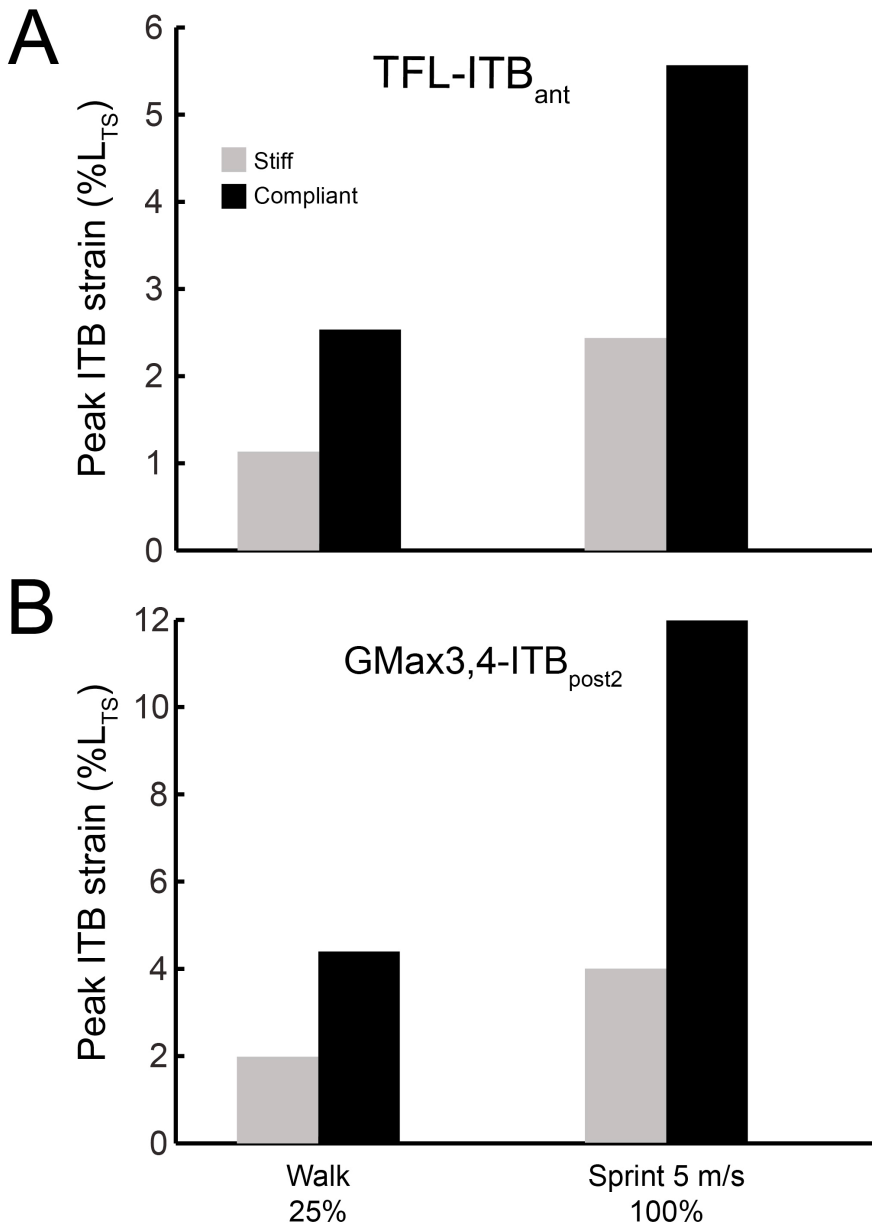

Figure 3.9. Estimates of peak ITB strain decrease by more than 50% with a 3-fold stiffer ITB force-length curve for the TFL-ITB$_{ant}$ (**A**) and GMax3,4-ITB$_{post1}$ (**B**) MTUs in walking and sprinting (5 m/s) with the indicated muscle activation levels for each gait.

Discussion

This is the first study to quantitatively characterize the 3D musculoskeletal geometry of the ITB and the inserting muscles. Detailed dissections confirmed that all TFL muscle fibers insert into the anterior ITB and that 40-70% of GMax mass inserts into the posterior ITB, indicating that substantial muscle forces are potentially transmitted to both the anterior and posterior ITB. Additionally, given the superficial position of the ITB and inserting muscles, the ITB and inserting muscles have large MAs throughout hip ranges of motion, indicating substantial length change with hip motion. In combination, these large forces and MAs indicate a substantial potential for ITB energy storage.

We used measured hip and knee moment arms to modify an existing lower limb model that included more compliant ITB properties. The modified model was combined with typical GMax and TFL EMG patterns to demonstrate a previously unrecognized role for the ITB in elastic energy storage. Analysis of the model supported our hypotheses. Forces generated by the TFL and GMax muscles stretch the ITB during walking and running, resulting in ITB energy storage in both gaits (Figure 3.8). The anterior and posterior ITB have distinct length change patterns and periods of predicted elastic energy storage because of different MAs (Figure 3.7). The TFL1,2-ITB_{ant} MTU potentially stores energy in stance phase. The GMax-ITB_{post} MTUs potentially store energy in mid to late swing phase, and estimates of posterior ITB energy storage are greater than the anterior ITB because of larger maximum muscle forces. These data also demonstrate that passive ITB energy storage is negligible, with less than 0.5 J stored in the anterior and posterior ITB MTUs when muscles are not active.

Results confirm our hypothesis that energy storage is potentially greater in running than walking. Using our model, we estimated that peak ITB energy storage is potentially eight times greater in the anterior ITB and 11 times greater in the posterior ITB in running compared to walking. By independently evaluating the effect of joint motion and muscle activation on peak ITB energy storage, our results demonstrate that the kinematic differences between walking and running are not large enough to influence ITB energy storage. The key difference between gaits is the amount of muscle activation, and hence, force required to support the body's mass and oscillate the limb faster in running versus walking.

Our study may have implications for understanding the evolution of human bipedalism. Many adaptations for bipedalism are beneficial for both walking and running, but selection for the capacity to run for long distances would have presented unique demands on the anatomy and physiology of *Homo* (see Bramble and Lieberman (2004) for review). Among these demands is the need to oscillate long and massive limbs (14% of body mass in humans compared to 9% in chimpanzees; Zihlman and Brunker, 1979) quickly and efficiently during running. During the swing phase of running, the limb must be decelerated and then reaccelerated with each step. We showed that the anterior ITB is stretched by hip extension and TFL forces during the late stance phase of running when the limb is decelerating and then shortens during swing phase. Anterior ITB recoil during swing may reaccelerate the limb, reducing the muscle work that would otherwise be provided by active hip flexion in swing. It is also feasible that the compliant ITB allows the TFL and GMax muscles to operate over more

favorable regions of their force-length and force-velocity curves, although this remains to be tested.

While the energetic cost of running is primarily determined by the force required to support the body's weight during stance (Kram and Taylor, 1990), the cost of decelerating and reaccelerating the limb during swing phase is not negligible. Kram and colleagues showed that a device which assisted the limb in initiating and propagating swing decreased the metabolic cost of walking by 10% (Gottschall and Kram, 2005) and of running by 20% (Modica and Kram, 2005), which is similar to the estimate of limb swing cost in running birds (Marsh et al., 2004). Thus, selection for reduced locomotor costs during running may have selected for traits increasing ITB energy storage in *Homo* in late stance phase that is returned in swing.

Additionally, expansion of GMax occurred in the genus *Homo* and is thought to play a role in trunk stabilization during endurance running (Lieberman et al., 2006). Our modeling results indicate that an expanded GMax may serve an additional function in human running by increasing the forces transmitted to the posterior ITB to increase its elastic energy storage capacity.

How does ITB elastic energy storage compare to the muscle work required to walk and run? Using forward dynamic simulations of walking and slow running (2 m/s), Neptune et al. (2008) and Sasaki and Neptune (2006) estimated the total positive muscle fiber and tendon work required during stance and swing phase. Comparing our estimates of peak posterior ITB energy storage in walking and running at 2.0-3.0 m/s to the total positive work required during stance phase, we find that the GMax-ITB MTUs each potentially store about 1.5% of the 70 J required in walking and 1-3% of the 115 J

in slow running assuming 95% recovery of elastic energy storage. The anterior ITB can potentially store up to 1.5% of the 17 J required during swing phase in walking and about up to 2% of the 33 J required in slow running. This analysis suggests that the elastic energy storage potential of the anterior and posterior ITB MTUs may perform similar work relative to the requirements in each phase because of the lower cost of swing versus stance phase. Additionally, while absolute ITB elastic energy storage may be greater in running, energy estimates as a proportion of the work required are more similar once we account for differences in work requirements in walking and running. Nonetheless, the proportion of work stored as elastic energy is greater in running than walking and because of higher peak energy storage in fast running and sprinting, greater energy is likely stored during these gaits.

It is important to acknowledge the limitations of our analysis. Based on experimental observations of discrete paths of strain when placing tension on the superior and inferior GMax, we assumed that GMax regions transmit force to different portions of the ITB. However, if GMax forces are transmitted to the same region of the posterior ITB, then the higher total GMax force would produce higher strains and greater energy storage in the posterior ITB. Our estimates of energy storage depend on ITB compliance. We based our ITB F-L curves on the best data available (Derwin et al., 2008). However, if ITB is stiffer, then our sensitivity analysis suggests peak ITB energy storage is decreased by more than 50% compared to a compliant ITB. Nonetheless, with a stiffer ITB, our modeling results remain consistent with the hypotheses that the ITB stores a greater magnitude of energy in running than walking. This finding also suggests that current musculoskeletal models that have stiff tendon force-length

properties may underestimate the contribution of tendons to elastic energy storage. In this study, we estimated the force generated by each muscle, at body positions corresponding to walking and running, ignoring the muscle's force-velocity (F-V) properties and assuming some level of activation. In a simulation of human running, Arnold et al. (2013) found that GMax muscle fiber velocity increases with running speed, resulting in decreased GMax muscle forces. However, the lower limb model used in this study has a number of limitations addressed previously including no ITB and a stiff tendon F-L curve, both of which may amplify the F-V effects on GMax forces during running. We are generating muscle-driven simulations, using our refined model, so that we can address these limitations in a future study.

References

Alexander, R. M. and Bennet-Clark, H. C. (1977). Storage of elastic strain energy in muscle and other tissues. *Nature (London)* **265**, 114-117.

Alexander, R. M. N. (1984). Elastic energy stores in running vertebrates. *American Zoologist* **24**, 85-94.

An, K. N., Takahashi, K., Harrigan, T. P. and Chao, E. Y. (1984). Determination of muscle orientations and moment arms. *Journal of Biomechanical Engineering* **106**, 280-282.

Andersson, E. A., Nilsson, J. and Thorstensson, A. (1997). Intramuscular EMG from the hip flexor muscles during human locomotion. *Acta Physiologica Scandinavica* **161**, 361-370.

Arnold, A. S., Salinas, S., Asakawa, D. J. and Delp, S. L. (2000). Accuracy of muscle moment arms estimated from MRI−based musculoskeletal models of the lower extremity. *Computer Aided Surgery* **5**, 108-119.

Arnold, E. M., Hamner, S. R., Seth, A., Millard, M. and Delp, S. L. (2013). How muscle fiber lengths and velocities affect muscle force generation as humans walk and run at different speeds. *Journal of Experimental Biology* **216**, 2150-2160.

Arnold, E. M., Ward, S. R., Lieber, R. L. and Delp, S. L. (2010). A model of the lower limb for analysis of human movement. *Annals of Biomedical Engineering* **38**, 269-279.

Arya, S. and Kulig, K. (2010). Tendinopathy alters mechanical and material properties of the Achilles tendon. *Journal of Applied Physiology* **108**, 670-675.

Bartlett, J. L., Sumner, B., Ellis, R. G. and Kram, R. (2014). Activity and functions of the human gluteal muscles in walking, running, sprinting, and climbing. *American Journal of Physical Anthropology* **153**, 124-131.

Biewener, A. A. (2003). Animal Locomotion. Oxford: Oxford University Press.

Birnbaum, K., Siebert, C. H., Pandorf, T., Schopphoff, E., Prescher, A. and Niethard, F. U. (2004). Anatomical and biomechanical investigations of the iliotibial tract. *Surgical and Radiologic Anatomy* **26**, 433-446.

Bramble, D. and Lieberman, D. (2004). Endurance running and the evolution of *Homo*. *Nature* **432**, 345-352.

Brand, P. W., Cranor, K. C. and Ellis, J. C. (1975). Tendon and pulleys at the metacarpophalangeal joint of a finger. *Journal of Bone and Joint Surgery* **57**, 779-784.

Butler, D. L., Grood, E. S., Noyes, F. R., Zernicke, R. F. and Brackett, K. (1984). Effects of structure and strain measurement technique on the material properties of young human tendons and fascia. *Journal of Biomechanics* **17**, 579-596.

Cruells Vieira, E., Vieira, E., Teixeira da Silva, R., dos Santos Berlfein, P., Abdalla, R. and Cohen, M. (2007). An anatomic study of the iliotibial tract. *Arthroscopy: The Journal of Arthroscopic & Related Surgery* **23**, 269-274.

Delp, S. L., Loan, J. P., Hoy, M. G., Zajac, F. E., Topp, E. L. and Rosen, J. M. (1990). An interactive graphics-based model of the lower extremity to study orthopaedic surgical procedures. *IEEE Transactions on Biomedical Engineering* **37**, 757-767.

Derwin, K. A., Baker, A. R., Spragg, R. K., Leigh, D. R., Farhat, W. and Iannotti, J. P. (2008). Regional variability, processing methods, and biophysical properties of human fascia lata extracellular matrix. *Journal of Biomedical Materials Research Part A* **84**, 500-507.

Dorn, T. W., Schache, A. G. and Pandy, M. G. (2012). Muscular strategy shift in human running: dependence of running speed on hip and ankle muscle performance. *The Journal of experimental biology* **215**, 1944-1956.

Eng, C. M., Pancheri, F. Q., Lieberman, D. E., Biewener, A. A. and Dorfmann, L. (2014). Directional differences in the biaxial material properties of fascia lata and the implications for fascia function. *Annals of Biomedical Engineering* **DOI: 10.1007/s10439-014-0999-3**.

Fredericson, M., Cookingham, C., Chaudhari, A., Dowdell, B., Oestreicher, N. and Sahrmann, S. (2000). Hip abductor weakness in distance runners with iliotibial band syndrome. *Clinical Journal of Sport Medicine* **10**, 169-175.

Gottschalk, F., Kourosh, S. and Leveau, B. (1989). The functional anatomy of tensor fasciae latae and gluteus medius and minimus. *Journal of Anatomy* **166**, 179-189.

Gottschall, J. S. and Kram, R. (2005). Energy cost and muscular activity required for leg swing during walking. *Journal of Applied Physiology* **99**, 23-30.

Gratz, C. M. (1931). Tensile strength and elasticity tests on human fascia lata. *The Journal of Bone and Joint Surgery* **13**, 334.

Gray, H., Williams, P. L. and Bannister, L. H. (1995). Gray's anatomy: the anatomical basis of medicine and surgery. Edinburgh: Churchill Livingstone.

Hamner, S. R. and Delp, S. L. (2013). Muscle contributions to fore-aft and vertical body mass center accelerations over a range of running speeds. *Journal of Biomechanics* **46**, 780-787.

Inman, V. T. (1947). Functional aspects of the abductor muscles of the hip. *The Journal of Bone and Joint Surgery* **29**, 607-619.

Jönhagen, S., Ericson, M., Nemeth, G. and Eriksson, E. (1996). Amplitude and timing of electromyographic activity during sprinting. *Scandinavian Journal of Medicine and Science in Sports* **6**, 15-21.

Kaplan, E. B. (1958). The iliotibial tract: Clinical and morphological significance. *The Journal of Bone and Joint Surgery* **40**, 817-832.

Ker, R. F., Bennett, M. B., Bibby, S. R., Kester, R. C. and Alexander, R. M. (1987). The spring in the arch of the human foot. *Nature* **325**, 147-149.

Kram, R. and Taylor, C. R. (1990). Energetics of running: a new perspective. *Nature* **346**, 265-267.

Lieber, R. L., Fazeli, B. M. and Botte, M. J. (1990). Architecture of selected wrist flexor and extensor muscles. *Journal of Hand Surgery. American Volume* **15A**, 244-250.

Lieber, R. L., Loren, G. J. and Fridén, J. (1994). In vivo measurement of human wrist extensor muscle sarcomere length changes. *Journal of Neurophysiology* **71**, 874-881.

Lieberman, D. E., Raichlen, D. A., Pontzer, H., Bramble, D. M. and Cutright-Smith, E. (2006). The human gluteus maximus and its role in running. *Journal of Experimental Biology* **209**, 2143-2155.

Maganaris, C. N. and Paul, J. P. (2002). Tensile properties of the in vivo human gastrocnemius tendon. *Journal of Biomechanics* **35**, 1639-1646.

Mann, R., Moran, G. and Dougherty, S. (1986). Comparative electromyography of the lower extremity in jogging, running, and sprinting. *The American journal of sports medicine* **14**, 501.

Marsh, R. L., Ellerby, D. J., Carr, J. A., Henry, H. T. and Buchanan, C. I. (2004). Partitioning the energetics of walking and running: Swinging the limbs is expensive. *Science* **303**, 80-83.

Mendez, J. and Keys, A. (1960). Density and composition of mammalian muscle. *Metabolism: Clinical and Experimental* **9**, 184-188.

Modica, J. R. and Kram, R. (2005). Metabolic energy and muscular activity required for leg swing in running. *Journal of Applied Physiology* **98**, 2126-2131.

Montgomery, W. H., Pink, M. and Perry, J. (1994). Electromyographic analysis of hip and knee musculature during running. *The American journal of sports medicine* **22**, 272-278.

Neptune, R. R., Sasaki, K. and Kautz, S. A. (2008). The effect of walking speed on muscle function and mechanical energetics. *Gait and Posture* **28**, 135-143.

Ober, F. R. (1936). The role of the iliotibial band and fascia lata as a factor in the causation of low-back disabilities and sciatica. *The Journal of Bone and Joint Surgery* **18**, 105-110.

Ounpuu, S., Gage, J. and Davis, R. (1991). Three-dimensional lower extremity joint kinetics in normal pediatric gait. *Journal of Pediatric Orthopaedics* **11**, 341&hyhen.

Paré, E., Stern, J. and Schwartz, J. (1981). Functional differentiation within the tensor fasciae latae. *The Journal of Bone and Joint Surgery* **63**, 1457-1471.

Powell, P. L., Roy, R. R., Kanim, P., Bello, M. and Edgerton, V. R. (1984). Predictability of skeletal muscle tension from architectural determinations in guinea pig hindlimbs. *Journal of Applied Physiology* **57**, 1715-1721.

Roberts, T. (2002). The integrated function of muscles and tendons during locomotion* 1. *Comparative Biochemistry and Physiology-Part A: Molecular & Integrative Physiology* **133**, 1087-1099.

Rolian, C., Lieberman, D. E., Hamill, J., Scott, J. W. and Werbel, W. (2009). Walking, running and the evolution of short toes in humans. *Journal of Experimental Biology* **212**, 713-721.

Sasaki, K. and Neptune, R. R. (2006). Muscle mechanical work and elastic energy utilization during walking and running near the preferred gait transition speed. *Gait and Posture* **23**, 383-390.

Stern, J. T., Jr. (1972). Anatomical and functional specializations of the human gluteus maximus. *American Journal of Physical Anthropology* **36**, 315-339.

Swanson, S. C. and Caldwell, G. E. (2000). An integrated biomechanical analysis of high speed incline and level treadmill running. *Medicine and Science in Sports and Exercise* **32**, 1146-1155.

Ward, S. R., Eng, C. M., Smallwood, L. H. and Lieber, R. L. (2009). Are current measurements of lower extremity muscle architecture accurate? *Clinical Orthopaedics and Related Research* **467**, 1074-1082.

Wickiewicz, T. L., Roy, R. R., Powell, P. L. and Edgerton, V. R. (1983). Muscle architecture of the human lower limb. *Clinical Orthopaedics and Related Research* **179**, 275-283.

Zajac, F. E. (1989). Muscle and tendon: properties, models, scaling, and application to biomechanics and motor control. *Critical Reviews in Biomedical Engineering* **17**, 359-411.

Zihlman, A. L. and Brunker, L. (1979). Hominid bipedalism: then and now. *Yearbook of Physical Anthropology* **22**, 132-162.

Chapter 4: Comparative anatomy and biomechanics of the chimpanzee fascia lata and human iliotibial band and their role in elastic energy storage

Abstract

This study tests the overarching hypothesis that the human iliotibial band (ITB) is specialized for elastic energy storage relative to the chimpanzee fascia lata (FL). To characterize the chimp FL's potential for elastic energy storage, we measured the muscle architecture and moment arms from TFL and the cranial and caudal GMax muscles of four chimpanzee cadavers. These data were used to refine a chimp lower limb musculoskeletal model, which we used with estimates of the chimp's hip and knee angles during bipedal walking to compute loading and displacement of the FL and to predict its capacity for elastic energy storage and recovery. We compared these data to analogous estimates from a human lower extremity model. Our modeling results support the hypothesis that the human ITB is anatomically derived compared to the chimp FL in ways that suggest the human ITB is specialized for elastic energy storage. Differences in both locomotor mechanics and anatomy contribute to the human ITB's greater capacity to store elastic energy compared to the chimp FL. Chimpanzees walk with a smaller range of hip flexion/extension than humans, so chimpanzee FL muscle-tendon units (MTUs) undergo smaller length changes during bipedal walking compared to human muscle-ITB MTUs. The combined mass-normalized PCSAs of the TFL and GMax muscles inserting on the human ITB are more than two times greater than the total normalized PCSA of the chimp muscles inserting on the FL, indicating a greater

capacity for ITB force transmission. Greater MTU strain along with greater muscle force-generating capacity suggests that the human ITB may store as much as 15 times more mass-specific elastic energy than the chimp FL per stride. We explore the implications of these findings for the evolution of bipedalism.

Introduction

Bipedalism appears to be the initial derived feature that set the human lineage on a separate evolutionary trajectory from the African great apes (Darwin, 1871; Haile-Selassie, 2001; Zollikofer et al., 2005). There are many hypotheses about the selective pressures that favored the origin of hominin bipedalism including reducing heat stress in open habitats (Wheeler, 1984), hand-assisted stabilization during arboreal movement (Thorpe et al., 2007), and increased ability to carry loads or use tools (Darwin, 1871; Hewes, 1964; Zihlman and Tanner, 1978). Perhaps the most widely accepted hypothesis is that natural selection favored a shift to bipedal walking from a more costly mode of quadrupedalism, such as knuckle-walking, to reduce the energetic costs of travel as climatic shifts increased the distance between food patches (Rodman and McHenry, 1980; Sockol et al., 2007). This hypothesis is supported by studies that have shown that many adaptations in the lower limb associated with bipedal locomotion, such as relatively longer limbs and shorter toes also benefit locomotor economy (Pontzer, 2007; Rolian et al., 2009).

The iliotibial band (ITB) is a unique structure in the human lower limb, derived from the fascia lata (FL) of the thigh, that may also contribute to locomotor economy. The ITB is not present in other apes and thus almost certainly evolved independently in

hominins, but its role in human locomotion is not well understood. While the human ITB has traditionally been considered a hip stabilizer (Inman, 1947; Kaplan, 1958; Gottschalk et al., 1989; Fredericson et al., 2000), we recently used a musculoskeletal model of the human lower extremity that shows that the human ITB likely stores and recovers elastic energy during walking and running (Chapter 3). We found that the tensor fascia lata (TFL) has the capacity to store 0.3-2.3 J of energy in the anterior ITB during the late stance and early swing phases, while the gluteus maximus (GMax) has the capacity to store as much as 12 J of energy in the posterior ITB during the mid to late swing phase. These findings suggest that the human ITB may have evolved, not necessarily as a mechanism for stabilizing the hip, but instead as an adaptation for increasing locomotor economy. This study tests these ideas within a broader comparative context, examining if the human ITB's ability to store and recover elastic energy or counteract adduction moments at the hip during walking is unique to humans among apes.

Chimpanzees (Hominidae: *Pan*) are a key comparative species for interpreting the derived nature of the ITB because chimps are the extant sister taxon to *Homo* (Ruvolo, 1994; Satta et al., 2000). Given the many morphological similarities between chimps and gorillas, with many differences likely resulting from the effects of size (Shea, 1985; Berge and Penin, 2004), we can infer that the last common ancestor (LCA) of *Pan* and humans resembled *Pan* in morphology and was a knuckle-walking ape with no ITB (Pilbeam, 1996; Wrangham and Pilbeam, 2001). It is also possible that the ITB was convergently lost in both gorillas and chimpanzees, but given the lack of an ITB in other apes it is most parsimonious to assume that the ITB is a human autapomorphy.

Therefore, this study compares human ITB function with chimp FL function using musculoskeletal models of the human and chimpanzee lower extremities.

The ability of the FL to store and recover elastic energy depends on the forces that it transmits, and the muscular forces transmitted to the chimp FL and human ITB during walking likely differ. However, descriptions of chimpanzee FL anatomy in the literature vary considerably and are limited by small sample sizes and methodological differences between studies (Stern, 1972; Swindler and Wood, 1973; Sigmon, 1975; Sigmon and Farslow, 1986). According to most studies, the chimp TFL inserts on the FL (Sigmon, 1974; Sigmon, 1975; Sigmon and Farslow, 1986), as it does in humans. However, compared to the human TFL, the chimp TFL is thought to be smaller and partially fused with the anteriormost portion of the cranial gluteus maximus muscle (Sigmon, 1974; Sigmon, 1975; Sigmon and Farslow, 1986). When referring to the gluteus maximus muscle in chimps, we distinguish between the cranial portion of the GMax (GMaxCr; also called gluteus maximus proprius) and the caudal portion of the GMax (GMaxCd; also referred to as ischiofemoralis). Authors agree that GMaxCr in chimps is thinner and less massive than the homologous GMax in humans (Stern, 1972; Swindler and Wood, 1973; Sigmon, 1975; Lieberman et al., 2006), but authors disagree about the insertion site of this muscle. Some claim that the chimp GMaxCr inserts on the FL (Swindler and Wood, 1973; Sigmon, 1974; Sigmon, 1975), while others report that insertion of GMaxCr on the TFL occurs in a few individuals but is an anomaly among chimps (Preuschoft, 1961; Stern, 1972). Stern (1972) states that the nonhuman ape GMaxCr inserts on the lateral femur and that insertion into the overlying ITB is a feature unique to humans among apes. The chimp GMaxCd originates on the ischial

tuberosity and is reported to insert along the femoral shaft from the gluteal tuberosity to the lateral epicondyle; this muscle is absent in humans (Stern, 1972; Sigmon, 1974; Sigmon, 1975). Thus, to estimate energy storage in the chimp FL, detailed dissections are needed to identify the force-generating capacity of the portions of GMaxCr, GMaxCd, and TFL that insert on the FL.

There have been previous efforts to estimate the muscle force-generating capacity of chimp muscles with a musculoskeletal model (O'Neill et al., 2013). However, this model has a number of limitations. The model's muscle paths were defined based on limited chimpanzee muscle moment arm data. Furthermore, the model does not include a TFL muscle and thus cannot accurately estimate FL function.

The ability of the FL to store and recover elastic energy also depends on the length changes of the FL muscle-tendon units (MTUs). MTU length changes that occur during walking depend on the MTUs' moment arms and the range of joint angles through which the limb moves. For a given joint motion, MTUs with larger moment arms will change length more than MTUs with smaller moment arms. MTU moment arms (MAs) generally vary as a function of joint angle (An et al., 1984; Hoy et al., 1990; Spoor et al., 1990), which is relevant because most comparisons of moment-generating capacity between chimps and humans are based on morphology and not direct measurements of MAs over the ranges of joint motion found in chimp and human locomotion. Though MA data are available for several chimp muscles (Thorpe et al., 1999; Payne et al., 2006), data are not available for TFL nor for the portions of GMax that insert on the FL (Payne et al., 2006). More detailed MA measurements on chimpanzees are therefore required to compare MAs of chimps and humans and to

explain how these differences affect the potential for human ITB and chimp FL energy storage.

While this study tests the hypothesis that the human ITB is specialized for elastic energy storage relative to the chimp FL, the prevailing hypothesis for ITB function is that it stabilizes the limb in the frontal plane during locomotion (Inman, 1947; Kaplan, 1958; Stern, 1972; Gottschalk et al., 1989). The transition from quadrupedalism to bipedalism in hominins required that the body's center of mass be stabilized over a smaller area of support. Selection for increased stability during locomotion may have acted on structures in bipedal hominins increasing stability in the lower limb such as the ITB. During stance, the contralateral pelvis tilts inferiorly in the frontal plane causing the center of mass to fall slightly towards the contralateral limb, which creates an adduction torque on the weight-bearing limb. Pelvic tilt can be counteracted if the muscles or passive structures in the weight-bearing limb such as the ITB generate an opposing abduction torque, causing the pelvis to tilt back towards the stance limb (Saunders et al., 1953). Previous studies have suggested that the human ITB may play a role in controlling pelvic tilt during the stance phase of walking and running (Inman, 1947; Kaplan, 1958; Gottschalk et al., 1989), but this lateral stability hypothesis has never been tested with a musculoskeletal model.

In this study, we tested the overarching hypothesis that the human ITB is specialized for elastic energy storage relative to the chimpanzee FL. To characterize the chimp FL's potential for elastic energy storage, we measured the masses, fiber lengths, and moment arms of the TFL and the cranial and caudal GMax in five chimpanzee cadavers. These data were used to refine a 3D musculoskeletal model of the

chimpanzee hindlimb that includes the 3D geometry of the bones, the attachments of the muscles, and the isometric force-generating properties of the muscles and tendons (O'Neill et al., 2013). The model was combined with kinematic descriptions of joint motion during bipedal walking to compute loading and stretch of the FL and to predict its capacity for elastic energy storage and recovery. Results from the chimp model were compared to results from a human model (Chapter 3) and used to test three specific hypotheses pertaining to elastic energy storage: first, that the muscles inserting on the human ITB have the potential to transmit larger forces to the ITB than the muscles inserting on the chimp FL (H1); second, that those larger muscle forces in humans have a greater potential to stretch the ITB compared to the chimp FL over the body positions corresponding to bipedal walking (H2); and, third, that these features give the human ITB the potential to store a greater amount of elastic energy during bipedal walking compared to the chimp FL (H3). We also used the chimp and human models to examine whether the human ITB is specialized for stabilizing the hip in the frontal plane relative to the chimp FL.

Materials and methods

Moment arm measurements

Detailed measurements of moment arms and muscle anatomy were collected from four fresh-frozen chimpanzee cadaveric pelvises (Table 4.1) obtained from the Texas Biomedical Research Institute (San Antonio, TX). MTU moment arms for the portions of TFL, GMaxCr, and GMAXCd inserting on the FL were determined for hip

flexion/extension, hip rotation, hip adduction/abduction, and knee flexion/extension using the tendon excursion method (Brand et al., 1975; An et al., 1984).

In each specimen, skin and subcutaneous fat were dissected from the gluteal region and thigh to expose the muscle origins and insertions. Subcutaneous fat was carefully removed from the surface of the fascia lata (FL), and its insertion on the tibia was exposed distally. Each muscle was separated into regions based on origins and insertions (Table 4.2). Muscle regions were each represented by a Kevlar thread path for tendon excursion measurements (Figure 4.1). Screw eyes were inserted in the origin and insertion of each muscle region (Table 4.2). We anchored Kevlar thread to a screw eye located at the MTU's insertion, routed the thread through plastic tubing to a screw eye located at the MTU's origin, and attached it to one of two cable-extension position transducers (PTX101, Celesco, Canoga Park, CA) that measured length changes with an accuracy of ±0.32 mm while applying a tension of 1.4 or 2.8 N. The plastic tubing ensured a repeatable path and decreased friction between the thread and underlying tissues. The 3D coordinates of each muscle path were digitized relative to segment coordinate systems, using a motion tracking system, and were used to accurately recreate the paths in the musculoskeletal model. We placed marker pairs in the anterior and posterior FL and tracked their locations with high-speed video (Photron USA Inc., San Diego, CA) while moving the limb through its ranges of hip and knee motion. These data were used to determine the hip and knee angles at which the anterior and posterior FL began to stretch.

Each specimen was mounted in a custom frame as described in Chapter 3, which allowed independent control of hip rotation, hip flexion/extension, hip

abduction/adduction, and knee flexion/extension after proper specimen alignment (Figure 4.2) Briefly, the pelvis was mounted on a table using threaded fixation half-pins (IMEX Veterinary, Inc., Longview, TX). The femur was fixed to the inner of two concentric rings mounted on a rotating cart. Rotating the inner ring relative to the outer ring rotated the femur. Rotating the cart flexed and extended the hip (when the specimen was mounted for hip flexion) and abducted and adducted the hip (when the specimen was mounted for hip adduction). Vertical translation of the rings on the cart adducted or flexed the hip when mounted for hip flexion or adduction, respectively.

Electromagnetic receivers were rigidly attached to the pelvis, femur and tibia, and were used to track the segments' positions and orientations in space using a motion tracking system (Polhemus Fastrak, Colchester, VT). Joint angles were computed from receiver data using custom LabView software (National Instruments, Austin, TX). Anatomical landmarks on each segment were marked with screws and digitized to define each segment's coordinate system based on anatomical axes. To find the hip joint center, the coordinates of the knee joint center (the midpoint between the medial and lateral epicondyles) were recorded while moving the femur through a range of hip flex/extension and hip ab/adduction angles. A sphere was fit to this cloud of knee joint center points, and the center of this sphere was defined as the hip joint center and the origin of the femoral coordinate system.

Specimen alignment was performed using LabView^{TM} (National Instruments, Inc.) with real-time feedback of the relevant segment positions and orientations as described in Chapter 3. After aligning the specimen, we ensured that coupling of hip flexion, hip

rotation, and hip adduction was less than 2° hip flexion, 2° hip adduction and 4° hip rotation over the hip adduction and flexion ranges of motion.

MTU excursion and joint angle data were simultaneously sampled at 10 Hz using a National Instruments BNC-2090 analog-to-digital converter. While MAs were measured in one plane of joint movement, the other planes were locked at the approximate joint positions found in midstance during bipedal walking (hip flexion = 35°, hip rotation = 0°, hip adduction = -15°, knee flexion = 45°) (Lee et al., 2013). Lengthening excursion versus joint angle data were fit with a fourth order polynomial and the polynomial derivative used to estimate MAs. A minimum of five trials was collected for each condition from each muscle, and MAs averaged across trials.

Comparative muscle anatomy and muscle architecture

We measured muscle architecture of the chimp TFL, GMaxCr, and GMaxCd to estimate the force-generating capacity of each muscle region. After measuring MAs, each muscle region was carefully dissected to its insertion on the femur or fascia lata (FL). Blunt dissection was used to identify and separate the muscle fibers inserting on the FL from fibers inserting in the femur. Insertion on the FL was confirmed by placing traction on the separated region and ensuring that force was transmitted distally through the FL and not to the tendon inserting in the femur. The masses of the portions inserting on the FL and femur were measured. The total mass of each muscle was calculated as the sum of all regions. These data were compared to the relative masses of the human TFL and GMax inserting on the ITB and femur reported in chapter 3. After measuring muscle length (L_M), two fascicles were dissected from each muscle region and their lengths measured and averaged to obtain fascicle length (L_f) for the region. Fascicle

length-to-muscle length ratio (L_f/L_M) was calculated by dividing muscle length by average fascicle length. Surface pennation angle was measured with a goniometer as the angle between the fascicles and the distal tendon. The physiological cross-sectional area (PCSA) of each muscle region was calculated using the following equation (Powell et al., 1984):

$$PCSA = \frac{M}{\rho \cdot L_f} \quad (1)$$

where M is the region's muscle mass, L_f is the region's average fascicle length, and ρ is muscle density (1.056 g/cm^3; (Mendez and Keys, 1960). In the musculoskeletal model used here pennation angle is used to relate muscle force to tendon force to calculate their respective length changes, so pennation angle was not included in the PCSA calculation. Because the muscle tissue was unfixed, sarcomere lengths could not be accurately measured to normalize fascicle lengths. Muscle masses were normalized by body mass to make comparisons between chimps and humans. Human muscle fiber lengths and pennation angles were obtained from fixed cadaveric lower limbs (n=3) reported in chapter 3, while masses of each muscle region were measured from fresh cadaveric limbs (n=5) used for moment arm measurements. The proportions of GMax and TFL muscle fibers inserting on the ITB were measured from a subsample of the fresh cadaveric limbs (n=2). PCSA was scaled to (body mass)$^{2/3}$ assuming geometric similarity. Because body mass was not available for the fixed human specimens, the average body mass of similarly-aged cadavers was used (Ward et al. 2009). Architectural parameters were compared between chimps and humans using a t-test. All data are presented as mean ± s.e.m, with a p-value <0.05 considered significant.

Representation of MTU paths in the musculoskeletal model

We modified paths of the TFL and GMax MTUs in the musculoskeletal model reported by O'Neill et al. (2013) to match our digitized muscle attachments, regional paths, and moment arm data (Figure 4.3). Using SIMM (*Software for Interactive Musculoskeletal Modeling*, v7.0, MusculoGraphics, Santa Rosa, CA), we created 2 paths for TFL, 1 path for GMaxCr, and 2 paths for GMaxCd. For GMaxCr and GMaxCd, we created two additional muscle paths to represent regions inserting on the femur, but the focus of this paper is the regions inserting in the FL. MTUs were represented as line segments spanning from origin to insertion and were constrained by "via" points (points through which a muscle is constrained to act) and wrap objects to replicate the anatomical structures near each muscle region. The skeletal segments in the model were re-oriented to match the segment coordinate systems used in our MA experiments. The experimentally measured MAs were used to adjust the model's paths and verify their accuracy.

Although multiple muscle paths were created and analyzed to gain insight into FL-MTU 3D anatomy, paths were combined to represent the three major paths of FL force transmission that we observed in our experiments, including the anterior FL (TFL1&2 combined as TFL-FL_{ant1} and GMaxCr-FL_{ant2}) and the posterior FL (GMaxCd3&4; GMaxCd-FL_{post}). Each path was adjusted to yield average MAs of the combined MTUs.

Active and passive force-length curves were scaled to each FL MTU path using two key parameters, maximum isometric force (F_{max}) and optimal fiber length (L_{opt}). We used measured fascicle lengths for L_{opt}, and we calculated F_{max} as the product of regional PCSA and the muscle specific tension of 31.5 N/cm^2 used in O'Neill et al.

(2013). F_{max} and tendon slack length (L_{TS}) were used to scale each MTU's "tendon" force-length curve. The tendon force-length curves were created using human ITB stress-strain data reported in Derwin et al. (2008). Measures of FL width and thickness were used to normalize the ITB stress values to average FL cross-sectional area. Tendon slack lengths were chosen for each MTU such that the FL began to stretch passively at hip and knee angles consistent with our experimental measurements. We verified that these L_{TS} values allow the muscles in our model to generate force over functional ranges of motion.

The capacity for FL energy storage during bipedal walking

We used our model along with joint kinematics and EMG activations to estimate the FL's ability to store and recover elastic energy during bipedal walking. First, we calculated the origin-to-insertion lengths of the MTUs at hip and knee angles corresponding to chimp bipedal walking (Lee et al., 2013). We identified periods of the stride when MTUs were near maximum length and also likely active (Stern and Susman, 1981), and we assumed that peak strains in FL_{ant} or FL_{post} would occur at these times. Next, we separated the MTU lengths into FL lengths and muscle fiber lengths by independently activating each MTU in the model and solving for the lengths at which the muscle force and FL force were equivalent, accounting for pennation angle. We set each muscle's activation to 25% (of its maximum activation) to assess FL strains during walking. Finally, we used FL force (F_{FL}) and FL length change (ΔL_{FL}) relative to L_{TS} to estimate elastic energy (E):

$$E = \tfrac{1}{2} F_{FL} \Delta L_{FL} \quad (2)$$

following Alexander (1984). Peak energy storage in the chimp FL was compared to estimates of mass-specific peak energy storage in the human ITB (normalized by model's estimated body mass of 83 kg) derived from the model reported in Chapter 3. In order to estimate the maximum energy storage capacity of the chimp FL and human ITB, energy storage estimates were also compared when the muscles were maximally activated.

The role of the FL in lateral stability

To assess whether the human ITB is specialized for lateral stability during stance phase compared to the chimp FL, we compared the maximum hip abduction moments generated by the FL and ITB MTUs when the muscles are fully activated at the joint positions found in midstance. These maximum abduction moments were compared to the total abduction moment generated by the muscles inserting in the femur. In addition, the total passive abduction moment at midstance were also compared. Moments were normalized by body mass and femur length to compare between chimp and human.

Figure 4.1. Posterolateral view of the chimpanzee hindlimb mounted in the custom frame with suture paths for tensor fascia lata (TFL1 and TFL2), the anterior region of the cranial GMax (GMaxCr1), and caudal GMax (GMaxCd3 and GMaxCd4).

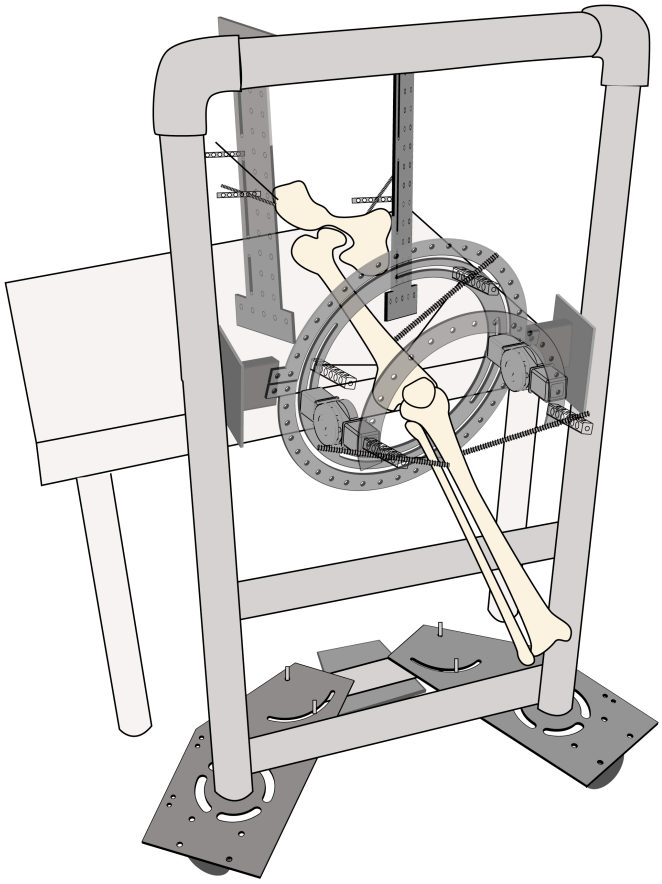

Figure 4.2. The specimen was mounted in a custom frame, comprising a fixed table for securing the pelvis, a rotating cart for moving the femur through a range of hip flex/extension and ab/adduction angles, and a set of concentric rings for rotating the femur, following Arnold et al. (2000). The cart consisted of two vertical support posts each mounted on a wheeled baseplate with a ball caster mounted on a rod between them. The limb is shown here with its pelvis mounted for hip ab/adduction, which is achieved by rotating the cart.

Table 4.1. Demographic information for the four chimpanzee cadaveric limbs used in this study.

Specimen number	Sex	Age (years)	Height (cm)	Weight (kg)	Cause of death
1	F	27	137.6	60.0	Heart problems
2	M	23	142.2	81.0	Heart problems
3	F	42	128.2	52.0	Heart problems
4	F	45	124.4	48.0	Heart and kidney problems

Table 4.2. Origin and insertion of MTU paths inserting on the FL used in moment arm measurements.

MTU	Origin	Insertion
TFL1	Anterior ilium 1.5 cm medial to ASIS	Proximal lateral tibia, 3 cm posterior to tibial tuberosity
TFL2	Anterior ilium 3.5 cm medial and 3 cm inferior to ASIS	Proximal lateral tibia, 3 cm posterior to tibial tuberosity
GMaxCr1	Posterior ilium, 1 cm medial and 1.5 cm inferior to posterior superior iliac spine	Distal femur 1 cm anterior to lateral epicondyle
GMaxCd3	Proximal ischial tuberosity	Distal femur 1 cm anterior to lateral epicondyle
GMaxCd4	Distal ischial tuberosity	Distal femur 1 cm anterior to lateral epicondyle

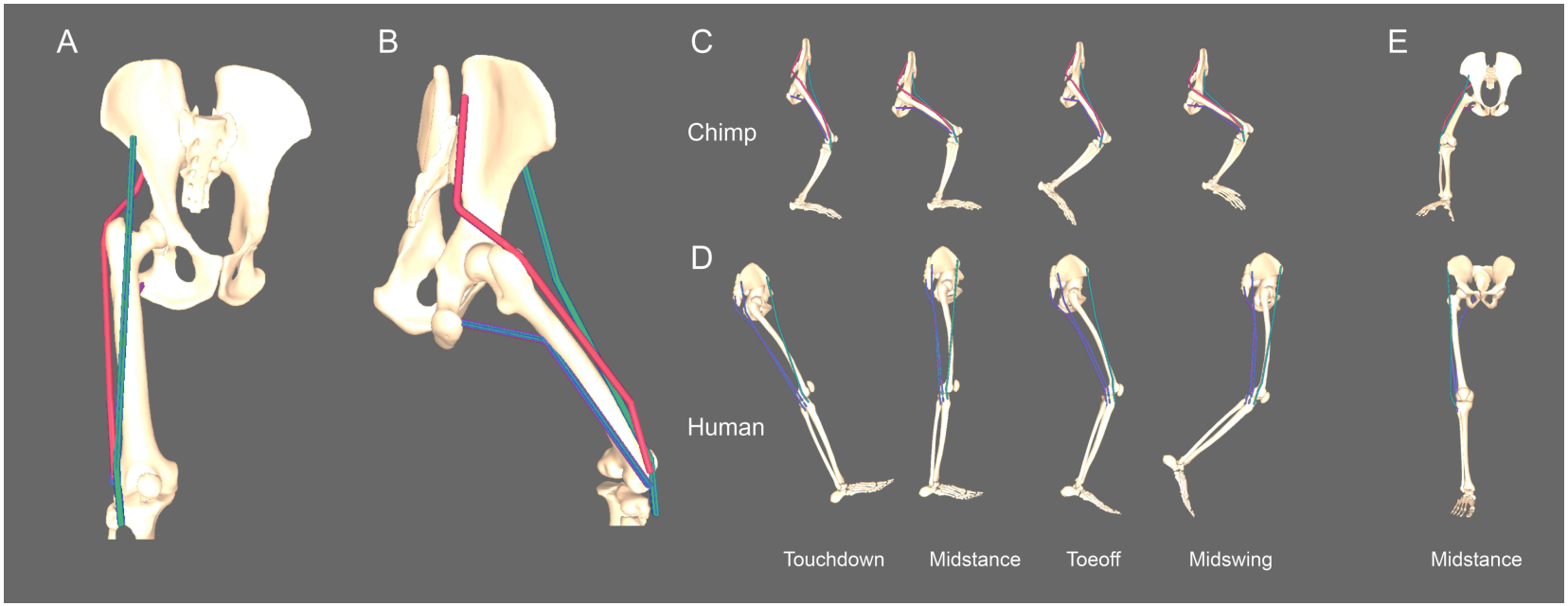

Figure 4.3. A: Anterolateral view of the chimp lower extremity model modified from (O'Neill et al., 2013) showing the TFL-FL_{ant1} MTU (green). B: Posterolateral view of the chimp model showing the GMaxCr-FL_{ant2} (red), and GMaxCd-FL_{post} (blue) MTUs. C: Lateral view of the chimp model showing FL MTUs during touchdown, midstance, toeoff, and midswing during bipedal walking. D: Lateral view of the human model from chapter 3 showing ITB MTUs during bipedal walking. E: Anterior view of the chimp (top) and human (bottom) models during midstance showing the abducted posture of the chimp limb during bipedal walking.

Results

Comparative muscle architecture

Examination of human ITB and chimpanzee FL anatomy confirmed that muscles inserting on the human ITB have the potential to transmit substantially larger forces to the ITB than muscles inserting on the chimp FL. Dissections of the chimp TFL, GMaxCr, and GMaxCd revealed that portions of all three muscles insert directly on the fascia lata. Similar to the human TFL, all chimp TFL muscle fibers insert in the anterior fascia lata. However, the force-generating capacity of the human TFL is greater than the chimp TFL. In particular, the normalized PCSA of the human TFL (0.23 ± 0.01 $cm^2/kg^{2/3}$) is nearly 4 times greater than the normalized chimp TFL PCSA (0.06 ± 0.03 $cm^2/kg^{2/3}$) (Figure 4.4A) because the human TFL has shorter fibers, relative to muscle length, than the chimp TFL ($p<0.05$; Figure 4.4B). Consistent with previous findings (Sigmon, 1974; Sigmon, 1975; Sigmon and Farslow, 1986), dissections confirmed that the anterior region of the chimp GMaxCr is fused distally with TFL (Figure 4.5). However, this region of GMaxCr that inserts in the anterior FL is relatively small, comprising less than 6% of the total chimp GMaxCr mass (Table 4.3). By contrast, approximately 50% of the human GMax mass inserts in the ITB. The normalized PCSA of this portion of the human GMax inserting on the ITB is more than ten times greater than the normalized PCSA of the chimp anterior GMaxCr inserting on the FL (0.72 ± 0.13 $cm^2/kg^{2/3}$ vs. 0.05 ± 0.03 $cm^2/kg^{2/3}$; $p <0.05$). When combined, the normalized PCSAs of the chimp TFL and GMaxCr inserting on the anterior FL is 0.11 $cm^2/kg^{2/3}$ while the normalized PCSA of the human TFL inserting on the anterior ITB is 0.18 $cm^2/kg^{2/3}$. The superficial fibers of the chimp GMaxCd (approximately 24% of the total

GMaxCd mass) insert in the posterior FL. The normalized PCSA of this muscle region is less than half as large as the normalized PCSA of the human GMax that inserts in the posterior ITB (0.28 ± 0.05 $cm^2/kg^{2/3}$ vs. 0.72 ± 0.13 $cm^2/kg^{2/3}$; $p < 0.05$). In total, the normalized PCSA of the human TFL and GMax portions inserting on the ITB is more than two times greater than the total normalized PCSA of the chimp muscles inserting on the FL (0.95 ± 0.13 $cm^2/kg^{2/3}$ vs. 0.39 ± 0.00 $cm^2/kg^{2/3}$; Figure 4.4A), indicating a relatively greater capacity for ITB force transmission compared to the chimp FL.

MTU length changes during bipedal walking

The FL MTUs in our chimp model undergo length changes during bipedal walking that are smaller than the length changes of the ITB MTUs in our human model (Figure 4.7). These differences in the MTU excursions are not simply a result of differences in limb lengths. Rather, these data reflect the moment arms of the FL MTUs (Figure 4.6), the moment arms of the muscle-ITB MTUs (see Chapter 3 figures 3.4&3.5), and measured changes in hip and knee angles during walking.

Moment arms of the chimp TFL-FL_{ant1}, GMaxCr1-FL_{ant2}, and GMaxCd3,4-FL_{post} predicted by our model are consistent with results from our tendon excursion measurements (Figure 4.6). The chimp TFL-FL_{ant1} MTU has a knee extension MA, although this knee extension MA is small when the knee is flexed (Figure 4.6C). With its small hip flexion MA (Figure 4.6D) and its large hip abduction MA (Figure 4.6E), the anterior GMaxCr in chimps is more similar in function to the TFL (Figures 4.6A,B) than to the posterior GMaxCr, which has a relatively large hip extension MA and a negligible hip ab/adduction MA.

The FL MTU moment arms and the hip and knee angles during bipedal walking determine the chimp FL MTU length changes (Figure 4.7). TFL-FL_{ant1} stretches in late stance when the hip is extending. GMaxCr-FL_{ant2} does not stretch in late stance but instead stretches in late swing when the hip is adducting. GMaxCd-FL_{post} stretches in early to mid stance and stretches again in early to mid swing when the hip flexes. EMG recordings from chimps confirm that TFL, GMaxCr, and GMaxCd are active when the MTU is stretched or at its maximum length (Stern and Susman, 1981).

Because chimps extend their hips very little during bipedal walking compared to humans, their FL MTUs undergo smaller length changes than human ITB MTUs throughout the gait cycle (Figure 4.8). The chimp TFL-FL_{ant1} stretches less than the human TFL-ITB_{ant1} as the hip extends in late stance due its smaller hip flexion MA (slope of the line in Figure 4.8A vs 4.8D) and the reduced hip flexion/extension excursion in chimps. Similarly, the chimp GMaxCr-FL_{ant2} undergoes very little length change during bipedal walking because of its small hip flexion MA.

The capacity for FL energy storage during bipedal walking

Because chimp FL MTUs undergo relatively small length changes during bipedal walking, and because the force-generating capacity of chimp muscles inserting on the FL is just a small fraction of the capacity of human muscles inserting on the ITB, the chimp FL has a reduced capacity for energy storage compared to the human ITB (Figure 4.9). The chimp FL's average cross-sectional area (CSA) is smaller than the human ITB's CSA (6.7 ± 1.8 mm^2 vs. 15.7 ± 5.1 mm^2), making the chimp FL in our model less stiff than the human ITB (Chapter 3). Consequently, the chimp FL stretches more per unit force. However, peak FL strains during isometric contractions are lower

in the chimp FL than in the human ITB because the chimp FL transmits less force. Also, peak FL strains are likely lower in the chimp anterior FL (around 1.5% strain) than in the posterior FL (3.6% strain), assuming the same activation level in anterior and posterior muscles, because of the lower force-generating capacity of the anterior muscles.

When muscles are assumed to be activated 25% during walking, peak mass-specific energy storage is lower in all chimp FL MTUs compared to the human ITB MTUs (Figure 4.9B). Mass-specific energy stored in the posterior ITB is over 15 times greater than the mass-specific energy stored in the posterior FL. Mass-specific energy stored in the anterior ITB is 5 times greater than that stored in the anterior FL. If we assume maximum activation in the muscles inserting in the ITB and FL, the difference in ITB and FL mass-specific energy storage increases with 6 times greater energy storage in the anterior ITB and 20 times greater energy storage in the posterior ITB compared to the anterior and posterior FL (Figure 4.9B).

The normalized maximum hip abduction moment transmitted in the human ITB is not substantially greater than the hip abduction moment transmitted in the chimp FL at midstance (Figure 4.10). Additionally, the ITB MTU with the greatest force-generating capacity, GMax3,4-ITB_{post2}, generates an adduction moment. Thus, the normalized (and absolute) net abduction moment of the ITB MTUs is actually smaller than the net abduction moment of the FL MTUs. Considering just the ITB MTUs with hip abduction MAs, TFL-ITB and GMax1,2-ITB transmit an abduction moment of -0.42 Nm/kgm at midstance, which is 10.3% of the total maximum hip abduction moment generated by muscles inserting on the ITB and femur. All chimp FL MTUs have hip abduction MAs at

midstance and the normalized hip abduction moment transmitted to the chimp FL is about 40% lower than the human TFL- and GMax1,2-ITB moment. The chimp FL MTUs transmit 7.2% of the total maximum abduction moment generated at midstance. The maximum abduction moment transmitted in the ITB does not vary with ITB stiffness.

The passive abduction moment at midstance is two times greater in the human versus chimp, but is negligible in both species (human: -0.017 Nm/kgm vs. chimp: -0.008 Nm/kgm).

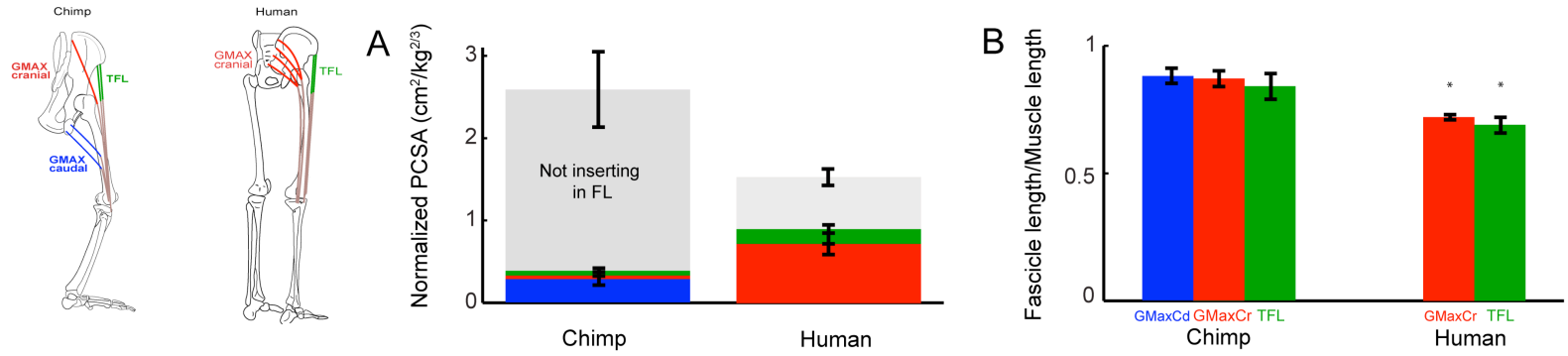

Figure 4.4. A: Normalized muscle PCSA (PCSA/BM$^{2/3}$) in the portions of the TFL (green), GMaxCr (red), and GMaxCd (blue) muscles inserting in the FL or ITB compared to the total normalized PCSA of the muscle regions not inserting in the FL or ITB. B: Fiber length to muscle length ratio in the muscles inserting in the FL and ITB. Asterisks indicate a significant difference between the chimp and human TFL and GMaxCr muscles.

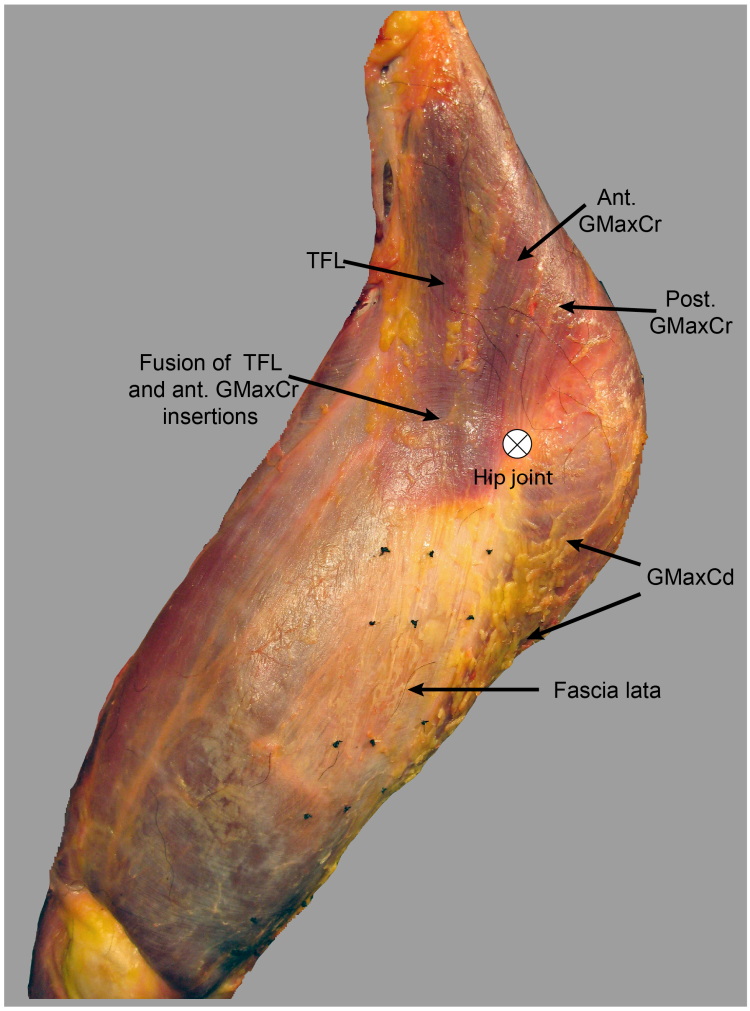

Figure 4.5. Lateral view of the chimpanzee hip showing the distal fusion of the TFL and anterior GMaxCr muscle fibers proximal to where they insert in the FL.

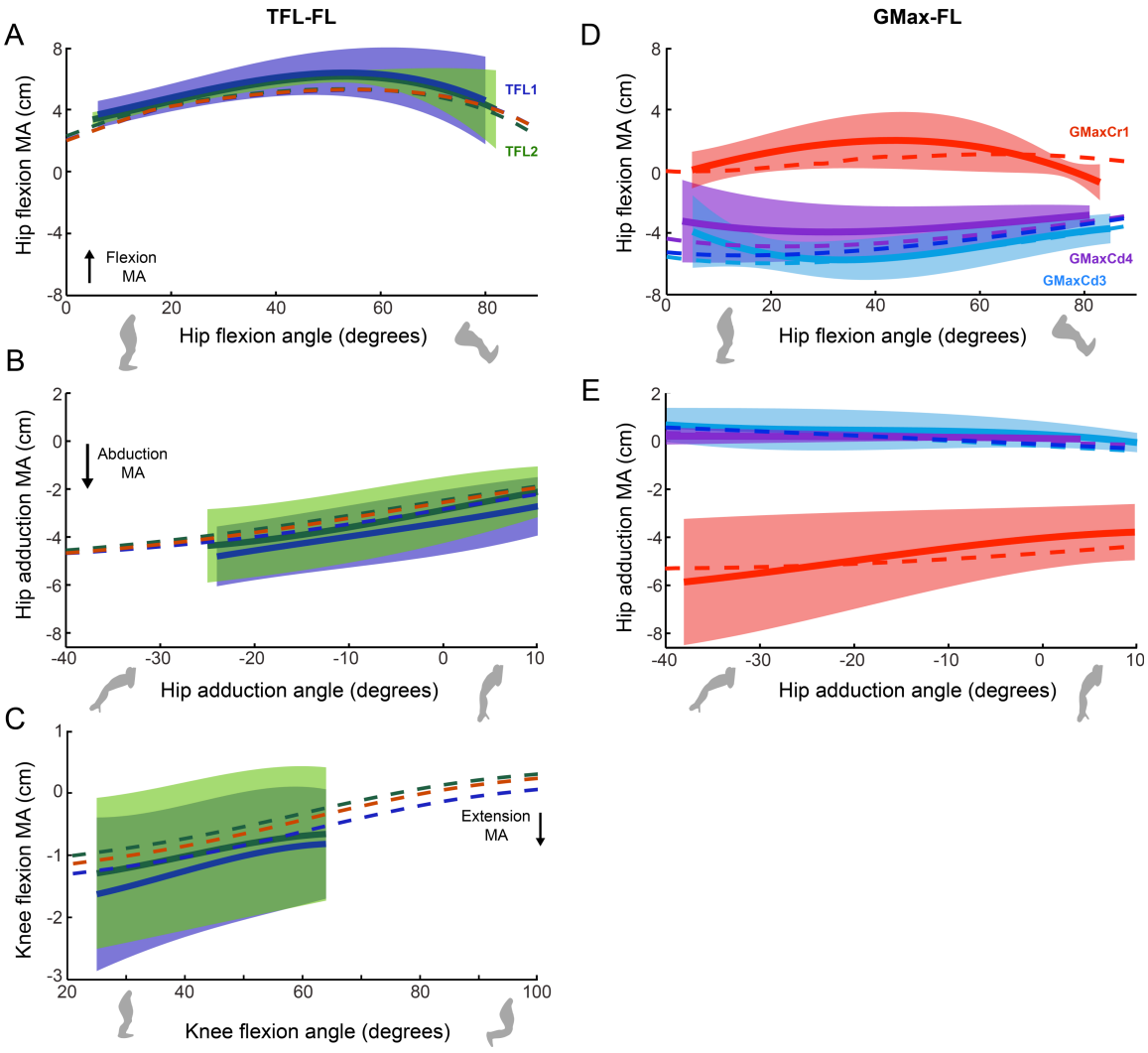

Figure 4.6. The moment arms of the MTUs inserting in the FL in the modified chimp model are consistent with experimental moment arm measurements. A: Hip flexion MA as a function of hip flexion/extension for TFL1- (green) and TFL2-FL_{ant1} (blue; shaded regions showing average across subjects). Dashed lines indicate modified model's TFL1- and TFL2-FL_{ant1} MAs and combined TFL-FL_{ant} (red) MAs. TFL-FL_{ant} MAs are shown for hip abduction/adduction (B) and knee flexion/extension (C). D: Hip flexion/extension MAs as a function of hip flexion/extension for GMaxCr1-FL_{ant2} (red) and GMaxCd3- (blue) and GMaxCd4- FL_{post} (purple). Shaded regions show average across specimens. Dashed lines indicate modified model's MAs for GMaxCr1-FL_{ant2} and GMaxCd3- and GMaxCd4- FL_{post} and GMaxCd-FL_{post} MAs (dark blue). E: GMaxCr1-FL_{ant2} and GMaxCd3- and GMaxCd4- FL_{post} abduction/abduction MAs.

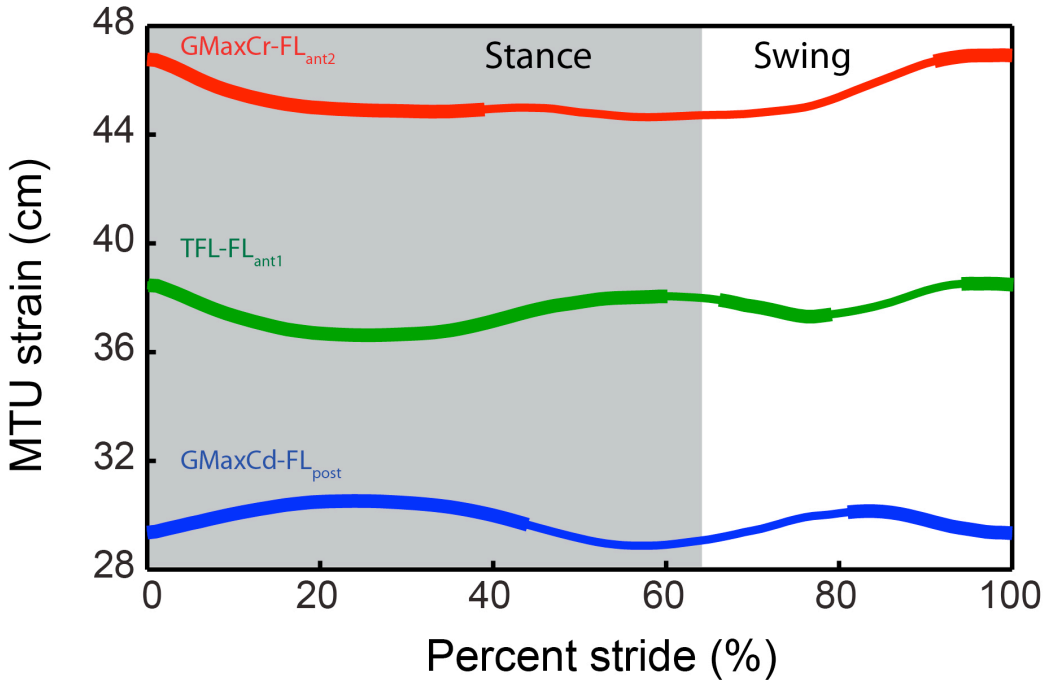

Figure 4.7. TFL-FL_{ant1}, GMaxCr-FL_{ant2}, and GMaxCd-FL_{post} MTU length during a stride of bipedal walking. Thickened portions of each curve denote period in stride when muscles are active as recorded in Stern and Susman (1981).

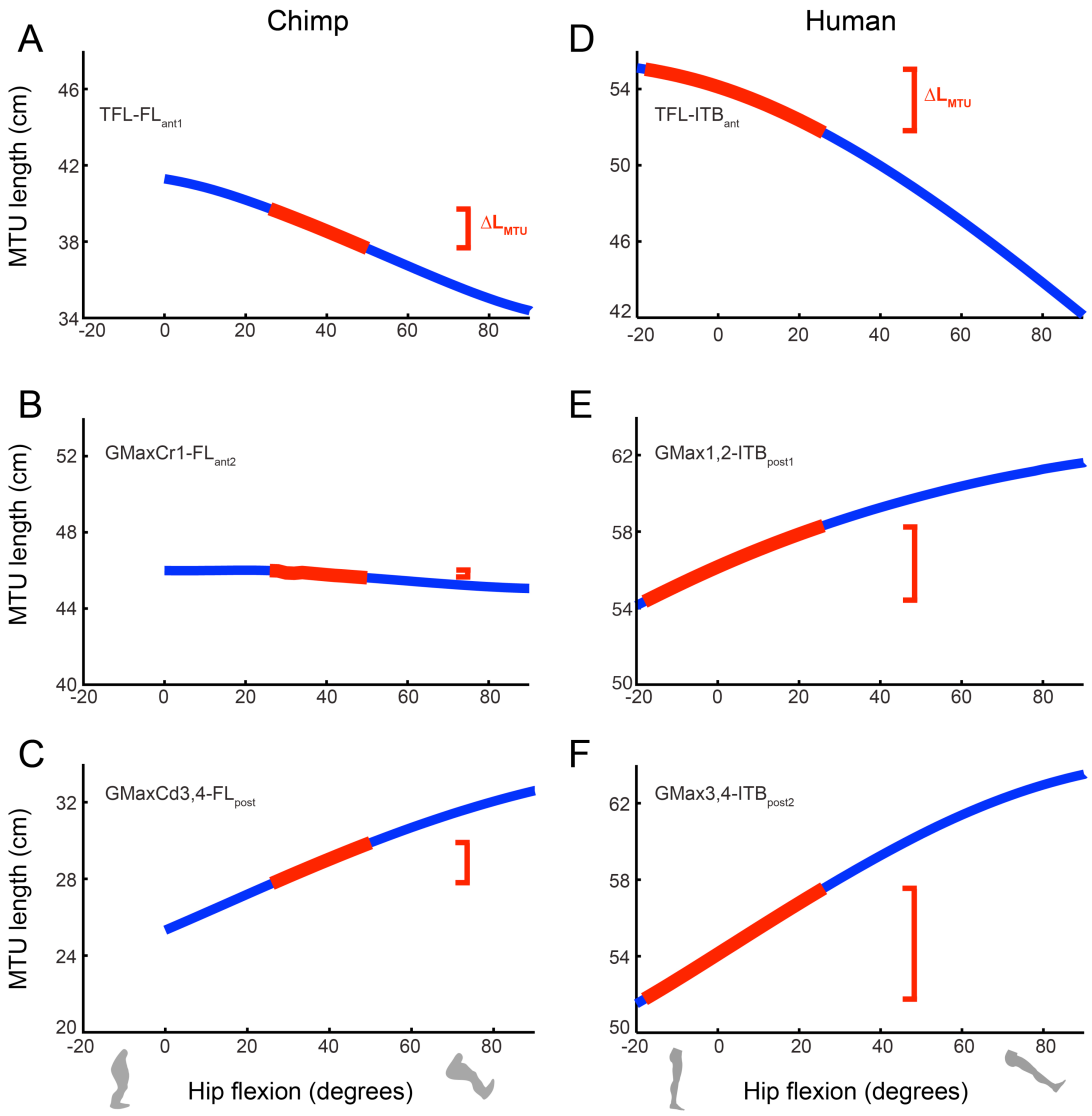

Figure 4.8. MTU length as a function of hip flexion in the chimp FL MTUs (A-C) and human ITB MTUs (D-F). The thickened red region on the curve shows the range of hip flexion/extension angles during bipedal walking, which is lower in chimps compared to humans. The bracket to the right of the curve shows the amount of MTU length change occurring during bipedal walking that is due to changes in hip flexion/extension. The slope of the curve is equivalent to the moment arm of the MTU.

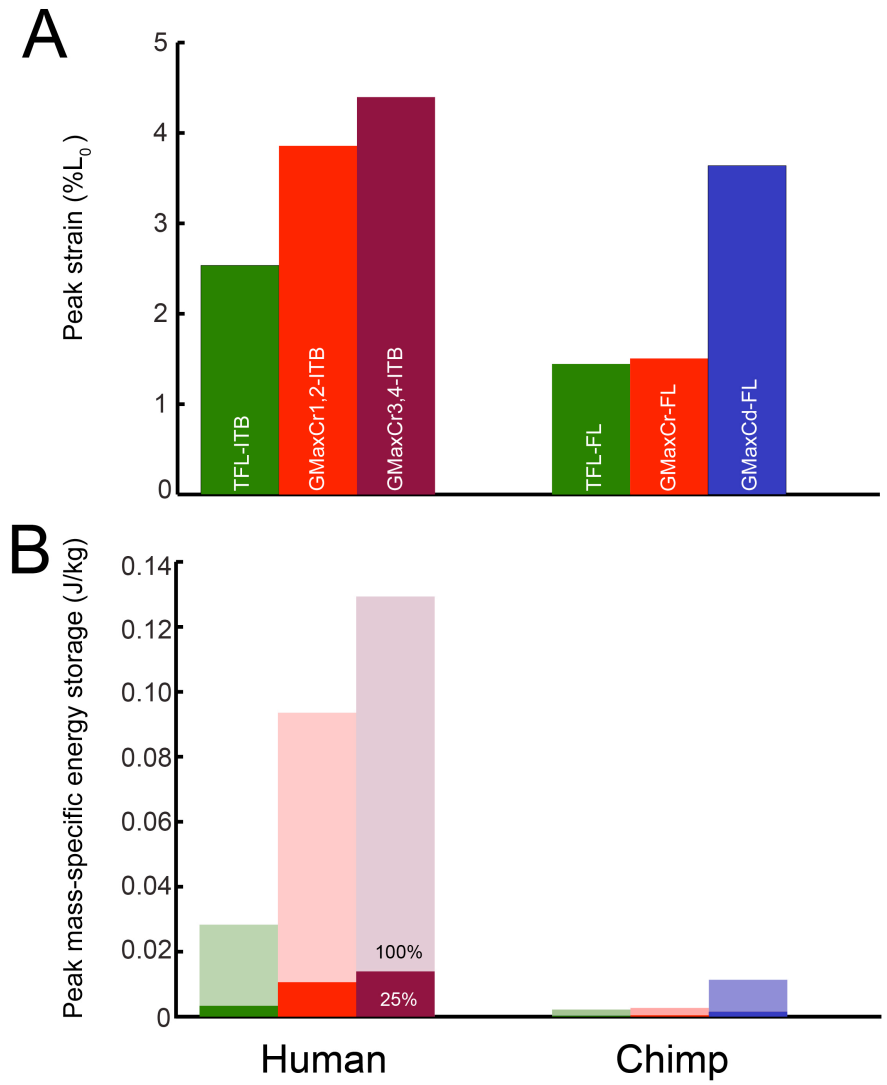

Figure 4.9. A: Peak chimp FL and human ITB MTU strain when the muscles are activated at 25% of maximum. B: Peak elastic energy storage in the human ITB and chimp FL MTUs during bipedal walking when the muscles are activated at 25% of maximum (dark bars) and 100% of maximum activation (light bars). Peak energy storage is greater in all ITB regions compared to the chimp FL for both activation levels.

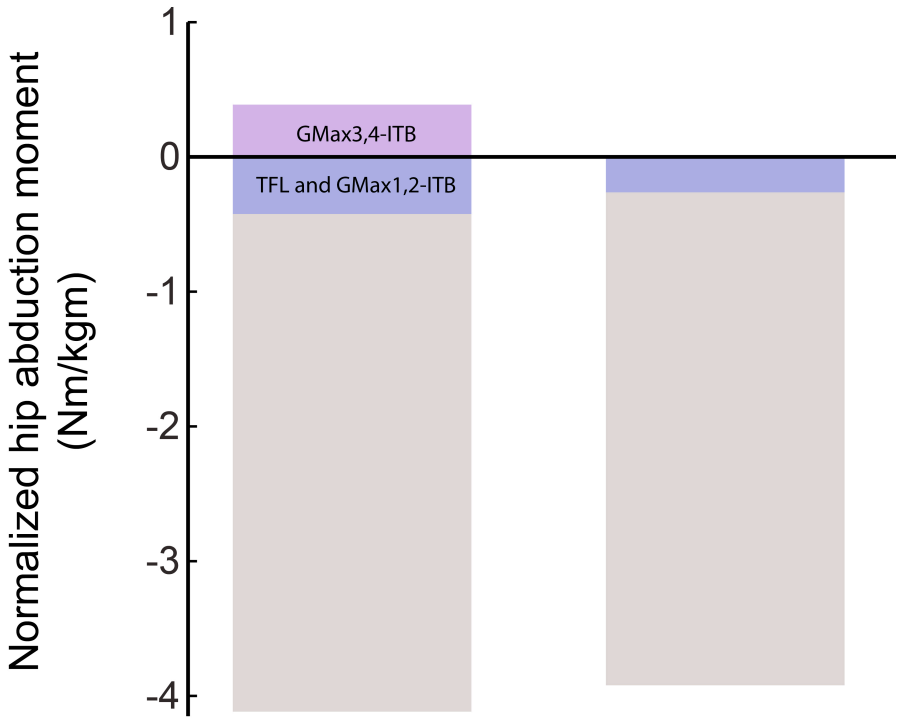

Figure 4.10. The normalized maximum hip abduction moment transmitted to the ITB and FL (lavender) relative to the maximum hip abduction moment transmitted to the femur. Hip abduction MAs are negative and the GMax3,4-ITB MTU has a positive hip adduction moment arm.

Table 4.3. Muscle architecture of the chimpanzee tensor fascia lata (TFL), cranial gluteus maximus (GMaxCr), and caudal gluteus maximus (GMaxCd) muscles.

Muscle	Mass (g)	Fascicle length[§] (cm)	Pennation angle (degrees)	PCSA[¥] (cm^2)
TFL[*]	10.8 ± 3.6	121.8 ± 1.5	1.7 ± 1.7	1.0 ± 0.7
GMaxCr1[*]	12.1 ± 4.0	107.2 ± 6.0	5.0 ± 2.9	0.9 ± 0.6
GMaxCr2	96.2 ± 24.5	85.2 ± 8.9	22.3 ± 6.7	11.0 ± 2.1
GMaxCr3	101.9 ± 30.3	85.3 ± 12.4	22.3 ± 6.7	10.7 ± 5.2
GMaxCd1	102.9 ± 29.1	123.0 ± 3.8	18.3 ± 3.3	8.7 ± 2.6
GMaxCd2	111.9 ± 43.7	170.0 ± 20.0	18.3 ± 1.7	6.7 ± 2.9
GMaxCd3[*]	26.4 ± 7.2	178.7 ± 11.3	16.7 ± 3.3	1.7 ± 0.3
GMaxCd4[*]	32.6 ± 6.8	149.0 ± 19.7	16.7 ± 1.7	2.8 ± 0.5

Data are expressed as mean ± s.e.m.

[¥]Pennation angle is not included in the PCSA calculation since our SIMM model multiplies PCSA, specific tension, and pennation angle to determine peak muscle-tendon force.

[*]Muscle region inserts on the FL

Discussion

To explore the function of the chimp FL relative to the human ITB, we made detailed measurements of chimp TFL, GMaxCr, and GMaxCd muscle architecture, FL anatomy, and FL MTU moment arms on the largest published chimp sample to date. We incorporated these data into an existing chimp musculoskeletal model to estimate the chimp FL's capacity to store and recover elastic energy during walking. The results support the hypothesis that the human ITB is anatomically derived compared to the chimp FL in ways that suggest that the human ITB is specialized for elastic energy storage (H3). Greater stretch occurs in human ITB MTUs compared to chimp FL MTUs during bipedal walking because humans walk with greater hip flexion/extension excursion. As hypothesized (H2), greater MTU length changes, along with the greater mass-specific force-generating capacity of muscles inserting in the ITB (H1), result in greater peak strains in the human ITB compared to the chimp FL. Approximately 10% of the chimp TFL, GMaxCr, and GMaxCd mass inserts in the FL while nearly 60% of the human TFL and GMaxCr mass inserts in the ITB. Thus, differences in both anatomy and locomotor mechanics between chimpanzees and humans determine the human ITB's greater elastic energy storage capacity compared to the chimp FL.

There are very few measures of chimp gluteal muscle architecture and moment arms in the literature for comparison to our data. Thorpe et al. (1999) report a normalized PCSA for GMaxCr and GMaxCd combined from a single juvenile specimen, which is smaller than the value measured here even after scaling to body mass (2.5 $cm^2/kg^{2/3}$ vs. 3.45 ± 0.6 $cm^2/kg^{2/3}$). We measured a small hip flexion MA for the anterior region of GMaxCr, which correponds with the data reported in Payne et al. (2006). We

measured large hip extension MAs for the more massive posterior GMaxCr regions (our unpublished data), which are not reported in Payne et al. (2006). There are no hip abduction/adduction MAs reported for GMaxCr, nor MAs for GMaxCd in any plane of hip motion. Measures of chimp MAs and muscle architecture for the TFL muscle are absent from the literature.

This study's descriptions of the chimpanzee muscle and FL anatomy are consistent with those reported by several previous studies. Stern (1972) found that the most anterior fibers of GMaxCr may insert in the fascia lata in some chimps. The anterior region of GMaxCr inserted in the FL in all four specimens examined here with this portion constituting, on average, 6% of the total GMaxCr mass. We also confirmed that the anteriormost region of the chimp GMaxCr muscle is partially fused with TFL as previously discussed. Contrary to Stern (1972) but consistent with other reports (Champneys, 1871; Sigmon and Farslow, 1986), we found that the superficial portion of GMaxCd (around 24% of the total muscle mass) inserts in the FL. Our findings also confirm previous studies reporting the diminutive size of the chimp TFL muscle relative to the human TFL muscle and its insertion in the FL (Sigmon, 1974; Sigmon, 1975).

While the human ITB and chimp FL differ in many respects, our dissections revealed that they also share some similarities. Like the human ITB, the chimp FL is relatively thick and fibrous compared to other deep fascia in the chimp lower limb. The chimp FL and human ITB both receive muscle fibers from GMaxCr and TFL. Part of the chimp FL inserts on the anterior tibia and plays a role in knee extension, similar to the human ITB. Taken together, our dissections suggest that the chimpanzee FL is a likely precursor to the human ITB. Assuming this anatomy was also present in the last

common ancestor of chimps and humans (see below), it is reasonable to hypothesize that the human ITB was elaborated from a chimplike condition by increasing the size of GMaxCr and TFL muscles inserting in the ITB and increasing ITB thickness. These changes likely have several functions. While the ITB was previously hypothesized to play a central role in lateral stability (Inman, 1947; Kaplan, 1958; Stern, 1972; Gottschalk et al., 1989), our model suggests that the human ITB does not have a substantially greater capacity to transmit abduction moments that stabilize the hip at midstance compared to the chimp FL. At a maximum, the human ITB transmits only 10% of the maximum hip abduction moment at midstance, which is comparable to the 7% of the total abduction moment transmitted by the chimp FL. Thus, our model does not suggest that the ITB is specialized for lateral hip stability. Instead, our results indicate that the human ITB is specialized to store elastic strain energy in comparison to the chimp FL.

Specialization of the human ITB for elastic energy storage has implications for the evolution of bipedalism. Bipedal walking is relatively inefficient in chimps compared to humans (Taylor and Rowntree, 1973; Pontzer et al., 2009; Pontzer et al., 2014) primarily because chimps locomote with a flexed hip and knee posture. A crouched posture reduces limb muscle effective mechanical advantage (Biewener, 1989) and requires a greater volume of active muscle to resist the effects of gravity (Biewener et al., 2004; Hicks et al., 2008). A crouched posture and compliant gait is common among extant primates (Schmitt, 1999), suggesting that the LCA of humans and other apes used a crouched gait. The relatively flexed hip of chimps during bipedal locomotion is due to their inferiorly oriented ischia, which reduces the hamstring muscle moment arms

when the hip is extended (Robinson, 1972). Indeed, the oldest hominin pelvis, ascribed to *Ardipithecus ramidus,* indicates an inferiorly oriented ischia, suggesting that early hominins used a crouched gait (Lovejoy et al., 2009; Fleagle and Lieberman, 2014).

Our model showed that the limited hip flexion/extension excursion of chimp bipedal walking compared to modern human walking reduced the stretch of chimp FL MTUs compared to human ITB MTUs. While the extreme hip flexion during chimp bipedal walking may put the posterior FL MTU in a relatively stretched position, energy is a function of length change (and force) and is not achieved by merely maintaining the MTU in a stretched position without changing length. Reduced MTU stretch along with a reduced muscle force-generating capacity resulted in a reduced capacity for chimp FL energy storage compared to the ITB. Thus, an energy-saving role for the FL is unlikely to have occurred in early hominins that walked with a crouched gait. However, models of hominin bipedalism have demonstrated that in order for habitual bipedalism to become economical in early hominins, changes to the locomotor morphology were necessary including a more upright lower limb posture, longer limbs, and shorter limb muscle fibers to increase muscle force-generating capacity (Crompton and Weijie, 1998; Sockol et al., 2007; Pontzer et al., 2009). *Australopithecus afarensis* (AL 288-1) and *Australopithecus africanus* (STS-14) have more dorsally oriented ischia compared to chimpanzees (Robinson, 1972; Stern and Susman, 1983), which would allow a more extended lower limb posture during locomotion. Although some paleontologists have suggested that australopiths walked with the bent hip-bent knee gait of earlier hominins (Stern and Susman, 1983; Susman et al., 1984; Stern, 2000; Schmitt, 2003), several recent studies have shown that they likely walked with a humanlike gait in terms of hip,

knee and ankle angles (Latimer et al., 1987; Tardieu and Trinkaus, 1994; Crompton et al., 1998; Ward, 2002; Carey and Crompton, 2005; Barak et al., 2013). FL energy storage may also have increased locomotor economy and may have occurred secondarily to muscular and kinematic changes accrued in early hominins including a more upright posture and increased muscle force-generating capacity. However, because the ITB is soft tissue and does not fossilize, we do not know when the ITB evolved in hominin evolution. While features of the locomotor apparatus in australopiths and *Homo* likely increased ITB energy storage, we lack the fossil evidence necessary to test this hypothesis.

Although selection for increased locomotor economy likely played a role in determining the unique structure of the human ITB, long-term exercise studies and comparisons of material properties in tendons subjected to high and low muscle loads demonstrate that tendons remodel in response to a high stress environment (Shadwick, 1990; Buchanan and Marsh, 2001; Foutz et al., 2007). While fascial plasticity has never been tested, similarities in the structure and composition of tendons and fascia indicate that fascia may also remodel in response to loading. Increased loading and stretch of the FL may have induced structural changes in the fascia including anteroposterior expansion or increased thickness.

Our study has a number of limitations. In our model, we scaled chimp muscle PCSAs by the specific tension of 31.5 N/cm^2 used in O'Neill et al. (2013). Because the human model's muscle parameters were based on data from elderly cadaveric specimens, muscle PCSAs were scaled by a specific tension of 61 N/cm^2 (Arnold et al., 2010); in Arnold et al.'s model, this value of specific tension predicts hip, knee, and

ankle joint moments that are consistent with the moments measured in healthy human subjects . If we use the higher specific tension value for both the human and chimp models, chimp peak FL energy storage values are doubled, but anterior and posterior ITB energy storage is still substantially greater. Because we lacked data describing chimp FL material properties, we assumed its material properties were similar to those of the human ITB, but we did take into account the lower FL cross-sectional area when calculating its tendon force-length curve from the human ITB stress-strain curve. In our model, we assumed that the chimp and human muscles were activated at 25% of maximum, but chimps may have greater muscle activation to maintain the bent hip-bent knee posture during walking. Higher activations and muscle forces would reduce differences in human and chimp peak energy storage. When maximally activated, the chimp FL MTUs store similar mass-specific elastic energy compared to the human ITB MTUs with 25% activation. We estimated the force generated by each muscle at body positions corresponding to bipedal walking and ignored the muscle's force-velocity properties. We can address these limitations in a future study by incorporating the modified chimp and human models within muscle-driven dynamic simulations. While the chimpanzee is a good model for the last common ancestor of humans and other apes, compromises between adaptations for walking and climbing probably explain why their cost of locomotion is unusually high among mammals (Taylor and Rowntree, 1973; Taylor et al., 1982; Sockol et al., 2007). Thus, while chimpanzee limb morphology may not be specialized to minimize energy expenditure, more terrestrial primates, such as baboons, may be under greater selective pressure to increase locomotor economy through energy storage and recovery. Future studies incorporating alternative primate

models of FL function are vital for understanding whether changes in the FL anatomy that influence energy storage are related to minimizing the cost of terrestrial locomotion.

References

Alexander, R. M. N. (1984). Elastic energy stores in running vertebrates. *American Zoologist* **24**, 85-94.

An, K. N., Takahashi, K., Harrigan, T. P. and Chao, E. Y. (1984). Determination of muscle orientations and moment arms. *Journal of Biomechanical Engineering* **106**, 280-282.

Arnold, A. S., Salinas, S., Asakawa, D. J. and Delp, S. L. (2000). Accuracy of muscle moment arms estimated from MRI−based musculoskeletal models of the lower extremity. *Computer Aided Surgery* **5**, 108-119.

Arnold, E. M., Ward, S. R., Lieber, R. L. and Delp, S. L. (2010). A model of the lower limb for analysis of human movement. *Annals of Biomedical Engineering* **38**, 269-279.

Barak, M. M., Lieberman, D. E., Raichlen, D. A., Pontzer, H., Warrener, A. G. and Hublin, J. J. (2013). Trabecular evidence for a human-like gait in *Australopithecus africanus*. *PloS One* **8**, e77687.

Berge, C. and Penin, X. (2004). Ontogenetic allometry, heterochrony, and interspecific differences in the skull of African apes, using tridimensional Procrustes analysis. *American Journal of Physical Anthropology* **124**, 124-138.

Biewener, A. A. (1989). Scaling of body support in mammals: Limb posture and muscle mechanics. *Science* **245**, 45-48.

Biewener, A. A., Farley, C. T., Roberts, T. J. and Temaner, M. (2004). Muscle mechanical advantage of human walking and running: implications for energy cost. *Journal of Applied Physiology* **97**, 2266-2274.

Brand, P. W., Cranor, K. C. and Ellis, J. C. (1975). Tendon and pulleys at the metacarpophalangeal joint of a finger. *Journal of Bone and Joint Surgery* **57**, 779-784.

Buchanan, C. I. and Marsh, R. L. (2001). Effects of long-term exercise on the biomechanical properties of the Achilles tendon of guinea fowl. *Journal of Applied Physiology* **90**, 164-171.

Carey, T. S. and Crompton, R. H. (2005). The metabolic costs of 'bent-hip, bent-knee'walking in humans. *Journal of Human Evolution* **48**, 25-44.

Champneys, F. (1871). The muscles and nerves of a Chimpanzee (Troglodytes Niger) and a Cynocephalus Anubis. *Journal of anatomy and physiology* **6**, 176.

Crompton, R. H., Li, Y., Wang, W., Günther, M. M. and Savage, R. (1998). The mechanical effectiveness of erect and “bent-hip, bent-knee” bipedal walking in *Australopithecus afarensis*. *Journal of Human Evolution* **35**, 55-74.

Crompton, R. H. and Weijie, L. Y. W. (1998). The mechanical effectiveness of erect and "bent-hip, bent-knee" bipedal walking in *Australopithecis afarensis*. *Journal of Human Evolution* **35**, 55-74.

Darwin, C. (1871). The Descent of Man and Selection in Relation to Sex. London: Murray.

Derwin, K. A., Baker, A. R., Spragg, R. K., Leigh, D. R., Farhat, W. and Iannotti, J. P. (2008). Regional variability, processing methods, and biophysical properties of human fascia lata extracellular matrix. *Journal of Biomedical Materials Research Part A* **84**, 500-507.

Fleagle, J. G. and Lieberman, D. E. (2014). Major transformations in the evolution of primate locomotion. In *Great Transformations: Major Events in the History of Vertebrate Life - Festschrift in Honor of Professor Farish A. Jenkins, Jr.*, eds. K. P. Dial E. L. Brainerd and N. H. Shubin). Chicago: The University of Chicago Press.

Foutz, T. L., Griffin, A. K., Halper, J. T. and Rowland, G. N. (2007). Effects of activity on avian gastrocnemius tendon. *Poultry Science* **86**, 211-218.

Fredericson, M., Cookingham, C., Chaudhari, A., Dowdell, B., Oestreicher, N. and Sahrmann, S. (2000). Hip abductor weakness in distance runners with iliotibial band syndrome. *Clinical Journal of Sport Medicine* **10**, 169-175.

Gottschalk, F., Kourosh, S. and Leveau, B. (1989). The functional anatomy of tensor fasciae latae and gluteus medius and minimus. *Journal of Anatomy* **166**, 179-189.

Haile-Selassie, Y. (2001). Late Miocene hominids from the Middle Awash, Ethiopia. *Nature* **412**, 178-181.

Hewes, G. (1964). Hominid bipedalism: Independent evidence for the food-carrying theory. *Science* **146**, 416-418.

Hicks, J. L., Schwartz, M. H., Arnold, A. S. and Delp, S. L. (2008). Crouched postures reduce the capacity of muscles to extend the hip and knee during the single-limb stance phase of gait. *Journal of Biomechanics* **41**, 960-967.

Hoy, M. G., Zajac, F. E. and Gordon, M. E. (1990). A musculoskeletal model of the human lower extremity: the effect of muscle, tendon, and moment arm on the moment-angle relationship of musculotendon actuators at the hip, knee, and ankle. *Journal of Biomechanics* **23**, 157-169.

Inman, V. T. (1947). Functional aspects of the abductor muscles of the hip. *The Journal of Bone and Joint Surgery* **29**, 607-619.

Kaplan, E. B. (1958). The iliotibial tract: Clinical and morphological significance. *The Journal of Bone and Joint Surgery* **40**, 817-832.

Latimer, B., Ohman, J. C. and Lovejoy, C. O. (1987). Talocrural joint in African hominoids: implications for Australopithecus afarensis. *American Journal of Physical Anthropology* **74**, 155-175.

Lee, L.-F., O'Neill, M. C., Demes, B., Confer, M. D., Thompson, N. E., Larson, S. G., Stern Jr, J. T. and Umberger, B. R. (2013). The mechanics of economical walking: Insights from chimpanzee and human bipedalism. In *American Society of Biomechanics*. Omaha, Nebraska.

Lieberman, D. E., Raichlen, D. A., Pontzer, H., Bramble, D. M. and Cutright-Smith, E. (2006). The human gluteus maximus and its role in running. *Journal of Experimental Biology* **209**, 2143-2155.

Lovejoy, C. O., Suwa, G., Simpson, S. W., Matternes, J. H. and White, T. D. (2009). The great divides: Ardipithecus ramidus reveals the postcrania of our last common ancestors with African apes. *Science* **326**, 73-106.

Mendez, J. and Keys, A. (1960). Density and composition of mammalian muscle. *Metabolism: Clinical and Experimental* **9**, 184-188.

O'Neill, M. C., Lee, L.-F., Larson, S. G., Demes, B., Stern, J. T. and Umberger, B. R. (2013). A three-dimensional musculoskeletal model of the chimpanzee (Pan troglodytes) pelvis and hind limb. *The Journal of experimental biology* **216**, 3709-3723.

Payne, R. C., Crompton, R. H., Isler, K., Savage, R., Vereecke, E. E., Günther, M. M., Thorpe, S. K. S. and D'Août, K. (2006). Morphological analysis of the hindlimb in apes and humans. II. Moment arms. *Journal of Anatomy* **208**, 725-742.

Pilbeam, D. (1996). Genetic and morphological records of the Hominoidea and hominid origins: a synthesis. *Molecular Phylogenetics and Evolution* **5**, 155-168.

Pontzer, H. (2007). Predicting the energy cost of terrestrial locomotion: a test of the LiMb model in humans and quadrupeds. *Journal of Experimental Biology* **210**, 484-494.

Pontzer, H., Raichlen, D. A. and Rodman, P. S. (2014). Bipedal and quadrupedal locomotion in chimpanzees. *Journal of Human Evolution* **66**, 64-82.

Pontzer, H., Raichlen, D. A. and Sockol, M. D. (2009). The metabolic cost of walking in humans, chimpanzees, and early hominins. *Journal of Human Evolution* **56**, 43-54.

Powell, P. L., Roy, R. R., Kanim, P., Bello, M. and Edgerton, V. R. (1984). Predictability of skeletal muscle tension from architectural determinations in guinea pig hindlimbs. *Journal of Applied Physiology* **57**, 1715-1721.

Preuschoft, H. (1961). Muskeln und Gelenke der Hinterextremitat des Gorillas. *Morphologisches Jahrbuch* **101**, 432-540.

Robinson, J. T. (1972). Early hominid posture and locomotion. Chicago: University of Chicago Press.

Rodman, P. S. and McHenry, H. M. (1980). Bioenergetics and the origin of human bipedalism. *American Journal of Physical Anthropology* **52**, 103-106.

Rolian, C., Lieberman, D. E., Hamill, J., Scott, J. W. and Werbel, W. (2009). Walking, running and the evolution of short toes in humans. *Journal of Experimental Biology* **212**, 713-721.

Ruvolo, M. (1994). Molecular evolutionary processes and conflicting gene trees: The hominoid case. *American Journal of Physical Anthropology* **94**, 89-114.

Satta, Y., Klein, J. and Takahata, N. (2000). DNA archives and our nearest relative: The trichotomy revisited. *Molecular Phylogenetics and Evolution* **14**, 259-275.

Saunders, J. B. d. M., Inman, V. T. and Eberhart, H. D. (1953). The major determinants in normal and pathological gait *Journal of Bone and Joint Surgery* **35**, 543-558.

Schmitt, D. (1999). Compliant walking in primates. *Journal of Zoology* **248**, 149-160.

Schmitt, D. (2003). Insights into the evolution of human bipedalism from experimental studies of humans and other primates. *Journal of Experimental Biology* **206**, 1437-1448.

Shadwick, R. (1990). Elastic energy storage in tendons: mechanical differences related to function and age. *American Journal of Physiology* **207**, 1033-1040.

Shea, B. T. (1985). Ontogenetic allometry and scaling. In *Size and scaling in primate biology*, pp. 175-205: Springer.

Sigmon, B. (1974). A functional analysis of pongid hip and thigh musculature. *Journal of Human Evolution* **3**, 161-185.

Sigmon, B. A. (1975). Functions and evolution of hominid hip and thigh musculature. In *Primate Functional Morphology and Evolution*, (ed. R. H. Tuttle). Paris: Mouton.

Sigmon, B. A. and Farslow, D. L. (1986). The Primate Hindlimb. New York: A.R. Liss.

Sockol, M., Raichlen, D. and Pontzer, H. (2007). Chimpanzee locomotion energetics and the origin of human bipedalism. *Proceedings of the National Academy of Sciences* **104**, 12265-12269.

Spoor, C., Van Leeuwen, J., Meskers, C., Titulaer, A. and Huson, A. (1990). Estimation of instantaneous moment arms of lower-leg muscles. *Journal of Biomechanics* **23**, 1247-1259.

Stern, J. T. (2000). Climbing to the top: a personal memoir of Australopithecus afarensis. *Evolutionary Anthropology Issues News and Reviews* **9**, 113-133.

Stern, J. T., Jr. (1972). Anatomical and functional specializations of the human gluteus maximus. *American Journal of Physical Anthropology* **36**, 315-339.

Stern, J. T., Jr. and Susman, R. L. (1981). Electromyography of the gluteal muscles in Hylobates, Pongo, and Pan: implications for the evolution of hominid bipedality. *American Journal of Physical Anthropology* **55**, 153-166.

Stern, J. T., Jr. and Susman, R. L. (1983). The locomotor anatomy of Australopithecus afarensis. *American Journal of Physical Anthropology* **60**, 279-317.

Susman, R. L., Stern Jr, J. and Jungers, W. L. (1984). Arboreality and bipedality in the Hadar hominids. *Folia Primatologica* **43**, 113-156.

Swindler, D. and Wood, C. (1973). An atlas of primate gross anatomy: baboon, chimpanzee, and man. Seattle: University of Washington Press.

Tardieu, C. and Trinkaus, E. (1994). Early ontogeny of the human femoral bicondylar angle. *American Journal of Physical Anthropology* **95**, 183-195.

Taylor, C. R., Heglund, N. C. and Maloiy, G. M. O. (1982). Energetics and mechanics of terrestrial locomotion. I. Metabolic comsumption as a function of speed and size in birds and mammals. *Journal of Experimental Biology* **97**, 1-21.

Taylor, C. R. and Rowntree, V. J. (1973). Running on two or on four legs: which consumes more energy? *Science (Washington D.C.)* **179**, 186-187.

Thorpe, S. K. S., Crompton, R. H., Günther, M., Ker, R. F. and Alexander, R. M. (1999). Dimensions and moment arms of the hind- and forelimb muscles of the common chimpanzees (*Pan troglodytes)*. *American Journal of Physical Anthropology* **110**, 179-199.

Thorpe, S. K. S., Holder, R. L. and Crompton, R. H. (2007). Origin of human bipedalism as an adaptation for locomotion on flexible branches. *Science* **316**, 1328-1331.

Ward, C. V. (2002). Interpreting the posture and locomotion of *Australopithecus afarensis*: Where do we stand? *Yearbook of Physical Anthropology* **45**, 185-215.

Wheeler, P. (1984). The evolution of bipedality and loss of functional body hair in hominids. *Journal of Human Evolution* **13**, 91-98.

Wrangham, R. W. and Pilbeam, D. (2001). African Apes as Time Machines. In *All Great Apes Great and Small, Volume I: African Apes*, eds. B. Galdikas N. Briggs L. Sheeran G. Shapiro and J. Goodall), pp. 5-17. New York: Kluwer Academics/Plenum Publishers.

Zihlman, A. and Tanner, N. (1978). Gathering and the hominid adaptation. *Female hierarchies*, 163-194.

Zollikofer, C., Ponce de Leon, M., Lieberman, D., Guy, F., Pilbeam, D., Likius, A., Mackaye, H., Vignaud, P. and Brunet, M. (2005). Virtual reconstruction of *Sahelanthropus tchadensis*. *Nature* **434**, 755-759.

Discussion

My dissertation research provides important insights into the function of fascia and has implications for human evolution. The biaxial materials testing experiments described in chapter 1 were critical for validating the assumptions of fascia material behavior used in the musculoskeletal models.

Chapter 2 demonstrated that the goat fascia lata stretches during locomotion with increased stretch potentially meeting the increased demand for mechanical work on incline versus level walking. The results of this study also indicate that the fascia lata (FL) may stretch passively with joint motion or actively through contraction of in series muscles. Measures of *in vivo* stretch in the goat fascia lata suggested that the human ITB, which shares many convergent features, also has the potential to store energy.

Chapter 3 confirmed that the human ITB has the potential to store elastic energy with greater energy stored in running than walking. Furthermore, the comparative analysis of human ITB and chimp FL energy storage in chapter 4 suggests that the ITB and its connections with GMax and TFL are derived features of the human lower limb that increase locomotor economy during bipedal walking relative to the chimp FL.

Future aims include using the refined human lower limb model to create a muscle-driven simulation of human walking and running. In addition to calculating energy storage, I can use this model to examine the influence of the compliant ITB on muscle fiber length operating ranges, power amplification, and force damping. Furthermore, the modified human lower limb model created here can be used to explore additional functions of the ITB and potential causes of and treatments for ITB syndrome, a common overuse injury among runners and cyclists.